Some Studies on Neutrino Oscillations, Scattering and their applications

Neelakshi Sarma

Department of Physics
Gauhati University

This thesis is submitted to
Gauhati University as requirement for the degree of
Doctor of Philosophy

Faculty of Science

April 2019

Certificate

This is to certify that the thesis titled "Some Studies on Neutrino Oscillations, Scattering and their applications" is the result of research work of Ms. Neelakshi Sarma, carried under my supervision, submitted to Gauhati University for the award of the degree of Doctor of Philosophy in Physics.

This thesis conforms to the standard of PhD thesis under Gauhati University including the standard related to plagiarism and has a similarity index not more than 20% (twenty percent), excluding the bibliography.

Kalpana
12/4/19

Dr. Kalpana Bora, Supervisor

April 2019

Members of the Research Advisory Committee:

Declaration

I hereby declare that this thesis is the result of my own research work which has been carried out under the guidance of Dr. Kalpana Bora of Gauhati University. I further declare that this thesis as a whole or any part thereof has not been submitted to any University (or Institute) for the award of any degree or diploma.

This thesis contains less than 90,000 (ninety thousand) words excluding bibliography and captions.

Neelakshi Sarma
12/4/19

Neelakshi Sarma

April 2019

I would like to dedicate this thesis to

Papa & Maa . . .

Acknowledgements

It gives me immense pleasure to express my deep sense of gratitude, to those people without whom this thesis would never have been possible. Words can not express how grateful I am to the people, who contributed in their own particular ways, to made this journey of mine a very pleasant and exciting experience, that has encouraged and allowed me to grow as a research scientist of physics!

First of all, I am indebted to my Alma Mater, Gauhati University and its authorities, specially our Honourable Vice Chancellor Dr. Mridul Hazarika Sir, for all the support that I have received during the entire period of my education and research here. I feel honoured and proud, for this association of mine with my University. My sincere gratitude goes to my supervisor, Dr. Kalpana Bora of Physics Department, Gauhati University for her persistent guidance and untiring support during these years. Her intense enthusiasm and passion for physics kept me committed to my research work, and it was her inspiring behaviour that helped my PhD research period so delightful and fruitful. She not only taught me to become a good physicist but also a good human being. She has been a true mentor!

I am truly grateful to Prof. M. P. Bora, Head of Physics Department for providing me with all the necessary infrastructure facilities, and for his unconditional support, invaluable advices and constructive criticism in different ways, at many occasions. All the faculty members of Physics Department, Gauhati University deserve special thanks for helping me in various aspects. In particular, I would like to thank Prof. D. K. Choudhury for his brilliant comments and valuable suggestions during the seminars that I have presented at the department at different occasions. I also want to thank all the members of the GU THEP group - Gayatri Ghosh, Baishali Saikia, Luxmi Machahari, Jugal Lahkar, Neelakshi N. K. Bora, Dr. Subhankar Roy, K. Shashikanta, Tapashi Das, Nilavjyoti Hazarika, Ricky Devi, and Paramita Deka. Their faithful and heart-warming company in the department always created a stimulating working environment, that made this challenging task an enjoyable and unforgettable one.

Next, some people of outstanding importance for my research work. I wholeheartedly thank Prof. Raj Gandhi, HRI, Allahabad for his kind support and suggestions, during my visits to HRI, where I learnt so many new things. Jaydip Singh also deserves thanks, for many discussions on simulations used in this thesis work. My heartfelt thanks are due to Prof. U. Mosel of Germany, for numerous positive interactions over email on works related to second Chapter. My sincere thanks also go to Dr. Debasish Borah of IIT Guwahati, with whom we did a fine piece of work. I would also like to thank the authorities of HRI, Allahabad for providing me financial assistance for the collaborative visits, and for providing me facilities to do part of my work there. Authorities of IIT Guwahati deserve thanks for providing me facilities to carry out part of work related to Chapter 4.

I acknowledge the financial support received during my PhD period from DST-SERB, Govt of India, Grant No. DST-SERB/EMR/2014/000296, as a Project Fellow.

And, of course I want to express my deepest gratitude to my parents, my brother Dr. Sandeep Sarma, my in-laws and my loving husband Debashis Thakur, for believing in me and for being there for practical support in all those things of life beyond Physics. They always stood beside me in all my difficult times during the period of my research. Thank you so much for all your blessings.

Finally, I thank the Almighty for giving me enough strength. I shall always cherish this wonderful and memorable experience of my life ...

Neelakshi Sarma 12.4.19

Neelakshi Sarma,
April 2019,
Guwahati.

Abstract

The aim of this thesis is to study neutrino oscillations, scattering and their applications.

We begin with a brief review of the historical developments leading to establishment of neutrino masses, mixings and oscillations. Then we briefly review theory of neutrino flavour conversion, methods of detection in some neutrino experiments, importance of neutrino-nucleon scattering cross sections (in Quasi- elastic and Ultra High Energy regime), and neutrino oscillation in the regime of sterile neutrinos. We also present experimental status of these ideas. Next, we move on to the studies on importance of nuclear effects in neutrino nucleus interactions at low three momentum transfer, in quasi-elastic (QE) regime. In particular, we have analysed the data from the MINERνA experiment. In this experiment, neutrinos are scattered off carbon target, using NuMI beamline at Fermilab, to observe neutrino oscillations. This experiment has reported data (number of events and double differential cross section) in the range $2 < E_\nu < 6$ GeV. Earlier, scientists have simulated these results using neutrino event generator GENIE, and some discrepancies between the data and their simulation results were found to be present. Therefore, in our work, we have studied improved nuclear effects, using another event Generator GiBUU (version 2016), taking into account FSI effects for the interaction channels like 2p2h/MEC and default (QE) process. We compare our results with the MINERνA data, and with earlier work done by P.A. Rodrigues et.al. After that, we have done investigations on neutrino nucleon cross section both for charged current and neutral current processes in ultra high energy limit ($10^9 GeV \leq E_\nu \leq 10^{12} GeV$), which will be relevant for analysing the high energy neutrinos coming from extra-galactic or astrophysical sources. Finally, we have studied the viability of various possible textures in light neutrino mass matrix within the framework of $3+1$ (one light (eV scale) sterile neutrino) scenario by considering a A_4 discrete flavour symmetric minimal extended seesaw mechanism (MES). This study would be relevant in future neutrino oscillation experiments in which existence of sterile neutrinos might be confirmed with precision. At the end, we present a brief summary of our works presented in the thesis followed by outlook and future prospects. A detailed list of references consulted during the work along with some appendices and a list of publications

is also given.

Keywords - Neutrino oscillation, neutrino scattering cross section, quasi-elastic scattering, 2p2h effects, final state interactions (FSI), charged current, neutral current, GENIE, GiBUU, proton structure function, double asymptotic limit, ultra high energy regime, sterile neutrino, A_4 discrete symmetry, minimal extended see saw, light neutrino mass matrix.

Table of contents

List of figures

List of tables

1 Introduction

1.1 Motivation and scope of the thesis

Motivation- Many properties of neutrino have been studied and measured experimentally, and neutrino physics has now entered precision era. But still, some parameters need experimental measurement as well as more intense theoretical studies. In this thesis, we have attempted to address some of these issues. The experimental measurements are inflicted with uncertainties in neutrino neucleon/nucleus scattering cross sections, which are one of the major causes of the errors in obtaining the values of neutrino oscillation parameters. Many experiments worldwide are thus regaining interest in making these measurements for neutrino scattering cross sections, in different energy regimes. Not only earth based experiments, but neutrinos coming to earth from extra-galactic and astrophysical sources serve as an important probe to investigate and know about the dynamics of ultra high energy (UHE) regimes. Since at the earth based experiments, the energy ranges that can be reached at the accelerators are constrained due to several limitations, the UHE neutrino studies become timely relevant, as a natural probe to investigate the dynamics at such scales. Neutrino interactions with nuclei play a crucial role in all these ongoing/planned experiments, as they make use of dense nuclear targets from which the incoming neutrinos are scatter off. Therefore, if the incoming neutrino energy is known precisely, one can extract neutrino oscillation parameters

from these experiments, provided the neutrino scattering cross section and its flux are known precisely. In fact, many experiments worldwide are ongoing/planned to measure $\nu - N$ scattering cross sections in low energy and UHE regime. This is the motivation for the work done in Chapters 2 and 3.

The anomalies in the measurements at LSND and MiniBoone experiments opened a new window for the existence of neutrino mass differences in the eV scale, which is very large as compared to the relatively small solar and atmospheric mass differences. This has led scientists to believe that active neutrinos may oscillate to a relatively heavy, sterile neutrino state. Many experiments worldwide are/will be making measurements to find stronger evidences for the existence of these sterile neutrinos. We would also like to mention here that the flavour structure of fermions is not yet well understood. And hence a unified theory that can explain neutrino masses and mixings along with the observed flavour structure would be the complete theory for the purpose. This is the motivation for the work done in Chapter 4.

Scope- With above motivation, the aim of this thesis is to study neutrino oscillations and neutrino-nucleus scattering in intermediate and ultra high energy regimes, and its application - specially the oscillation of active neutrinos to sterile neutrino, in presence of a discrete flavour symmetry.

In the first Chapter, we first review the historical developments leading to establishment of neutrino masses, mixings and oscillations. Then we briefly review theory of neutrino flavour conversion, methods of detection in some neutrino experiments, importance of neutrino-nucleon scattering cross sections (in Quasi- elastic and Ultra High Energy regime), and neutrino oscillation of active to sterile neutrinos. We also present experimental status of these experiments. A very brief discussion on the Methodology adopted to carry out the work done in this thesis has also been presented. In Chapter 2, we have studied neutrino-nucleus scattering cross section in intermediate energy regime ($0.1 - 20$ GeV), relevant for measurements done at the MINERνA experiment at Fermi Lab, USA, for Carbon target. We have simulated the number of events and double scattering cross-section, including nuclear effects, using an event generator GiBUU, and compare our results with the experimental data and those available in literature (using GENIE). In Chapter 3, we have studied neutrino nucleon scattering cross section, both for charged current and neutral current processes, in the energy range of $10^9 GeV \leq E_\nu \leq 10^{12} GeV$, using double asymptotic limit of the proton structure function. Chapter 4 is devoted to the studies on the viability of various possible textures in light neutrino mass matrix within the framework of $3+1$ (one light sterile neutrino) scenario

by considering a A_4 discrete flavour symmetric minimal extended seesaw mechanism (MES). This work would help us build and understand new theories and models to explain the neutrino masses, mixings and oscillations in 3 active flavours along with the existence of a fourth eigenstate of neutrino - the sterile neutrino. In the last Chapter, we present summary, outlook, and future prospects of the work carried out in the thesis.

In a nutshell, we can say that neutrino-nucleus interaction cross section calculations are important because they are used in any neutrino oscillation experiment. In any neutrino experimental set-up, if we know the flux, cross section, number of events then from probability, some of the unknown neutrino parameters like absolute mass squared differences, mixing angle in active-sterile neutrino sector, a Dirac CP-violating phase can be known with precision. Our $\nu - N$ interaction cross section calculation predictions, will indeed help to solve such unsolved issues in future oscillation experiments like DUNE [1]. We can say that if the existence of a light sterile neutrino of eV scale gets well established in future, then the predictions for the unknown neutrino oscillation parameters obtained in our analysis can be tested for further scrutiny of the model.

The work presented in this thesis is the compilation of the papers published for this purpose.

1.2 Historical background of neutrino oscillation

W. Pauli proposed at Tubingen in 1930 the existence of a neutral weakly interacting fermion emitted in β decay. He named this as 'neutron'. Later in 1932, Chadwick discovered a neutral, strongly interacting particle which we know as 'neutron' today. Enrico Fermi proposed the name of Pauli's particle to be as 'neutrino'. In early times, experiments showed that in β decay, nucleus decays to another nucleus (having same mass number) along with emission of an electron. Beta particle distribution is unique, unlike alpha particle energy distribution, it has a continuous spectrum which starts from zero, reaches a maximum height and then falls down and attains upper limit which is called 'end point energy' [2]. End point energy is the energy difference between initial and final nuclear states. If we consider β decay to be like a two body process then all the beta particles would have a unique energy but what we find in reality is that all the particles are emitted with smaller energy. This indicates that there must be some energy 'missing' in β decay process.

In 1931, W. Pauli proposed that a third particle might be emitted in the decay process which shared this missing energy, later the particle was named as 'neutrino' by Fermi. For instance, if we consider E_{beta} to be the energy carried by beta particles, E_{max} is the end point energy, then the energy carried by 'neutrino' is $E_\nu = (E_{max} - E_{beta})$ which is the missing energy. Experiments showed that there exist two different types of neutrinos emitted in beta decay. They are neutrino and its antiparticle called anti-neutrino ($\bar{\nu}$). The general beta decay process can be written as

$$X_N \rightarrow Y_{N-1} + \beta^- + \bar{\nu} \quad (\beta^- decay) \quad \text{and} \quad X_N \rightarrow Y_{N+1} + \beta^+ + \nu \quad (\beta^+ decay). \tag{1.1}$$

In early 1950's, F. Reines and C. L. Cowan encouraged by B. Pontecorvo performed an

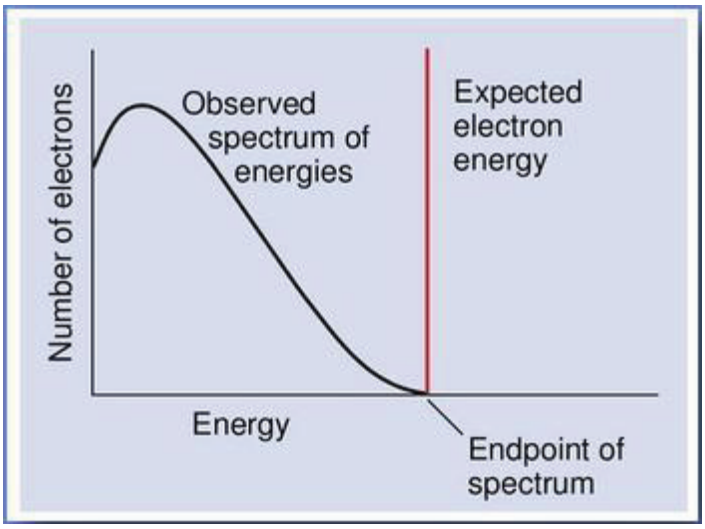

Fig. 1.1 β energy spectrum (taken from [3]).

experiment at Savannah River nuclear reactor in South Carolina which was the first reactor neutrino experiment [2–7]. They measured inverse beta decay in which an anti-neutrino produced a positron. The reaction is $\bar{\nu} + p \rightarrow n + e^+$. This reaction was observed by Reins and Cowan where they used a nuclear reactor as a source of $\bar{\nu}$. They used a liquid scintillator (in which a cadmium compound was embedded) for their neutrino detector. Reines and Cowan took lot of pain to carry out the experiment which proved the existence of neutrino experimentally. Ray Davis et al [8] in 1968 reported the first experiment to measure solar neutrinos, where they used a huge tank of chlorine in the Homestake mine in South Dakota. The famous Homestake experiment was able to observe solar neutrino flux [9] which was about 2.2 ± 0.4 SNU (Solar Neutrino Unit) [10, 11]. This value was smaller than the amount predicted by theoretical solar model. This is known as solar neutrino problem. In the year 1998, in Japan, the Super Kamiokande collaboration [12] was able to find evidence for

oscillation of atmospheric neutrinos. The scientists at Sudbury Neutrino Observatory (SNO) [13] measured the boron (B^8) solar neutrinos through the following reactions

$$\begin{aligned} \nu_e + d &\rightarrow p + p + e^- \quad \text{(charged current)}, \\ \nu_a + d &\rightarrow p + n + \nu_a \quad \text{(neutral current)}, \\ \nu_a + e^- &\rightarrow \nu_a + e^- \quad \text{(elastic scattering)}, \end{aligned} \tag{1.2}$$

where 'd' is deuteron, 'p' is proton, 'n' is neutron and $a = e, \mu, \tau$. After the discovery of electron and muon neutrino, search for the third flavour of neutrino finally ended in the year 2001. The DONUT collaboration at Fermilab [14] was able to observe tau neutrino interactions. For a long time it was believed that there exist three neutrino flavours but in the Liquid Scintillator Neutrino Detector (LSND) experiment located at Los Alamos [15], (electron antineutrinos were observed in a pure muon antineutrino beam) scientists could explain the existence of fourth type of neutrino called 'sterile neutrino'. The LSND experiment searched for $\bar{\nu}_\mu \rightarrow \bar{\nu}_e$ oscillations in the appearance mode and reported an excess of $\bar{\nu}_e$ interactions that could be explained by incorporating at least one additional light neutrino with mass in the eV range. This result was supported by the subsequent measurements at the MiniBooNE experiment [16]. Similar anomalies have been observed at reactor neutrino experiments and also at gallium solar neutrino experiments [17, 18]. Sterile neutrino can be defined as a neutral lepton with no gauge interaction. Sterile neutrinos in principle can have any mass. Very heavy sterile neutrinos are utilized in the minimal type I seesaw model and play a significant role in leptogenesis . We know that the Standard Model (SM) is based on the gauge group $SU(3)_c \times SU(2)_L \times U(1)_Y$, the elementary particle interactions are guided by this gauge group. Sterile neutrino is a singlet under both $SU(3)_c$ and $SU(2)_L$ and its hypercharge $Y = 0$. Recently in 2015, Nobel Prize in Physics was awarded jointly to Takaaki Kajita who belonged to Super-Kamiokande Collaboration, University of Tokyo, Japan and Arthur B McDonald belonged to Sudbury Neutrino Observatory, Queen's University, Canada, for the discovery of neutrino oscillations which shows that neutrinos are not massless.

1.3 Neutrino oscillation and flavour conversion

1.3.1 Solar Neutrino Problem

The reactions that occur in the core of the sun are [4]

$$\begin{aligned} p+p &\rightarrow D+e^{+}+\nu_e \quad (E_\nu \sim \text{0-0.42 MeV}),\\ p+p+e^{-} &\rightarrow D+\nu_e \quad (E_\nu \sim \text{1.44 MeV}),\\ Be_4^7+e^{-} &\rightarrow Li_3^7+\nu_e \quad (E_\nu \sim \text{0.861 or 0.33 MeV}),\\ Be_5^8 &\rightarrow Be_4^{*8}+e^{+}+\nu_e \quad (E_\nu \sim \text{0-14.1 MeV}). \end{aligned} \tag{1.3}$$

The net reaction is

$$4p \rightarrow He_2^4+2e^{+}+2\nu_e+28\text{MeV}. \tag{1.4}$$

In 1983, the first phase of Kamiokande experiment i.e. Kamiokande-I started, later in 1986 Kamiokande-II started which was an upgradation of its first one. Kamiokande-II was able to observe B^8 solar neutrinos. They measured solar neutrino flux through the following elastic scattering process Kamiokande experiment recorded an average of B^8 neutrino flux from 1987 to 1995 to be $\phi_{B^8}^{Kamiokande} = (2.80 \pm 0.38) \times 10^6 cm^{-2}s^{-1}$. Kamiokande used a large detector of pure water in order to measure the rate at which electrons present in water scattered high energetic neutrinos emitted from the sun. The Kamiokande experiment observed that the number of neutrino events was less as compared to the theoretical model of the sun.
Another solar neutrino experiment i.e. SK water Cherenkov detector located in Kamioka mine is based on the elastic scattering of electron neutrino on electron. SK could measure precisely high energy neutrinos and confirmed the high energy neutrino deficit as recorded by chlorine and Kamiokande experiment.

1.3.2 Atmospheric neutrino problem

The interactions of primary cosmic rays with the nuclei in the atmosphere produce atmospheric neutrinos. These interactions produce secondary cosmic rays. In particular, many secondary pions are produced which decay mainly into muons and muon neutrinos [4]. The processes for production of atmospheric neutrinos are :

$$\begin{aligned} \pi^{+} \rightarrow \mu^{+}+\nu_\mu, \qquad \mu^{+} \rightarrow e^{+}+\nu_e+\bar{\nu_\mu} \quad \text{and}\\ \pi^{-} \rightarrow \mu^{-}+\bar{\nu_\mu}, \qquad \mu^{-} \rightarrow e^{-}+\bar{\nu_e}+\nu_\mu. \end{aligned} \tag{1.5}$$

Above Eq (1.5) indicates that the fluxes of $\nu_e, \nu_\mu, \bar{\nu_e}, \bar{\nu_\mu}$ are related to each other by the relation [19]

$$\phi(\nu_\mu + \bar{\nu_\mu}) \simeq 2\phi(\nu_e + \bar{\nu_e}). \tag{1.6}$$

where ϕ represents the neutrino flux. In 1960, atmospheric neutrino experiments were started, an experimental set up was built in Kolar Gold Field in India, another was carried out at the East Rand Proprietary Mine in South Africa. The neutrino interactions that occurred in the rocks which surrounded a neutrino detector were measured. It was found that some ν_μ were missing - flux of ν_μ was less than that predicted. This is called atmospheric neutrino problem.

1.3.3 Solution of above problems

Scientist at SNO studied neutrinos coming from the sun. In the year 2001, the SNO research group proved that these neutrinos switch their identities. As the ν_e neutrinos travel from sun to earth, they oscillate to other flavours say to ν_μ type neutrino or to ν_τ type neutrino. This phenomenon is called 'neutrino oscillation'. The process of neutrino oscillation shows neutrinos are not massless but are massive. Neutrino oscillation can be explained with the help of neutrino mixing and neutrino mixing exist only if mass of neutrinos is non zero. Also, the atmospheric neutrino problem was solved if we assume conversion of atmospheric ν_μ to ν_e or ν_τ.

1.3.4 Theory of neutrino oscillation

Neutrino oscillation is a quantum mechanical phenomenon where a neutrino created with a specific flavour transforms into a different flavour which can be measured later. In 1968, Bruno Pontecorvo proposed that electron neutrino produced in the sun are transformed into a different type of neutrino (say ν_μ) while travelling in vacuum i.e. $\nu_e \longleftrightarrow \nu_\mu$. The flavour eigenstate of neutrino is 'ν_α' where $\alpha = e, \mu, \tau$. The mass eigenstates 'ν_j' are different from flavour eigenstates [4] i.e.

$$\mid \nu_\alpha >= \sum_{j=1}^{3} U_{\alpha j} \mid \nu_j >, \tag{1.7}$$

$$U = \begin{pmatrix} c_{12}c_{13} & s_{12}c_{13} & s_{13}e^{-i\delta_{CP}} \\ -s_{12}c_{23} - c_{12}s_{13}s_{23}e^{i\delta_{CP}} & c_{12}c_{23} - s_{12}s_{13}s_{23}e^{i\delta_{CP}} & c_{13}s_{23} \\ s_{12}c_{23} - c_{12}s_{13}c_{23}e^{i\delta_{CP}} & -c_{12}s_{23} - s_{12}s_{13}c_{23}e^{i\delta_{CP}} & c_{13}c_{23} \end{pmatrix}, \tag{1.8}$$

where $c_{ij} = cos\theta_{ij}$ and $s_{ij} = sin\theta_{ij}$. Here U is the unitary mixing matrix known as Pontecorvo-Maki-Nakagawa-Sakata (PMNS) matrix. For a 3×3 neutrino mixing case, we have three mix-

ing angles θ_{12}(solar angle), θ_{13}(reactor angle), θ_{23}(atmospheric angle), and one complex phase δ_{CP}, which is responsible for CP violation in the neutrino sector. Also, $\nu_j = \nu_1, \nu_2, \nu_3$ are the mass eigenstates with mass eigen values m_1, m_2, m_3.

If a neutrino of a given flavour [20], say ν_e , with energy 'E' is produced at ν_e source then the probability of finding a neutrino of a different flavour, say ν_μ, P ($\nu_e \rightarrow \nu_\mu$; E, L) at a distance L away from the source, is called transition probability. Consider a beam of pure ν_e states produced at time $t = 0$, we have [4],

$$\mid \nu_e(0) >= U_{e1} \mid \nu_1 > + U_{e2} \mid \nu_2 > + U_{e3} \mid \nu_3 > . \tag{1.9}$$

We consider all neutrino particles in the beam have a common momentum 'p' then mass eigenstates have energy as $E_j^2 = p^2 + m_j^2$. At some later time, say 't', we have

$$\mid \nu_e(t) >= U_{e1} e^{-iE_1 t} \mid \nu_1 > + U_{e2} e^{-iE_2 t} \mid \nu_2 > + e^{-iE_3 t} U_{e3} \mid \nu_3 > . \tag{1.10}$$

The probability of finding a neutrino of flavour , say ν_β at time 't' is given by $|< \nu_\alpha \mid \nu_\beta(t) >|^2$ i.e.

$$P_{\nu_\alpha \rightarrow \nu_\beta}(t) = |< \nu_\alpha \mid \nu_\beta(t) >|^2 = \sum_{j,k=1}^{3} U_{\alpha j} U^*_{\beta j} U^*_{\alpha k} U_{\beta k} e^{-i(E_j - E_k)t}. \tag{1.11}$$

For relativistic neutrino, $p >> m_j$ we have

$$E_j = \sqrt{p^2 + m_j^2} = p + \frac{m_j^2}{2p}$$

and

$$E_j - E_k = \frac{1}{2E}(m_j^2 - m_k^2) = \frac{\Delta m_{jk}^2}{2E}. \tag{1.12}$$

As neutrinos are ultra-relativistic particles, we can use ($t = L$), and the transition probability is

$$P_{\nu_\alpha \rightarrow \nu_\beta}(t) = \sum_{j,k=1}^{3} U_{\alpha j} U^*_{\beta j} U^*_{\alpha k} U_{\beta k} e^{-i(\frac{\Delta m_{jk}^2}{2E} L)}. \tag{1.13}$$

The above equation can be written as

$$P_{\nu_\alpha \rightarrow \nu_\beta} = \sum_{j=1}^{3} \mid U_{\alpha j} \mid^2 \mid U_{\beta j} \mid^2 + 2Re \sum_{j>k} U_{\alpha j} U^*_{\beta j} U^*_{\alpha k} U_{\beta k} exp^{-i(\frac{\Delta m_{jk}^2}{2E} L)}, \tag{1.14}$$

where,

$$\sum_{j=1}^{3} \mid U_{\alpha j} \mid^2 \mid U_{\beta j} \mid^2 = \delta_{\alpha\beta} - 2Re \sum_{j>k}^{n} U_{\alpha j} U^*_{\beta j} U^*_{\alpha k} U_{\beta k}. \tag{1.15}$$

The transition probability thus can be written as

$$P_{\nu_\alpha \to \nu_\beta} = \delta_{\alpha\beta} - 2Re \sum_{j>k}^{n} U_{\alpha j} U^*_{\beta j} U^*_{\alpha k} U_{\beta k} [1 - e^{-i(\frac{\Delta m^2_{jk}}{2E} L)}]. \tag{1.16}$$

The identity Re(ab) = Re(a)Re(b)-Im(a)Im(b), is used to write the transition probability as [20]

$$P_{\nu_\alpha \to \nu_\beta} = \delta_{\alpha\beta} - 4\Sigma Re(U_{\alpha j} U^*_{\beta j} U^*_{\alpha k} U_{\beta k}) sin^2(\frac{\Delta m^2_{jk}}{4E} L) + 2 \sum_{j>k} Im(U_{\alpha j} U^*_{\beta j} U^*_{\alpha k} U_{\beta k}) sin(\frac{\Delta m^2_{jk}}{2E} L). \tag{1.17}$$

The above expression for the survival probability can be written as

$$P_{\nu_\alpha \to \nu_\beta} = 1 - 4 \sum_{j>k} \mid U_{\alpha j} \mid^2 \mid U_{\alpha k} \mid^2 sin^2(\frac{\Delta m^2_{jk}}{4E} L). \tag{1.18}$$

The appearance probability ($\alpha \neq \beta$) can be written as

$$P_{\nu_\alpha \to \nu_\beta} = -4 \sum_{j>k} (U_{\alpha j} U_{\beta j} U_{\alpha k} U_{\beta k}) sin^2(\frac{\Delta m^2_{jk}}{4E} L). \tag{1.19}$$

There are two kinds of neutrino oscillation experiments i.e. disappearance and appearance experiments. Suppose in a pure neutrino beam of known flavour say ν_μ, one looks to see how many neutrinos have disappeared then this is called 'disappearance' experiment which measures the survival probability ($P_{\nu_\mu \to \nu_\mu}$). On the other hand, suppose in a pure beam of known flavour say, ν_μ one looks how many neutrinos of a different flavour say, ν_e are detected. This is called 'appearance experiment'. CP violating effects cannot be studied in disappearance experiments - they arise only in appearance experiments.

In three neutrino mixing schemes, the three squared mass differences can be written as $\Delta m^2_{21}(solar) = m^2_2 - m^2_1$, $\Delta m^2_{31}(atmospheric) = m^2_3 - m^2_1$, $\Delta m^2_{32} = m^2_3 - m^2_2$. Out of the three squared mass differences, [4] only two are independent since $\Delta m^2_{32} + \Delta m^2_{21} - \Delta m^2_{31} = 0$. The observed hierarchy $\Delta m^2_{sol} << \Delta m^2_{atm}$ can be accomodated in the two types of three neutrino mixing schemes i.e. Normal hierarchy (NH) and Inverted hierarchy (IH) schemes.

In Normal ordering: $m_1 < m_2 < m_3$,

$\Delta m^2_A = \Delta m^2_{31} > 0$, $\Delta m^2_{solar} = \Delta m^2_{21} > 0, m_{2(3)} = \sqrt{m^2_1 + \Delta m^2_{21(31)}}$,

In Inverted ordering: $m_3 < m_1 < m_2$
$\Delta m^2_A = \Delta m^2_{32} < 0$, $\Delta m^2_{solar} = \Delta m^2_{21} > 0, m_2 = \sqrt{m_3^2 + \Delta m^2_{23}}, m_1 = \sqrt{m_3^2 + \Delta m^2_{23} - \Delta m^2_{21}}$.

1.3.5 Two flavour neutrino oscillation

For the sake of completeness, we discuss here briefly the two-flavour neutrino oscillations. The effective mixing matrix in case of two flavour neutrino oscillation is given as

$$U = \begin{pmatrix} cos\theta & sin\theta \\ -sin\theta & cos\theta \end{pmatrix}. \tag{1.20}$$

The flavor eigenstates are written as a function of the mass eigenstates as:

$$\nu_\alpha = \nu_1 cos\theta + \nu_2 sin\theta \qquad \nu_\beta = -\nu_1 sin\theta + \nu_2 cos\theta, \tag{1.21}$$

where θ is the mixing angle. For two flavour neutrino oscillation there is one mixing angle (θ) and no CP phase. From Eq (1.21), the transition probability can be written as

$$P_{\nu_\alpha \to \nu_\beta} = sin^2 2\theta sin^2(\frac{\Delta m^2 L}{4E}). \tag{1.22}$$

For survival probability, $\alpha = \beta$ and thus Eq (1.20) gives

$$P_{\nu_\alpha \to \nu_\alpha} = 1 - sin^2 2\theta sin^2(\frac{\Delta m^2 L}{4E}). \tag{1.23}$$

In Eq (1.23), when the mixing angle $\theta = 0$ the mass eigenstates will be equal to flavour eigenstates. When $\theta = \frac{\pi}{4}$, neutrino mixing is maximum. In order to have neutrino oscillation we must have non zero and non degenerate neutrino masses and mixing angles. In natural units of high energy physics, we express Δm^2 in terms of eV^2, L in kilometers and energy in GeV. The oscillation probability becomes

$$P_{\nu_\alpha \to \nu_\beta} = sin^2 2\theta sin^2(1.27\frac{\Delta m^2 L}{E}). \tag{1.24}$$

In Eq (1.24), 'L' is the distance from the source (also called baseline), and 'E' is the neutrino energy. The oscillation wavelength depends upon 'L', 'E', and Δm^2 and the amplitude depends upon $sin^2 2\theta$. For the oscillation probability to be maximum, $\frac{L}{E}$ is chosen such that

$$1.27\frac{\Delta m^2 L}{E} = \frac{\pi}{2} \quad or \quad \frac{L}{E} = \frac{\pi}{2.54\Delta m^2}. \tag{1.25}$$

1.3.6 Two flavour neutrino oscillation in matter

When neutrinos travel through matter, there is change in the pattern of neutrino oscillations. Changes come due to forward scattering interactions with electrons and nuclei giving rise to effective potentials. Neutrinos interact with matter through charged current (CC) (they mediate through $W^{\pm}$ boson) and neutral current (NC) (they mediate through Z^0 boson) interaction. When different flavours of neutrino interact with matter through NC process, then they give rise to an effective potential i.e. $V_{NC} = -\frac{G_F N_n}{\sqrt{2}}$ where N_n is the number density of neutron of the matter.

On the other hand electron neutrinos, in addition to neutral current interaction also undergo charged current interaction giving rise to an additional effective CC potential i.e. $V_{CC} = \sqrt{2} G_F N_e$ where N_e is the number density of electrons in the matter. Time evolution of flavour states [4] can be written as

$$i\frac{d}{dt}\begin{pmatrix} \nu_e(t) \\ \nu_\mu(t) \end{pmatrix} = H \begin{pmatrix} \nu_e(t) \\ \nu_\mu(t) \end{pmatrix}, \tag{1.26}$$

where H is the total Hamiltonian. The flavour eigenstates can be related to mass eigenstates by the following matrix

$$\begin{pmatrix} \nu_e \\ \nu_\mu \end{pmatrix} = \begin{pmatrix} cos\theta & \sin\theta \\ -sin\theta & cos\theta \end{pmatrix} \begin{pmatrix} \nu_1 \\ \nu_2 \end{pmatrix}. \tag{1.27}$$

In terms of effective Hamiltonian matrix , 'H', Eq (1.26) can be expressed as

$$i\frac{d}{dx}\begin{pmatrix} A_{ee}(x) \\ A_{e\mu}(x) \end{pmatrix} = H' \begin{pmatrix} A_{ee}(x) \\ A_{e\mu}(x) \end{pmatrix}, \tag{1.28}$$

where $A_{\alpha\beta} =< \nu_\beta \mid \nu_\alpha(t) >$ ($\alpha = e$ and $\beta = \mu$) is the probability amplitude of transition of $\nu_\alpha \to \nu_\beta$. Thus we have

$$H' = \frac{1}{4E}\begin{pmatrix} -\Delta m^2 cos2\theta + A_{CC} & \Delta m^2 sin2\theta \\ \Delta m^2 sin2\theta & \Delta m^2 cos2\theta - A_{CC} \end{pmatrix}, \tag{1.29}$$

where $\Delta m^2 = m_2^2 - m_1^2$ and $A_{CC} = 2EV_{CC} = 2\sqrt{2}EG_F N_e$. Diagonalising the above matrix by orthogonal transformation we have

$$U_M^T H' U_M = H_M = \frac{1}{4E}\begin{pmatrix} -\Delta m_M^2 & 0 \\ 0 & \Delta m_M^2 \end{pmatrix}, \tag{1.30}$$

where H_M is the effective Hamiltonian matrix in matter. Effective mixing matrix in matter can be written as

$$U_M = \begin{pmatrix} cos\theta_M & \sin\theta_M \\ -sin\theta_M & cos\theta_M \end{pmatrix}. \tag{1.31}$$

Effective mass square difference Δm^2_M in matter is

$$\Delta m^2_M = m^2_{2M} - m^2_{1M} = \sqrt{(\Delta m^2 cos2\theta - A_{CC})^2 + (\Delta m^2 sin2\theta)^2}. \tag{1.32}$$

Effective mixing angle θ_M in matter is

$$\theta_M = \frac{1}{2} tan^{-1}\left(\frac{tan2\theta}{1 - A_{CC}/\Delta m^2 cos2\theta}\right). \tag{1.33}$$

It is observed from Eq (1.33) that at resonance condition we have

$$A_{CC} = \Delta m^2 cos2\theta, \tag{1.34}$$

and hence $\theta_M = \pi/4$. At resonance, mixing among neutrino flavours in matter becomes maximum. This phenomenon was first observed in 1985 by Mikheyev, Smirnov, Wolfenstein (or MSW) effect also called Resonant Enhancement in Matter [21, 22].

1.3.7 Neutrino oscillation with sterile neutrinos

We know that neutrinos interact solely through weak interaction in the standard model (SM). As a consequence only left handed component in the SM is active, and is a part of a weak isospin doublet with its partner charged lepton. Here a question arises i.e. whether right-handed neutrinos exist or not. If right handed neutrinos exist in SM then it would be weak isospin singlets with no weak interactions except through mixing with the left-handed neutrinos. That is why right handed neutrinos are referred to as 'sterile' neutrinos [23]. Following is the mixing matrix between flavour eigenstates ν_α ($\alpha = e, \mu, \tau, s$) and mass eigenstates ν_j ($j = 1, 2, 3, 4$). We denote sterile neutrinos as ν_s .

$$\begin{pmatrix} \nu_e \\ \nu_\mu \\ \nu_\tau \\ \nu_s \end{pmatrix} = \begin{pmatrix} U_{e1} & U_{e2} & U_{e3} & U_{e4} \\ U_{\mu 1} & U_{\mu 2} & U_{\mu 3} & U_{\mu 4} \\ U_{\tau 1} & U_{\tau 2} & U_{\tau 3} & U_{\tau 4} \\ U_{s1} & U_{s2} & U_{s3} & U_{s4} \end{pmatrix} \begin{pmatrix} \nu_1 \\ \nu_2 \\ \nu_3 \\ \nu_4 \end{pmatrix}. \tag{1.35}$$

This unitary matrix can be parametrized [24] as

$$U = R_{34}(\theta_{34},0)R_{24}(\theta_{24},0)R_{23}(\theta_{23},\delta_3)R_{14}(\theta_{14},0)R_{13}(\theta_{13},\delta_2)R_{12}(\theta_{12},\delta_1), \tag{1.36}$$

where $R_{ij}(\theta_{ij},\delta_k)$ is the complex rotation matrix in the $i-j$ plane and the elements of the matrix are given by

$$[R_{ij}]_{pq} = \begin{cases} cos\theta \quad p=q=i \quad or \quad p=q=j \\ 1 \quad p=q\neq i \quad and \quad p=q\neq j \\ sin\theta e^{-i\delta} \quad p=i \quad and \quad q=j \\ -sin\theta e^{i\delta} \quad p=j \quad and \quad q=i \\ 0 \quad otherwise, \end{cases} \tag{1.37}$$

where θ_{ij} is the angle of rotation in $i-j$ plane. If we consider $\theta_{14},\theta_{24},\theta_{34}=0$ then the above matrix takes the form of Pontecorvo-Maki-Nakagawa-Sakata (PMNS) matrix for three flavour mixing. We have two kinds of neutrino schemes with the four flavours of neutrinos i.e. (2+2) scheme and (3+1)-scheme. These schemes are categorised depending on how the mass eigenstates are separated by the largest mass squared difference. In (2+2) scheme two mass eigenstates [25] are separated by other two. On the other hand, in (3+1) scheme one mass eigenstate is separated by other three mass eigenstates.
In (2+2) scheme, the fraction of sterile neutrino contributions to solar oscillation is given by $|U_{s1}|^2+|U_{s2}|^2$ and that of atmospheric oscillations is given by $|U_{s3}|^2+|U_{s4}|^2$. In (3+1) scheme, the probabilities for disappearance and appearance oscillations are as follows:

$$P(\nu_\alpha \to \nu_\beta) \simeq 4|U_{\alpha4}|^2|U_{\beta4}|^2 sin^2(1.27\frac{\Delta m^2_{41}L}{E}), \tag{1.38}$$

$$P(\nu_\alpha \to \nu_\alpha) \simeq 1-4(1-|U_{\alpha4}|^2)|U_{\alpha4}|^2 sin^2(1.27\frac{\Delta m^2_{41}L}{E}). \tag{1.39}$$

1.4 Processes for detection of neutrino oscillation

1) **Radiochemical method (Homestake experiment)**:
The Homestake Solar Neutrino Observatory is located in the Homestake Gold Mine, in South Dakota, USA. It detects solar neutrino through inverse beta decay chlorine-argon reaction

$$\nu_e + Cl^{37} \to Ar^{37} + e^-. \tag{1.40}$$

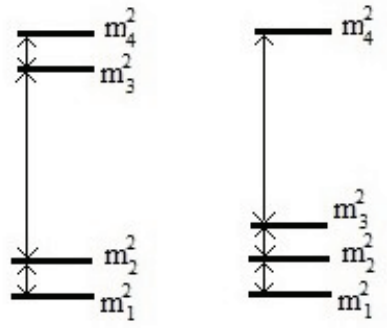

Fig. 1.2 Left figure shows four–neutrino mass spectra for (2+2) scheme and the right figure shows for (3+1) scheme.

Number of radioactive Ar^{37} atoms are counted to know how many solar neutrino have been detected. The argon is extracted through chemical methods and hence the name radiochemical method.

2) **Gallium experiment (GALLEX; SAGE)**:

The GALLEX/GNO and SAGE experiments were successful in measuring low energy neutrinos produced in the fundamental pp chain. In solar neutrino experiments GALLEX/GNO and SAGE, the solar neutrinos are detected through the reaction

$$\nu_e + Ga^{71} \rightarrow Ge^{71} + e^-. \tag{1.41}$$

The Ge^{71} atoms are extracted by chemical methods and counted in small proportional counters by observing their decay back to Ga^{71}.

3) **Water cherenkov detectors (Kamiokande, Superkamiokande)**:

In Water cherenkov detectors, neutrinos are detected through the elastic scattering reaction

$$\nu_e + e^- \rightarrow \nu_e + e^-. \tag{1.42}$$

When incoming electron neutrino interacts with electron of water, the produced electron travels with velocity greater than velocity of light in the medium. Cherenkov radiation is emitted in a cone around the direction of motion. The Cherenkov radiation is detected by the PMTs (photo multiplier tubes).

4) **Heavy water detector (SNO)**:
The large detectors are fitted with heavy water D_2O and incoming solar neutrino are detected by the Cherenkov radiation emitted. SNO detects solar neutrino through three reactions as given in Eq (1.2). Neutral current reaction is very important to detect all three flavours of neutrino (hence for detection of total flux of incoming solar neutrino) which offered solution to SNP. Heavy water (D_2O) Cherenkov detector, Sudbury Neutrino Observatory (SNO) studied high energy solar neutrinos that was previously investigated by Kamiokande and SK detectors. SNO alone demonstrated that about two out of three electron solar neutrinos, change their flavour to other flavours i.e. muon neutrinos (ν_μ) or tau neutrinos (ν_τ) as they traverse from core of sun down to earth. SNO detected all the three types of neutrinos i.e. ν_e, ν_μ and ν_τ.
5) **Detection of atmospheric neutrinos**:
In one of the first experiments that detected atmospheric neutrinos (performed in India, Kolar Gold mine), the detectors were made of scintillator, which recorded tracks of muons. Kamiokande and SK also detected atmospheric neutrino by detecting muon like events. In atmospheric neutrino experiments, neutrino fluxes of different flavours are measured by detection of the charged lepton produced in $\nu - N$ reactions

$$\nu_l + N \rightarrow l^- + X^- \quad \bar{\nu}_l + N \rightarrow l^+ + X, \tag{1.43}$$

where $l = e, \mu, \tau$. In the neutrino unmagnetized detector, charge of the lepton could not be distinguished. But it would become possible at magnetized detectors like future INO experiment. Also, it is extremely difficult to detect tau neutrinos, because the produced tau leptons decay immediately to leptons and hadrons, without leaving a clear track. Water cherenkov detector can detect both μ^- and e^-, muons produce a sharp ring of PMTs, while electron produce a fuzzy ring.
6) **Reactor neutrino experiments**:
Fission reactors are copious sources of electron antineutrinos produced in beta decays of neutron-rich nuclei. Reactor $\bar{\nu}_e$ are detected through inverse beta decay processes

$$\bar{\nu}_e + p \rightarrow n + e^-. \tag{1.44}$$

The emitted positron annihilates immediately with a surrounding electron and the released gamma are detected in scintillator detectors.
7) **Liquid scintillator experiments (KamLAND)**:
The detector is a liquid scintillator, the luminiscence from scintillator is picked by the PMTs. KamLAND is designed to detect $\bar{\nu}_e$ produced by reactors in Japan's Kamioka mine. $\bar{\nu}_e$ are

detected by inverse beta decay

$$\bar{\nu}_e + p \rightarrow n + e^-, \tag{1.45}$$

liquid scintillators are rich in hydrogen, which acts as target for this reaction. CC interactions are easier to work with since electron and muon have characteristic signatures in particle detectors and they are fairly easy to identify. If an electron is detected, electron neutrino must have arrived, if a muon neutrino is detected, means muon neutrino must have arrived, at the detector.

8) **Tracking experiment**:

Tracking detectors reconstruct the path of the charged leptons produced in CC interactions, either by ionisation that they cause or by the energy that they deposit. These detectors are best suited to higher energy neutrinos since distance travelled by a particle will increase as its energy increases and longer tracks are easier to reconstruct. Muons leave well defined tracks than electron which produce electromagnetic showers as they travel through dense material. Tracking detectors are good in separating muons from electrons. Examples of tracking detectors are MINOS, MINERνA, ICARUS, T2K.

9) **Emulsion detector**:

Detectors of CC events from tau neutrinos is very challenging since they decay extremely rapidly. The OPERA experiment at Gran Sasso and DONUT experiment at Fermilab addressed this change by using technique of nuclear emulsions. They can detect tracker produced by extremely short lived particles. Water cherenkov detectors can detect electron or muon from CC or recoil electron from neutrino electron elastic scattering.

1.5 More on solar, atmospheric and reactor experiments

In solar neutrino experiments, borexino is a scintillator detector, has intrinsic high luminosity, the liquid scintillation technology used by such detectors is extremely suitable for massive calorimetric low energy spectroscopy. In reactor neutrino experiments liquid scintillator technology is widely used because such technology has doping capability, mass production, uniformity and low cost. Daya Bay, Double Chooz, and RENO experiments used Gadolinium doped liquid scintillator as the medium to detect inverse beta decay events. The Gadolinium isotopes contain large cross sections of thermal neutron capture. Borexino [26] and KamLAND [27] were the two experiments that measured solar neutrinos from reactions other than B^8 [28]. Four experiments namely Super-K, MINOS, SNO, and IceCube study atmospheric neutrinos. The long baseline neutrino oscillation experiment, MINOS is the first magnetized tracking detector for detecting atmospheric neutrinos. IceCube is a neutrino telescope in which very high energy astrophysical neutrinos are studied. The

main background for searching these astrophysical neutrinos are high energy atmospheric neutrinos. Solar and atmospheric neutrino experiments showed that neutrinos oscillate with two different mass squared differences i.e. Δ^2_{sol} and Δ^2_{atm} respectively which was confirmed by KamLAND and K2K experiments [4], among others. DUNE is a very promising future long baseline (1300 km), underground experiment, being planned at the Fermilab, USA, with a liquid Ar detector. It is proposed to study about hierarchy problem, CP violation in neutrino sector etc, among other rich physics.

Reactor neutrinos are mainly produced through beta-decay of neutron-rich fission reactions of the four isotopes namely $U^{235}, U^{238}, Pu^{239}, Pu^{241}$. Another important source of anti-electron neutrinos apart from fission reaction processes come from neutron capture on U^{238}. In addition to inverse beta decay processes there are various methods for detection of reactor neutrinos.
First method is the charged current (CC) i.e.

$$\bar{\nu}_e + d \rightarrow n + n + e^+, \tag{1.46}$$

and neutral current (NC) process i.e.

$$\bar{\nu}_e + d \rightarrow n + p + \bar{\nu}_e. \tag{1.47}$$

Second method is the antineutrino-electron elastic scattering i.e.

$$\bar{\nu}_e + e^- \rightarrow \bar{\nu}_e + e^-. \tag{1.48}$$

The third method is the coherent antineutrino-nucleus interaction [29]. KamLAND which was built at the site of former Kamiokande experiment, aimed to search for reactor $\bar{\nu}_e$ oscillations. It was found that the results of KamLAND experiment was consistent with solar neutrino experiments and confirmed large mixing angle (LMA) solution to be the solution of SNP. Precise measurements from the combination of SNO and KamLAND experiments indicated : $tan^2\theta_{12} = 0.47^{+0.06}_{-0.05}$ and $\Delta m^2_{21} = 7.59^{+0.21}_{-0.21} \times 10^{-5} eV^2$.
Around 2002, neutrino oscillation was well established. Both atmospheric and long-baseline accelerator neutrino experiments determined the value atmospheric angle θ_{23} to be $\sim 45^\circ$ also the solar neutrino experiments and KamLAND found the value of solar angle θ_{12} to be $\sim 33^\circ$. It was assumed earlier that reactor mixing angle θ_{13} is zero but with advent of time, later in the year 2012 it was measured with accuracy at the reactor experiments, and found to have a large value of about 9° [30]. Daya Bay [31], Double Chooz [32], and RENO [33],

were the three reactor neutrino experiments proposed around 2006, to probe θ_{13} [34]. These experiments have successfully found non zero value of θ_{13}. Discovery of a large value of θ_{13} reactor mixing angle is a great achievement for physicists. Precise measurement of θ_{13} plays pivotal role not only in model-building in neutrino physics, but also encourages new reactor neutrino experimentalists to investigate some of the important issues such as determining neutrino mass hierarchy, CP violation in leptonic sector and searching for sterile neutrinos.

1.6 Neutrino nucleon scattering and cross section

Many properties of neutrino have already been measured experimentally, still some of them are yet to be measured. Some of unknown quantities are mass hierarchy, nature of neutrinos which can be either of Dirac or Majorana type, CP violation phase, exact mass of neutrinos, whether neutrino can help to explain matter-antimatter asymmetry of the universe, whether sterile neutrinos exist or not, etc. This provides a strong and active area of research for many researchers worldwide in both nuclear and particle physics. Precise knowledge of neutrino-nucleon interaction cross sections are required not only to measure the unknown quantities in several planned/ongoing experimental set ups, worldwide but also these cross sections help to minimise systematic errors in the analysis of neutrino oscillation experiments. Neutrino nucleon scattering cross sections are used in neutrino oscillation experiments, at different stages of calculations like signal cross section, ratio of quasi elastic - (ν_μ/ν_e) cross section and signal efficiency. Number of events (of signal process) are observed experimentally, which is proportional to the flux of the incoming neutrinos, cross section and probability of the signal process. The phenomenon of neutrino oscillation is equally important for both theorist and experimentalist since neutrino has non zero mass which is beyond the Standard Model. Neutrino-nucleon cross sections have an uncertainty of about 20-30 percent [35]. The main reasons behind it are poor knowledge of neutrino fluxes and the fact that any cross section measurements make use of nuclear targets.

1.6.1 Neutrino interaction across various energy scales

Neutrino interaction cross sections across various energy scales can be divided into five categories [36].

1) **Thresholdless processes ($E_\nu \sim 0-1$ MeV)**: The first interaction process is thresholdless processes which include coherent scattering (where neutrino interacts coherently with the target nucleus) and neutrino capture. Such processes occur when energy of neutrino ranges

from 0 to 1 MeV. Coherent process is similar to neutral current exchange process i.e.

$$\nu + A_N^Z \rightarrow \nu + A_N^{*Z}. \tag{1.49}$$

Another neutrino interaction is the stimulated or enhanced beta decay emission which falls under thresholdless process. The reaction is

$$\nu_e + A_N^Z \rightarrow e^- + A_{N-1}^{Z+1}. \tag{1.50}$$

2) **Low energy nuclear process** ($E_\nu \sim 0 - 100$ **MeV**): The second interaction process include low energy nuclear processes where energy of neutrino ranges from 1 to 100 MeV.
3) **Intermediate energy process** ($E_\nu \sim 0.1 - 20$ **GeV**): Third interaction process is the intermediate energy scale where neutrino energy ranges from 0.1 to 20 GeV. Mainly three processes - elastic and quasi-elastic scattering, resonance production and deep inelastic scattering fall under this category. Quasi-elastic (QE) also called charged current (CC) neutrino scattering process occur when neutrinos scatter elastically off an entire nucleon (within target nucleus) emitting a nucleon/multiple nucleons from target. The CCQE scattering processes for neutrino and its antineutrino are

$$\nu_\mu + n \rightarrow \mu^- + p \qquad \bar{\nu_\mu} + p \rightarrow \mu^+ + n. \tag{1.51}$$

Similarly we have neutral current NC or elastic process where neutrinos elastically scatter from nucleons of the target nucleus i.e.

$$\nu + p \rightarrow \nu + p, \qquad \bar{\nu} + p \rightarrow \bar{\nu} + p. \tag{1.52}$$

We have another inelastic scattering process where neutrinos with sufficient energy excite the struck nucleon within the target and produces a baryon resonance state (N^*) which decays to nucleon and other single pion final state. Typical resonant single pion reaction is

$$\nu_\mu + N \rightarrow \mu^- + N^* \rightarrow \pi + N^{'}, \tag{1.53}$$

where $N, N^{'} = n, p$. The baryonic resonance state can possibly give rise to multipion final state particles. With sufficient neutrino energy, inelastic process like deep inelastic scattering can produce abundant source of multipion final state particles.
Another coherent process i.e. coherent pion production falls within the intermediate energy range. Neutrino can coherently scatter from entire nucleus, transferring very less amount of

energy to the target nucleus. The reactions for both CC and NC coherent pion production are

$$\begin{aligned} \nu_\mu + A &\to \nu_\mu + A + \pi^0, \\ \bar{\nu_\mu} + A &\to \bar{\nu_\mu} + A + \pi^0 \\ \nu_\mu + A &\to \mu^- + A + \pi^+, \\ \bar{\nu_\mu} + A &\to \mu^+ + A + \pi^-. \end{aligned} \tag{1.54}$$

Lastly in this intermediate energy range, kaons/strange quarks are also produced in the final state . Both CC and NC processes are possible

$$\nu_\mu + n \to \mu^- + K^+ + \Lambda^0, \quad \nu_\mu + p \to \nu_\mu + K^+ + \Lambda^0. \tag{1.55}$$

4) **High energy process** ($E_\nu \sim 20 - 500$ **GeV**): In the high energy cross section energy range, neutrinos with high energy are able to probe the internal structure of target nucleus. Neutrinos are able to scatter off individual quark content of the target nucleus. Such process is referred to as Deep Inelastic Scattering (DIS). DIS process for CC and NC are

$$\begin{aligned} \nu_e + N \to e^- + X, \quad \bar{\nu_e} + N \to e^+ + X, \\ \nu_e + N \to \nu_e + X, \quad \bar{\nu_e} + N \to \bar{\nu_e} + X, \end{aligned} \tag{1.56}$$

where N = target nucleus and X = hadronic system in final state.
5) **Ultrahigh energy (UHE) process** ($E_\nu \sim 0.5TeV - 1EeV$): In the ultra high energy (UHE) regime ($1EeV = 10^{18}eV$), knowledge of neutrino nucleon cross section becomes particularly interesting because it provides opportunity for the experimentalist for observation of ultra high energy neutrinos from astrophysical and extragalactic sources.

1.6.2 Experimental status of neutrino cross section

Since we have already entered precision era of neutrino physics, studies of neutrino oscillations have been further extended in the long baseline accelerator and reactor experiments. With the precise determination of five known oscillation parameters i.e. two squared mass differences and three mixing angles, the present and future neutrino oscillation experiments aim to find the unknown parameters i.e. Dirac CP-violating phase and neutrino mass ordering. In addition to these unknown parameters, modern oscillation experiments are giving tremendous efforts to investigate the existence of additional massive neutrinos i.e. 'sterile neutrinos'. In what follows, we present a brief review on the status of neutrino cross section

measurements.

Neutrino experiments make use of reliable neutrino fluxes to remeasure absolute QE scattering cross sections. In the intermediate energy range, several neutrino-nucleon scattering cross section measurements were made. Using carbon as target, high statistics measurements of QE interaction cross section (as a function of neutrino energy), done by MiniBooNE and NOMAD experiments appeared to differ by about 30 percent. This problem is called 'MB-NOMAD' anomaly [37]. Low energy MB results are found to be higher than that from theoretical models such as Fermi gas model and impulse approximation calculations. Nuclear effects beyond impulse approximation are responsible for the discrepancies in the data. A better understanding of neutrino nucleus interactions is important to reduce systematic uncertainties in neutrino oscillation experiments. Over the past years, experiments in the intermediate energy range measured NC elastic cross section ratios w.r.t QE scattering in order to reduce systematics. For example MiniBooNE experiment measured such ratios using carbon in bins of Q^2. BNL E734 and MiniBooNE reported measurements of differential cross sections, using carbon as target for NC elastic scattering. P. Coloma et. al. [38] calculated total cross section (using oxygen as target) for various neutrino interaction channnels using event generators so as to determine neutrino oscillation parameters for an experimental set up similar to T2K. In another work by P. Rodrigue et. al. [39], they have calculated double differential cross section for various neutrino interaction channels (using carbon as target) so as to study nuclear effects in Minerva experiment. Nuclear effects in neutrino interactions is one of the leading source of systematic errors in present and future neutrino beam oscillation experiments.

Accelerator based neutrino experiments measure rate of neutrino interactions which comprises of three most important factors i.e. neutrino flux, neutrino cross section interaction and the detector efficiency [40]. Out of all the three factors, neutrino-nucleus cross section interaction in the hundreds-MeV to few-GeV energy regime poses one of the most important sources of systematic errors. For the past decade, for experiments like MiniBooNE and T2K, there was strong urge to understand neutrino interaction systematics around 1 GeV but at present time energy region of 2-10 GeV has become significant for oscillation experiments like NOvA, PINGU, ORCA, Hyper-K, DUNE and INO. For the future accelerator based neutrino experiments, two targets become most important, namely argon (for liquid argon time projection chambers (LArTPCs)) and water for water/ice -Cherenkov detectors.

1.7 Ultra High Energy Neutrino experiments

Knowledge of neutrino cross section in Ultra High Energy regime is important ingredient in the event rate calculation in high energy neutrino telescopes. Most striking experimental result of observation of ultra-high energy neutrino events was reported at IceCube. At IceCube, Ultra high energy neutrinos are detected by observing Cherenkov light produced in ice by charged particles created when neutrinos interact [41]. From May 2010 to May 2012, sufficient data were collected by the IceCube detector which provided the first evidence for a high-energy neutrino flux of extraterrestrial origin. The two neutrino events whose energies are in between 1 to 10 PeV were detected in IceCube on August 9, 2011 and January 3, 2012 which could be of atmospheric or astrophysical origin [42]. A number of experiments are geared towards observation of UHE neutrinos from astrophysical sources. The experiments are namely Baikal [43, 44], Antares [45], Antartic Muon And Neutrino Detector Array (AMANDA) [46], Radio Ice Cerenkov Experiment (RICE) [47], ANITA [48], HiRes [49] and Goldstone Lunar Ultra-High Energy experiment (GLUE) [50].

1.8 Sterile neutrino experiments

LSND experiment made use of coincidence of the prompt Cherenkov radiation from the positron and the delayed neutron capture by a hydrogen and was able to measure $\bar{\nu}_e$ events. $\bar{\nu}_\mu \to \bar{\nu}_e + p \to e^+ + n$. This experiment could observe an excess of $\bar{\nu}_e$ events. It was found that this statistically significant signal is consistent with the presence of sterile neutrinos ($\bar{\nu}_\mu \to \nu_{sterile} \to \bar{\nu}_e$) [51].

In a recent study [52], they have investigated the capability of planned Tokai to Hyper Kamiokande (T2HK) experiment to supply information regarding the unknown parameters like mass hierarchy, CP phases, and the octant of θ_{23}, in the presence of a light eV scale sterile neutrino. In another recent work [53] they have shown the impact of sterile neutrino oscillation parameters on the expected sensitivity of planned T2HK and T2HKK experiments to the neutrino unknown parameters. Recently K.Abe et al., [54] from T2K collaboration collected data from the T2K far detector which has been used to search oscillation signatures due to light sterile neutrinos in the (3+1) framework. They have used both CC $\bar{\nu}_\mu$ and $\bar{\nu}_e$ samples and NC samples at far detector at baseline of 295 km. In another work by Igor Krasnov, [55] it was found that they calculated the sensitivity of DUNE to the active-sterile neutrino mixing for sterile neutrinos having mass at GeV scale. In atmospheric neutrino oscillation experiments like SK and IceCube, one can probe muon neutrino disappearance channel. It was found that IceCube can probe highest energy range from 6 GeV to 20 TeV. In

Parameters	Hierarchy	Best Fit	NH	IH
$\Delta m^2_{21}[10^{-5}eV^2]$	NH or IH	7.37	$6.93-7.97$	$6.93-7.97$
$sin^2\theta_{12}/10^{-1}$	NH or IH	2.97	$2.50-3.54$	$2.50-3.54$
$sin^2\theta_{13}/10^{-2}$	NH and IH	2.14 (NH) and 2.18 (IH)	$1.85-2.46$	$1.86-2.48$
$sin^2\theta_{23}/10^{-1}$	NH and IH	4.37 (NH) and 5.69 (IH)	$3.79-6.16$	$3.83-6.37$
δ_{13}/π	NH and IH	1.35 (NH) and 1.32 (IH)	$0-2$	$0-2$
$\Delta m^2_{41}eV^2$	NH and IH	1.63	$0.87-2.04$	$0.87-2.04$
$\lvert V_{e4}\rvert^2$	NH and IH	0.027	$0.012-0.047$	$0.012-0.047$
$\lvert V_{\mu 4}\rvert^2$	NH and IH	0.013	$0.005-0.03$	$0.005-0.03$
$\lvert V_{\tau 4}\rvert^2$	NH and IH	–	< 0.16	< 0.16

Table 1.1 The latest global fit 3σ range data as well as sterile bounds are shown [61, 62].

this energy regime, matter effects becomes significant. For example a large matter-induced resonance would be expected at 3 TeV neutrino energy, for a 1 eV^2 sterile neutrino search at such detectors [56]. Future/planned reactor neutrino experiments aim to explore short baseline $\bar{\nu}_\mu$ disappearance channel, keeping the measurements of the energy spectrum at different distances so as to gather information on neutrino oscillations that are independent of the neutrino flux calculations. In near future the LSND $\bar{\nu}_\mu \rightarrow \bar{\nu}_e$ appearance channel will be monitored in the short baseline neutrino experiment at Fermilab [57]. In one of recent paper by Alan M. Knee et al., they used Planck data to obtain cosmological constraints on the sterile-neutrino oscillation parameters [58]. In [59], the authors have explained a way to search sterile neutrinos of keV scale, which are candidates of dark matter. TRISTAN project will extend the experimental set up of Karlsruhe Tritium Neutrino experiment (KATRIN) in order to search for such keV-scale sterile neutrino. In a recent work [60] by MINOS and MINOS+ collaboration, it was found that, these experiments achieved high sensitivity to the sterile neutrino eigenstate in the mass splitting parameter i.e. Δm^2_{41} over the magnitude of seven orders. In Table 1.1, the latest global fit 3σ range data [61, 62] are given.

1.9 Methodology

In **Chapter 2** of the thesis, we will calculate number of events and double differential cross section for neutrino-carbon scattering in MINERνA experiments (Fermilab). The methodology for this work would be - to simulate the number of events and double differential cross section using the event generator GiBUU. Using a low three momentum transfer (q_3) subsample of neutrino-carbon scattering data from MINERνA experiment, separation of two processes i.e. QE and Delta (1232) resonance processes are done using event generator

GENIE 2.8.0 in [39], where they used GENIE. We have used another simulation software i.e. GiBUU in order to investigate about the discrepancy in the region between QE and Δ processes.

In **Chapter 3**, we will calculate neutrino cross section for charged current and neutral current neutrino interaction in ultra high energy regime using QCD inspired double asymptotic limit fit of electron-proton structure function F_2^{ep}. The methodology here is - we will use the double asymptotic form of proton structure function, and use it to calculate the neutrino nucleon scattering cross section. We have not used any standard softwares available for the calculation of these cross sections, rather we will do our calculation using Monte Carlo (MC) integration technique. We will also do a comparative analysis of our results with those available in literature.

In **Chapter 4** of the thesis, we will consider 4×4 neutrino mass matrix and classify different possible textures of the matrix based on generic A_4 vacuum alignments for triplet flavons. The methodology here would be - from the 4×4 light neutrino mass matrix, we solve the constraint equations, to obtain the correlations among the light neutrino mass parameters, allowed by the 3σ global best fit ranges. And from that, one can see which flavon VEVs give reasonably good agreement with the present data. We will use Mathematica to solve these complex constraint equations.

1.9.1 GENIE and GiBUU event generators

GENIE stands for Generates Events for Neutrino Interaction Experiments which is a ROOT based neutrino Monte Carlo generator designed using object-oriented methodologies. Validity of GENIE generator extends over a wide spectrum of energies ranging from $\sim$ 1 MeV to $\sim$ 1 PeV and also to all nuclear targets and neutrino flavors [63]. GENIE makes use of nuclear physics models, cross section models, neutrino induced Hadron Production models for simulation of cross section, event rates, final state particle interaction etc for various neutrino experimental set-ups functioning worldwide. When a neutrino is scattered off from a nuclear target, GENIE can simulate complex physics processes within it. Complex physical processes includes primary scattering process, the neutrino-induced hadronic multiparticle production and the intra-nuclear hadron transport and re-scattering. Inside GENIE, there are inbuild flux drivers that enables users to use the desired flux for their experimental set up. GENIE installation requires 3rd party installation which includes external packages like ROOT, GSL, LHAPDF, PYTHIA6, log4cpp, libxml2. This is followed by main installtion of GENIE package. In this thesis, we have used GENIE 2.8.0 version to calculate cross sections and event rate in Chapter 2.

GiBUU stands for Giessen Boltzmann–Uehling–Uhlenbeck. It is a simulation code for electron, photon, neutrino, hadron and heavy-ion induced reactions on nuclei [64]. It is a transport model based on a coupled set of semi-classical kinetic equations, which describe the dynamics of a hadronic system explicitly in phase space and in time. GiBUU is based on Kadanoff-Baym (KB) equations which describe the time development of the Wigner-transform of the nuclear one-body density matrix [65, 66]. The neutrino event generator GiBUU can calculate cross sections, event rate for all neutrino flavour. Within GiBUU, various flux files, potentials, nuclear models are written in fortran 90. The software is user friendly, one has to run jobcards to generate events, cross sections, reconstructed neutrino energy etc by choosing appropriate modules within the jobcard. Running a jobcard is simple, one can just write the command i.e. "./GiBUU.x < "jobcard name" in the terminal, provided proper directory path is given. Once output files are generated, one can immediately obtain desired cross section, event rate etc by writing their own analysis program using ROOT/ FORTRAN 90.

2

Neutrino-carbon interactions at low three-momentum transfer

In this chapter, we intend to study neutrino-carbon interaction for some neutrino channels like quasi-elastic scattering, 2p2h/MEC process in the intermediate energy regime, with reference to data taken by the MINERνA experiment at Fermilab, USA.

2.1 Introduction

Neutrino Main Injector (NUMI) beamline located at Fermilab produces intense neutrino beam which has provided a platform for many experimental set ups like MINERνA, MINOS, NOνA etc for studying various neutrino/anti-neutrino interactions with nuclei, and neutrino oscillations. Accurate measurements of differential, double differential cross sections for various scattering processes like QE scattering, single and multi-pion production, as a function of (reconstructed) neutrino energy are done by such experiments, among other measurements. These along with other accelerator based experiments like T2K, DUNE (planned) etc, and reactor based experiments aim to study the unknown neutrino properties from the observation of neutrino oscillations, at different baselines and neutrino energies. Comparison of neutrino event rates at the far and near detectors, at a given neutrino energy

is done so as to extract neutrino oscillation parameters, mixing angles and CP-invariance violating phase, with reduced systematic uncertainties.

We know that neutrino beams are not mono-energetic, and they contain several flavours. Correct identification of neutrino flavour as well as detailed knowledge of final state particles after a neutrino interaction takes place, becomes essential to minimize systematic uncertainties in neutrino oscillation experiments [67]. Modern neutrino oscillation experiments make use of heavy nuclear targets. This is because event rate scales roughly linearly with mass of target, so use of dense target material will increase statistics. Unfortunately, due to use of heavy target nucleus, complex nuclear effects also must be taken care of in the interactions. When neutrino interacts with a heavy target nucleus, generally interaction takes place among the individual nucleons which are bound inside the target nucleus. At low energy interactions, distribution of energies and momenta inside the nucleus is not known properly which leads to uncertainties. Another complicated situation arises when interaction with target nucleons take place in nuclear medium - in the initial interaction, produced hadrons travel through dense nuclear medium and undergo further strong interactions giving rise to final state interactions (FSI). When FSI effects take place in such medium then some particles are absorbed by nucleus, and many new types of particles may also be created with different kinematics [68]. Because of FSI, it is not possible to precisely separate different interaction channels in an experiment, but one can possibly measure the post FSI particle contents [69]. Similar to FSI, another effect may be Pauli blocking (in a nucleus, Pauli exclusion principle prevents multi occupation of states by the nucleons, i.e. it ensures that the nucleons in a nuclear state cannot occupy states that are already filled up). Details of how Pauli blocking applies to nucleons in a target nucleus is not well understood, and can depend on the nuclear model used. Apart from FSI effects, Pauli blocking, other nuclear effects may be impulse approximation (scattering cross section is calculated as the incoherent sum of scattering from the target nucleons), random phase approximation (RPA) (in RPA correlations, the nucleons in a nucleus interact via two body NN potential) which collectively can cause difficulties in the precision measurements at the present/planned oscillation experiments.

Monte Carlo event generators play a vital role in every ongoing / planned experiment because they provide a model for all possible interactions for a given measurement with which analyses can be performed. In general, an event generator provides for any neutrino flavour, energy and target nucleus, the total cross section for each interaction mode, energy and direction of all secondary produced particles. It also simulates particle re-interactions inside target nucleus whenever necessary. Among the most important event generators are GENIE [63],

NUANCE [70], NEUT [71], GiBUU [65] etc. In GiBUU, the FSI effects are modeled by solving the semi-classical Boltzmann-Uehling-Uhlenbeck equation.

In [39], the authors have attempted to isolate two different nuclear-medium effects using a low 3-momentum transfer subsample of neutrino-carbon scattering data from the Minerνa experiment, using the event generator GENIE. They combined observed hadronic energy in CC ν_μ interactions, with muon kinematics, to separate QE and $\Delta(1232)$ resonance processes. They observed a small cross section at very low energy transfer that matches the expected screening effect of long-range nucleon correlations. Also, they observed that additions to the event rate in the kinematic region between the QE and the Δ resonance processes are needed to describe the data. The data in this kinematic region are also found to have an enhanced population of multi proton final states. Though contributions predicted for scattering from a nucleon pair is believed to have both the properties - the model tested in that work did not fully describe the data. Improved description of the effects of the nuclear environment are required - as observed by the authors.

Most of the earlier available event generators, for example, relied on free-particle Monte Carlo cascade simulations that are applicable at very high energies but are of only limited applicability in the description of relatively low energy FSI of hadrons inside the target nuclei. A basic feature of nuclei, their binding, is neglected from the outset in these Monte Carlo calculations. Furthermore, the generators often still rely on outdated nuclear and hadron physics and consist of a patchwork of descriptions of different reaction channels without internal consistency. There is, therefore, now a growing realization in the neutrino long-baseline community that the description of nuclear effects has to be improved.

Hence, in this work, we include the improved nuclear environment effects for the lepton-nucleus interaction, using implementation of quantum-kinetic transport theory, with improvements in its treatment of the nuclear ground state and 2p2h interactions. This is done by using another versatile event generator i.e. GiBUU so as to obtain results that could show a better agreement with the present MINERνA data.

2.2 MINERνA experiment

MINERνA (Main Injector Experiment for v-A) experiment is a neutrino scattering experiment which uses NuMI beamline at Fermilab. The experimental set up consists mainly of three parts - namely an active scintillator tracking detector, an electromagnetic calorime-

ter and a hadron calorimeter, including various nuclear targets like carbon, water, helium, iron and lead. In addition to this, MINOS near detector is used as a muon spectrometer by MINERνA experiment [72]. Both MINOS and MINERνA are low energy (LE) mode and medium energy (ME) mode on-axis experiments. The energy range of neutrinos in MINERνA flux is from $2 < E_\nu < 6$ GeV which peaks at approximately 3.5 GeV as shown in Fig. 2.3. The experiment does not provide neutrino flux below 1.5 GeV [40]. The MINERνA data were taken from the year 2010 to 2012, exposed to NuMI beam with 3.33×10^{20} protons on target. The experiment has baseline of approximately about 1300 km.

2.3 Quasi-elastic and MEC/2p2h processes

In Quasi-elastic (QE) scattering, neutrinos can elastically scatter off an entire nucleon emitting multiple nucleons from target nucleus. The formalism related to CCQE process was first laid in the Llewellyn Smith model [73]. For a CCQE process, the neutrino energy can be reconstructed from the kinematic variables of the charged lepton l in the final state interaction as:

$$E_\nu^{QE} = \frac{2(M_n - E_b)E_l - (E_b^2 - 2M_nE_b + \Delta M^2)}{2(M_n - E_b - E_l + p_l cos\theta_l)}, \tag{2.1}$$

where M_n is free neutron rest mass, E_b is the binding energy and $\Delta M^2 = M_n^2 - M_p^2 + m_l^2$. The above equation is valid for a CCQE process, where neutron is at rest.

Meson exchange current (MEC) also known as 2 particle-2 hole (2p-2h) effect, is an interaction where a weak boson from the leptonic current is exchanged by a pair of nucleons (two body current), and it is expected to lead to two nucleon emission [74]. MEC/2p2h effects are responsible for event excesses observed by various neutrino oscillation experiments. Both GENIE and GiBUU event generators use Llewellyn Smith model to calculate CCQE interaction. Schematic diagram of both CCQE and MEC/2p2h processes are shown in Fig. 2.1 and Fig. 2.2 respectively. In Fig. 2.2, diagram (a) represent one particle-one hole interaction, diagram (b) is a 2p2h/MEC interaction between two nucleons, diagram (c) shows pion production. These three diagrams collectively represent many body contributions to the polarisation propagator. The solid (dashed) lines correspond to free nucleon (pion) propagators and the dotted lines shows interaction between nucleon-nucleon. There is a blob with solid lines which represent full (dressed) nucleon propagators. In case of nucleons, the lines pointing to the right (left) denote particle (hole) states.

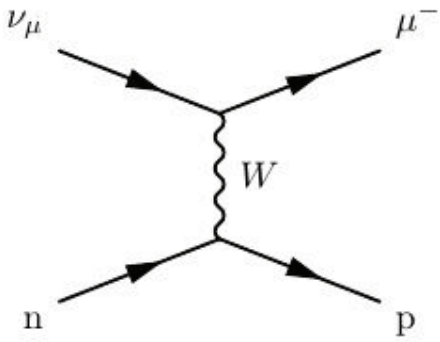

Fig. 2.1 Schematic diagram of charged current quasi-elastic scattering process (taken from [36]).

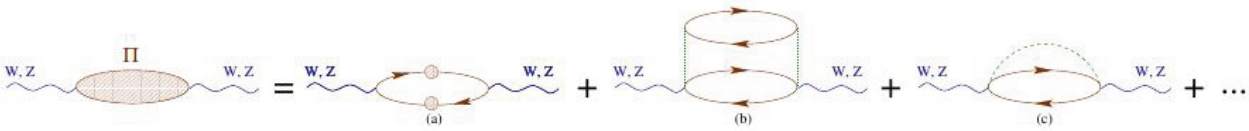

Fig. 2.2 Schematic diagram of 2p2h/MEC process (taken from [72]).

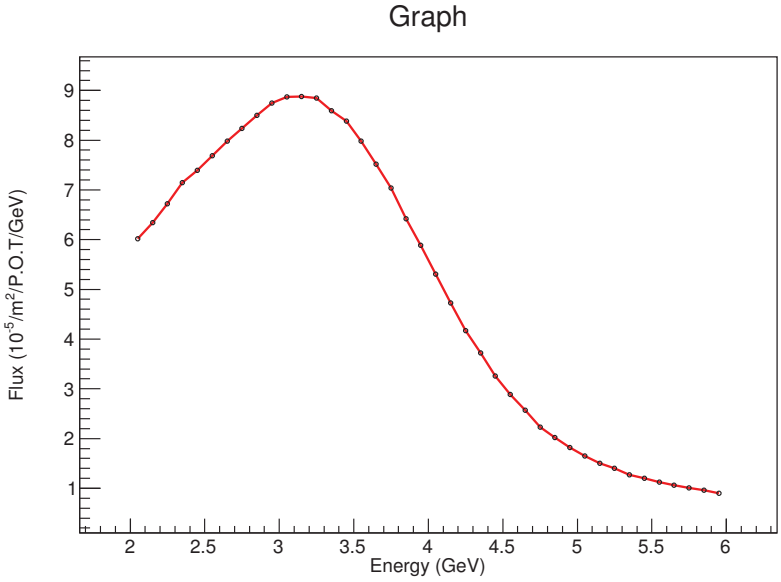

Fig. 2.3 Flux of MINERνA experiment [75].

2.4 Neutrino-carbon interaction using transport kinetic theory for nuclear effects

As discussed earlier in Chapter 1 and in this Chapter, due to discrepancy observed between the data of MINERνA for neutrino-carbon scattering in quasi-elastic regime, and theoretical results obtained by the authors of [39], in this work, we analyse this data using transport model based on a set of coupled set of semi-classical kinetic equations. This is done with the help of the event generator GiBUU 2016. In GiBUU, all nucleons are bound in a coordinate - and momentum-dependent potential, which is obtained from an analysis of nuclear matter binding properties and *pA* reactions. The momentum distribution is such that a high-momentum nucleon sees a less attractive potential than the one with a low momentum. The momentum distribution is modelled by the local Fermi gas distribution with $p_F \sim \rho^{1/3}$. The significant shift of strength towards lower momentum values, as compared with the distribution of the global rFG (relativistic Fermi gas) is reproduced in [64]. The preparation of the ground state uses a realistic nuclear density profile, then calculates potential from an energy density functional, and finally inserts the nucleons into this potential with moments distributed according the local Fermi-gas model. In GiBUU 2016, they have fixed the value of E_F from the outset. This is achieved by calculating the potential for a conventional, realistic Woods-Saxon density distribution [76]. Then, by keeping the functional form of the potential and the value of the Fermi-energy fixed, a nonlinear equation for the density is solved by iteration.

We would now describe the kinematics of the interaction. Let E_ν be the energy of the incoming neutrino, E_μ be that of the muon produced in CC, Q^2 be the square of four-momentum transferred to the nucleus, three momentum transfer is q_3, E_{avail} is the the hadronic energy available to produce activity in the detector. Then, they can be defined as follows:

$$E_\nu = E_\mu + q_0, \tag{2.2}$$

$$Q^2 = 2E_\nu(E_\mu - p_\mu cos\theta_\mu) - M_\mu^2 \quad (M_\mu \text{is the muon mass}), \tag{2.3}$$

$$q_3 = \sqrt{Q^2 + q_0^2}, \tag{2.4}$$

$$E_{avail} = \text{proton K.E + charged pion K.E + neutral pion K.E + electron + photon total energy.} \tag{2.5}$$

In next section, we present our results and discussion on them.

2.5 Results and Discussion

We have calculated double differential cross section for carbon target for MINERνA experiment for some interaction channels like default, 2p2h/MEC processes as shown in Figs 2.4 and 2.6. For the sake of completeness, we also reproduced the results for the same processes of [39] using GENIE 2.8.0 version (shown in Figs 2.5 and 2.7). We then compare our results with the available MINERνA neutrino carbon scattering data.

In calculating double differential cross section, we have calculated approximately one lakh events for both the interaction channels i.e. default and 2p2h/MEC processes, then created a two dimensional histogram of q_3 (along y axis) versus available energy (along x axis), then no of events in each bin of x and y axes were divided by average MINERνA flux and 3.17×10^{30} nucleon targets, to obtain the value of double differential cross section. From the definition mentioned in Section 2.4, the available energy (E_{avail}) was calculated from 0 to 0.5 GeV energy range corresponding to each value of calculated double differential cross section. We have followed this procedure for both the generators GENIE and GiBUU. The double differential cross section $\frac{d^2\sigma}{dE_{avail}dq_3}$ in six region of q_3 i.e. $0 < q_3/GeV < 0.2$, $0.2 < q_3/GeV < 0.3$, $0.3 < q_3/GeV < 0.4$, $0.4 < q_3/GeV < 0.5$, $0.5 < q_3/GeV < 0.6$ and $0.6 < q_3/GeV < 0.8$ was calculated using both the generators.

In case of GiBUU, for each interaction channel i.e. default and 2p2h/MEC processes, we used separate jobcards and gave runs selecting appropriate modules in the jobcard. We have incorporated the available MINERνA flux which ranges from $2 < E_\nu < 6$ GeV within the GiBUU package. Using our own analysis programs, we have extracted the kinematic variables from the generated files and plotted our results. Though there are various versions of GENIE available but we performed our analysis using GENIE version 2.8.0 since it is considered to be the most stable version. Since both the generators are unique in terms of nuclear models, potentials and for various other reasons, the operating technique in both the generators are quite different. In GENIE, there is no such jobcard, we have created our own cross section splines for neutrino carbon interaction. Then using appropriate commands we generated the events and followed the procedure as mentioned above in this Section.

It is seen from Fig 2.4, for the 2p2h/MEC process, we observe that the overall behaviour of the curves in the six q_3 regions are nearly same i.e. double differential cross section starts from zero value of available energy, slowly rises to some height and then falls down and attains zero at some value of available energy. In the region $0.6 < q_3/GeV < 0.8$, we observe that our results almost coincide with the MINERνA data.

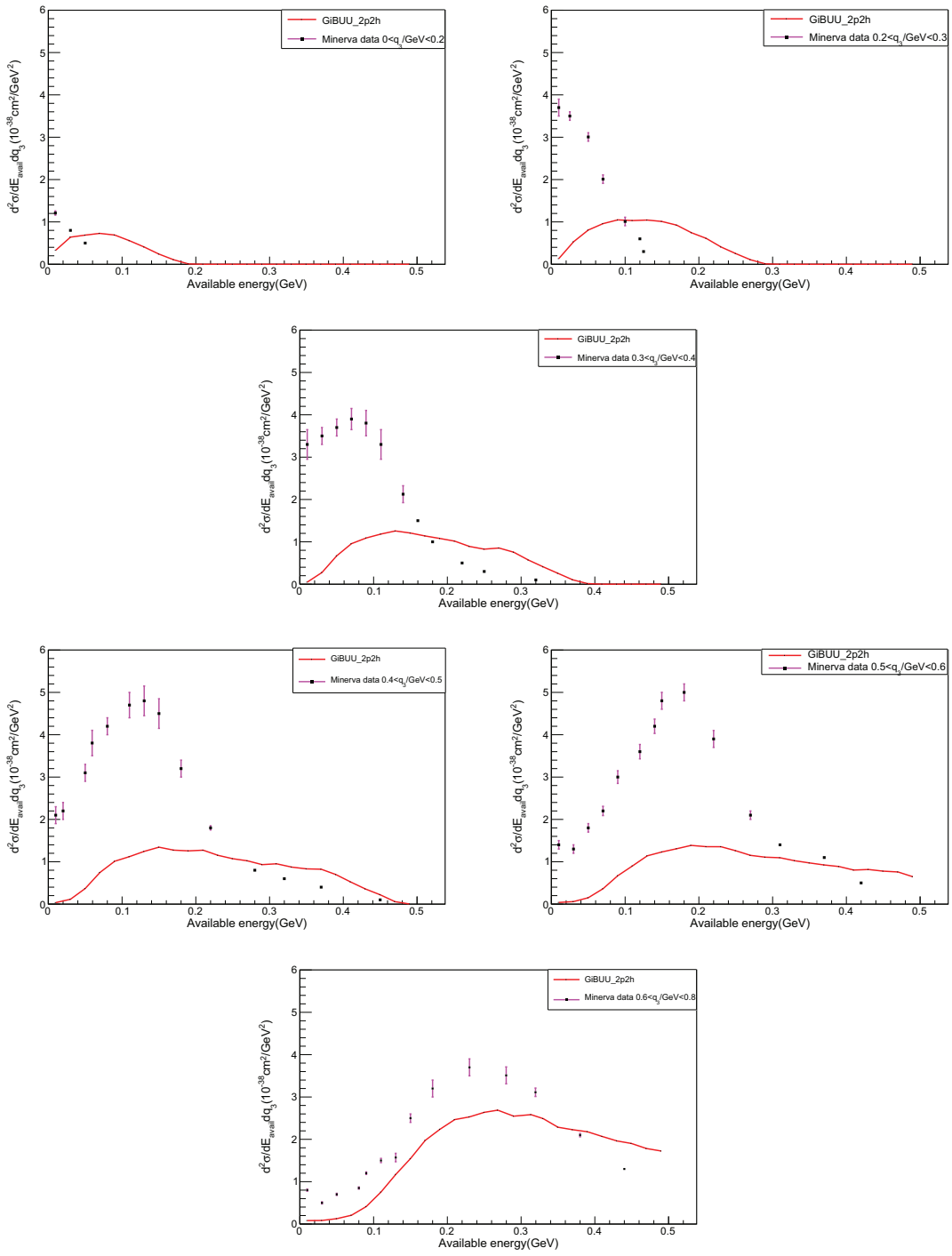

Fig. 2.4 The double differential cross section $\frac{d^2\sigma}{dE_{avail}dq_3}$ in six regions of q_3 using GiBUU 2016 are plotted for 2p2h process (red line) and the MINERνA experimental data are shown with their respective error bars.

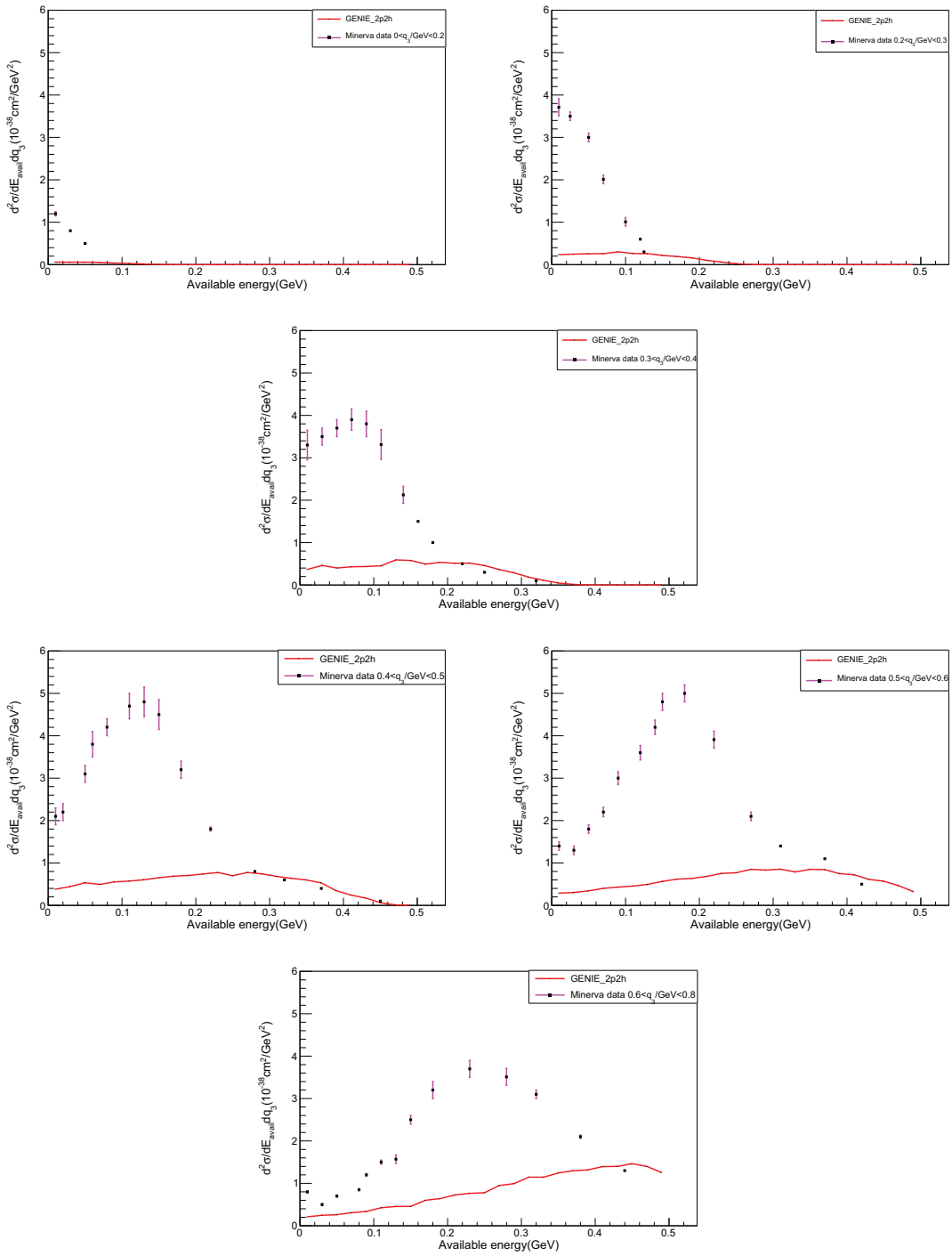

Fig. 2.5 The double differential cross section $\frac{d^2\sigma}{dE_{avail}dq_3}$ in six regions of q_3 using GENIE 2.8.0 are plotted for 2p2h process (red line) and the MINERνA experimental data are shown with their respective error bars.

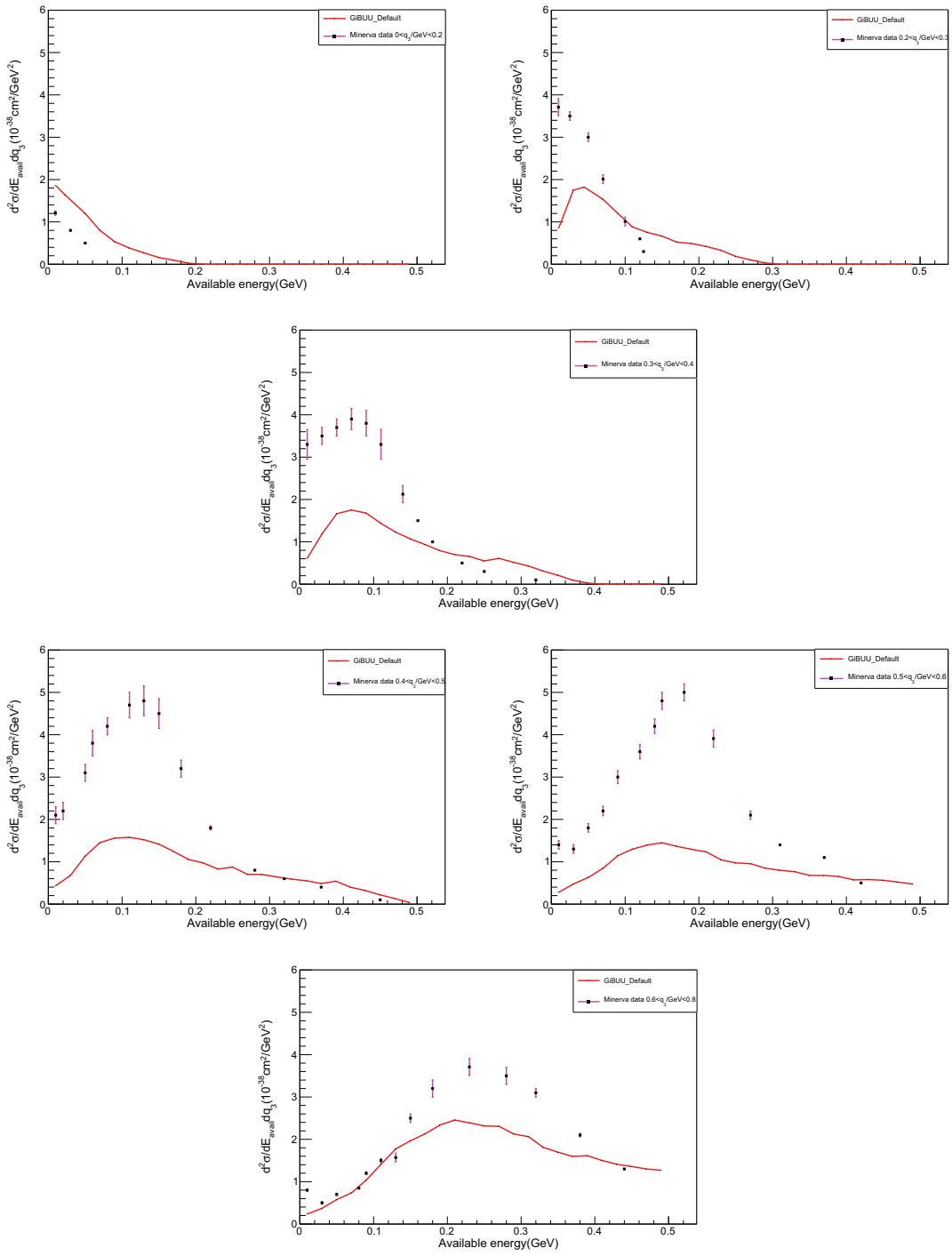

Fig. 2.6 The double differential cross section $\frac{d^2\sigma}{dE_{avail}dq_3}$ in six regions of q_3 using GiBUU 2016 are plotted for default process (red line) and the MINERνA experimental data are shown with their respective error bars.

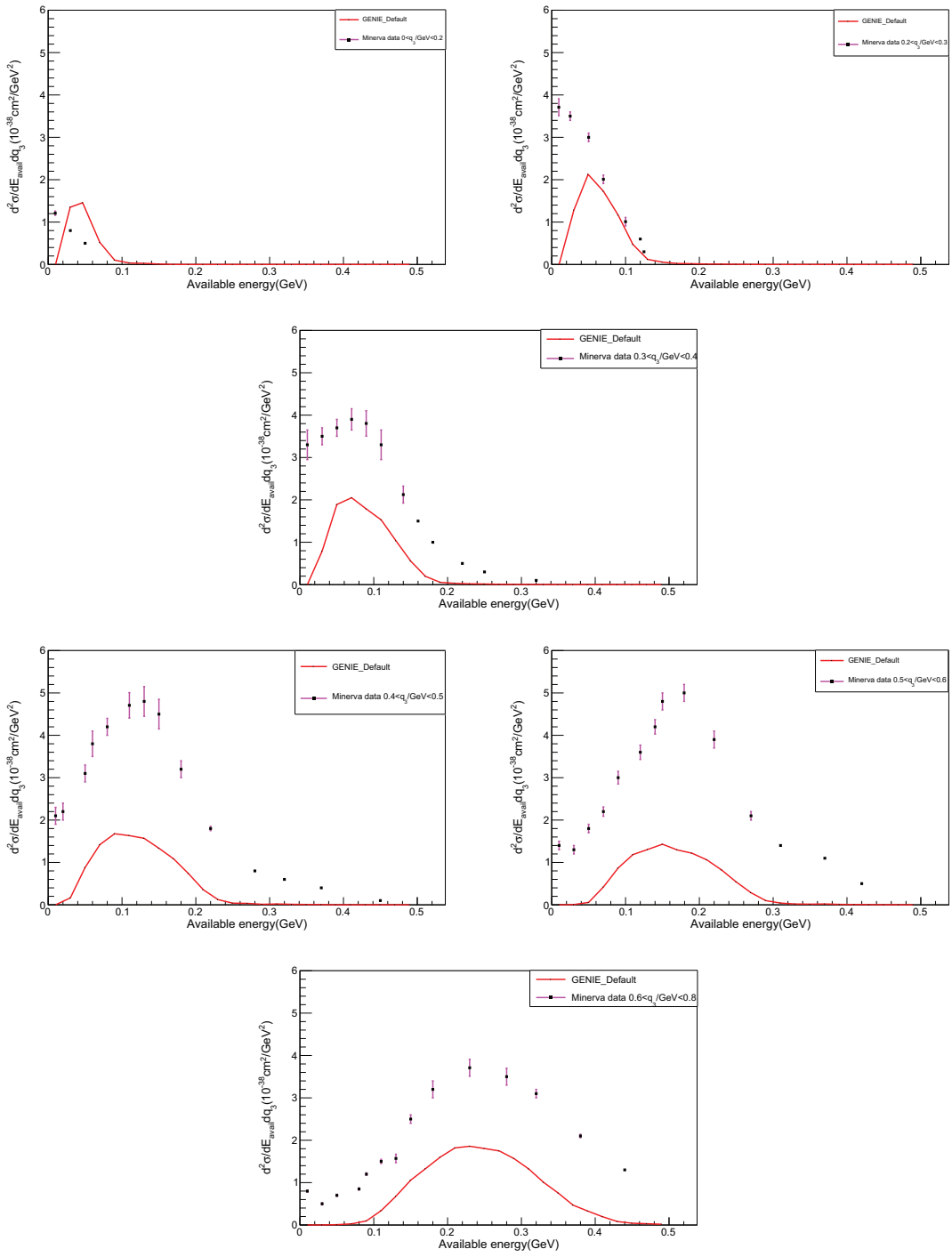

Fig. 2.7 The double differential cross section $\frac{d^2\sigma}{dE_{avail}dq_3}$ in six regions of q_3 using GENIE 2.8.0 are plotted for default process (red line) and the MINERνA experimental data are shown with their respective error bars.

From Fig 2.5, we observe that the double differential cross section for 2p2h/MEC process, indeed rises from zero value of available energy, attains some height and then slowly fall down and becomes zero for some value of available energy. This trend is observed for the five q_3 regions i.e. $0 < q_3/GeV < 0.2$, $0.2 < q_3/GeV < 0.3$, $0.3 < q_3/GeV < 0.4$, $0.4 < q_3/GeV < 0.5$, $0.5 < q_3/GeV < 0.6$. But it is observed that in the last region of q_3 i.e. $0.6 < q_3/GeV < 0.8$, the cross section curve increases with the increasing values of E_{avail} energy. It is expected that at some value of $E_{avail} > 0.5$ GeV, the curve may merge along with x axis. The double differential cross section results obtained using GENIE, are not in good agreement with the MINERνA data. Thus, using GiBUU, we can say that our results have improved as compared to those produced with the other generator GENIE.
From Fig 2.6, we observe that double differential cross section for the default process using GiBUU, is not zero at zero value of available energy, infact the curves slowly rises and attain some height and then slowly fall down to zero at nearly $E_{avail} = 0.5GeV$. This trend is observed for the four q_3 regions i.e. $0 < q_3/GeV < 0.2$, $0.2 < q_3/GeV < 0.3$, $0.3 < q_3/GeV < 0.4$, $0.4 < q_3/GeV < 0.5$. But for the last two regions of q_3 i.e. $0.5 < q_3/GeV < 0.6$ and $0.6 < q_3/GeV < 0.8$ we observe that our cross section curve increases with the increasing values of E_{avail} energy. Similarly from Fig 2.7, we observe that double differential cross section for the default process using GENIE is zero at zero value of available energy, then the curves slowly rises and then slowly fall down to zero at some values of available energy. This trend is observed for the entire six q_3 regions i.e. $0 < q_3/GeV < 0.2$, $0.2 < q_3/GeV < 0.3$, $0.3 < q_3/GeV < 0.4$, $0.4 < q_3/GeV < 0.5$, $0.5 < q_3/GeV < 0.6$ and $0.6 < q_3/GeV < 0.8$. What we can comment from this plot is that the GENIE results are not in good agreement with the available MINERνA data.

We would like to point out here, that from the theory of electroweak (EW) gauge interactions, this variation of cross section with energy can be explained very well [36].

2.6 Summary

To summarize, we find that our results obtained including 2p2h process for double differential cross section of neutrino carbon scattering, produced using GiBUU, are in better agreement with the MINERνA data, than those reported in [39]. The 2p2h results using GENIE are low as compared to our results using GiBUU. This differences may be attributed to use of better nuclear environment effects, through the use of GiBUU. Fine tuning of our GiBUU results for the two interaction processes i.e. default and 2p2h/ MEC is required. We are also

working on a different and interesting interaction process i.e. (2p2h + RPA). We expect that by incorporating RPA effects with 2p2h/MEC process, our GiBUU results will improve and will indeed agree well with the available MINERνA data.

3

Neutrino cross section in UHE regime using double asymptotic limit of QCD.

In Chapter 2, we discussed neutrino carbon scattering at low three momentum transfer in quasi-elastic regime. In this chapter, we focus on neutrino nucleon scattering in ultra high energy (UHE) regime.

3.1 Introduction

As discussed in Chapter 1, neutrino nucleon scattering cross sections play a pivotal role in all neutrino oscillation experiments. Such experiments make use of neutrinos coming from natural resources as well as from artificial (man-made) resources [36]. In any neutrino experiment, neutrinos are scattered off a nucleon/nucleus of the detector. Neutrinos coming to the earth from natural sources have their origin in the sun, active galactic nuclei (AGN) and core of supernovae-they are believed to play crucial role in various astrophysical phenomenon. The information obtained from astrophysical objects and mechanisms is complimentary to that available from electromagnetic or hadronic interactions. It was already mentioned in Chapter 1 that neutrino interactions across various energy scales can be categorised into five classes [36] - thresholdless process, low energy nuclear process,

intermediate energy process, high energy (DIS) process and Ultra high energy (UHE) process.

Neutrino DIS processes have been used to validate the standard model (SM) and to also probe nucleon structure. Cross sections, electroweak (EW) parameters, coupling constants and scaling variables etc. have also been measured by experimentalists through such processes. In the νN DIS, the neutrino scatters off a quark in the nucleon via the exchange of a virtual W (CC) or Z (NC) boson, producing a lepton and hadronic system in the final state. Similarly, UHE neutrino cross sections have gained importance as many experiments worldwide are ongoing/planned to observe processes involving them. The natural sources of UHE could be - supernovae core collapse, cosmic rays, gamma ray burst, AGN etc and they serve as windows of understanding highest energy processes in the universe. Since attenuation of these neutrinos due to their travel is very low (as they are only weakly interacting), they act as a powerful tool to help us know about their sources. Various experiments measuring UHE neutrinos, ongoing and planned, worldwide are - Baikal [77], ANITA [78], RICE [79], AMANDA [80], HiRes [81], ANTARES [82] , IceCube [83], GLUE [84], Pierre Auger Cosmic Ray Observatory [85], ARIANNA [86], JEM-EUSO [87]. A number of studies on UHE neutrino cross sections (CC and NC) are available in literature. R. Gandhi, et al., [88] (GQRS1998) reported results based on u,d,c,s quark PDFs (Parton Distribution Function) from 1998 CTEQ4 analysis of the early HERA-ZEUS small x data. In the results presented by A. Connolly, et al., [89] (CTW 2011) and A. Cooper-Sarkar, et al., [90] (CSMS 2011) they included b-quark contribution to both CC and NC scattering and are based on updated PDFs obtained from newer data. Froissart bound inspired behaviour of F_2^{ep} of DIS $(e-p)$ scattering was used by Martin M. Block, et al., [91] (BDHM 2013) to evaluate UHE neutrino cross section off an isoscalar nucleon $N = \frac{n+p}{2}$, upto $E_\nu \sim 10^{17}$ GeV. It may be noted that $E_\nu \sim 10^{17}$ GeV is the highest reach of the experimental search for UHE cosmic neutrino [83, 84].

In this work, we calculate CC and NC neutrino-nucleon scattering cross section in $E_\nu \sim (10^9 - 10^{12}$ GeV) using QCD inspired Double Asymptotic limit (DAL) of the proton structure function $F_2^{ep}(x, Q^2)$. The preliminary results of this analysis were presented in [92]. In [94], it has been shown that the e-p structure function exhibits a dynamic pomeron type behaviour:

$$F_2^{ep} \sim x^{-\lambda(Q^2)}, \tag{3.1}$$

which can be obtained from DGLAP (Dokshitzer-Gribov-Lipatov-Altarelli-Parisi) evolution equation. It was found to describe the HERA H1 data, available at that time, for F_2^{ep} in the range $1 \leq x \leq 10^{-4}$ and $5 \leq Q^2 \leq 5000\ GeV^2$ within 10 % error. In high energy physics, the

pomeron is a Regge trajectory, a family of particles with increasing spin, postulated to explain the slowly rising cross section of hadronic collisions at high energies [95]. At high energies (and low Q^2) $\gamma^* p$ cross section is believed to have similarities to that of hadron-hadron interactions. Pomeron type behaviour of F_2 at small x can explain the logarithmic rise of cross section with energy. In Fig 3.2 we present the result from the computation for CC, NC and total cross section for $10^9 \leq E_\nu \leq 10^{12}$ GeV. We then compare our results (shown in Fig 3.3 and Fig 3.4) in the energy range $10^9 \leq E_\nu \leq 10^{12}$ GeV with those already available in literature (as no data is available at present). While overall behaviour is found to be similar, the values of our cross sections are found to be lower than those of BDHM2013, CTW2011 and CSMS2011 for $E_\nu \geq (10^9 - 10^{11})$ GeV for CC . On the other hand, our values are lower than those of GQRS1998, for energy of $E_\nu = 10^9$ GeV. For NC, for $E_\nu \geq (10^9 - 10^{12})$ GeV , our values are almost same as GQRS1998 whereas for $E_\nu \geq (10^9 - 10^{10})$ GeV our values are slightly lower than BDHM2013, CTW2011 and CSMS2011. In our view, this could be attributed to the form of structure function Eq (3.1), used to calculate νN cross section. It may be noted that the rising behaviour of F_2^{ep} can be controlled due to screening corrections and we intend to do it in our future work. Then we present analytical form of total cross section, fitted to the forms, Eq (3.19) and Eq (3.20) both for CC and NC.

It has been stated in [36] that for a more accurate prediction of the νN cross-section, a well formulated model of the nucleon structure function is needed and that this predictive power is specially important in the search of New Physics (NP). At such Ultra High Energies, the νN cross section can depart substantially from the standard model predictions, if NP is at play. Study of such UHE neutrino interaction thus could be a possible probe of new physics. Determination/measurement of νN cross section could also be useful to constrain the underlying QCD dynamics of the nucleon. Detection of UHE neutrino events may shed light on the observation of air shower events with energies $\geq 10^{10}$ GeV, as well. Moreover, the behaviour of UHE νN cross section can also be used to discriminate among different models of gluon dynamics at play at very low x. The energy dependence of total νN cross section measurement may have important implications for hadronic interactions at such UHE, not accessible otherwise. If cross section much outside the limits of ongoing/planned neutrino experiments are observed, then predictions presented in this work could be very important. This commands attention also, since many experiments worldwide are planned/ongoing in DIS/UHE regime.

We would like to emphasize here that, we have not used any software available in public domain, in our work we have done the computation of νN cross section, using our own

computer program and this is a novely in this work. Another novel feature is dynamic pomeron type behaviour of F_2^{ep} used in our work, which also gives pomeron type behaviour for νN cross section at UHE.
The Chapter has been organised as follows. In Section 3.2, we present a brief review on neutrino scattering at UHE regime, in Section 3.3, a review on DAL behaviour of F_2^{ep}, following [94] is given. In Section 3.4, total $\sigma_{\nu N}^{CC}$ and $\sigma_{\nu N}^{NC}$, cross sections using above form of F_2^{ep} are presented. Section 3.5 contain numerical calculations, results and analysis. Lastly we summarize and draw conclusions in Section 3.6.

3.2 Neutrino scattering at UHE regime

In DIS, the neutrino scatters off a quark in the nucleon via the exchange of a virtual W or Z boson producing a lepton and a hadronic system in the final state [4]. Both charged current (CC) and neutral current (NC) processes are possible like $\nu_l + N \to l^- + X$ and $\bar{\nu}_l + N \to l^+ + X$. where $N = p, n$ and X denotes any set of final hadrons.
We now describe the kinematic variables for the process $\nu_l(p_\nu) + N(p_N) \to l^-(p_l) + X(p_X)$
• the four momentum transfer, q = $(p_\nu - p_l)$ = $(p_X - p_N)$
• Lorentz invariant squared center of mass energy, $s = (p_\nu + p_N)^2$
The other quantities are $-Q^2 = q^2 = (p_\nu - p_l)^2$
• Bjorken variable, $x = Q^2/(2.p_N.q)$. It is the fraction of longitudinal momentum of the nucleon carried by parton.
• Inelasticity, $y = p_N.q/p_N.p_\nu$. where p_ν, p_l, p_N and p_X are the four momenta of neutrino, the charged lepton, the nucleon and the sum of the four-momenta of the final hadrons respectively.
The Feynman diagram for the process $\nu_l(p_\nu) + N(p_N) \to l^-(p_l) + X(p_X)$ is shown in Figure 3.1(a) and in the quark-parton model with elementary $W^+(q) + d(p_i) \to u(p_f)$ transition is shown in Figure 3.2(b).

3.3 A brief review of $F_2^{ep}(x, Q^2)$ using DAL of QCD

In this section, we describe briefly about electron-proton structure function $F_2^{ep}(x, Q^2)$ utilising DAL of QCD, following [94], for the sake of completeness of this work. It is well known that in DIS $(e-p)$ scattering, the incoming electron scatters off the target proton, via the exchange of a virtual photon, producing a hadronic system in the final state. A typical $(e-p)$ DIS event can be described with the help of two independent variables, x and Q^2, where x is the Bjorken variable (fraction of proton's momentum carried by its constituent

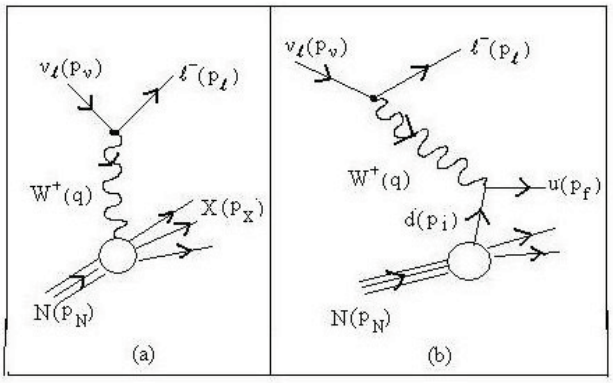

Fig. 3.1 (a) Diagram of the $\nu_l(p_\nu)+N(p_N)\rightarrow l^-\ (p_l)+X(p_X)$ charged-current DIS process. (b) Diagram of the same process in the quark-parton model.

partons, in Breit's frame) and Q^2 is the transverse momentum squared of the virtual exchanged photon. The scattering cross section can be described in terms of two structure functions, $F_2(x,Q^2)$ and $F_1(x,Q^2)$. Bjorken variable $x=\frac{Q^2}{2M\nu}$, here ν is the electron's energy loss and Q^2 depends on the scattering angle. The squared mass W^2 of the observed hadronic system is

$$W^2=(p+q)^2=M^2-Q^2+2M\nu, \tag{3.2}$$

(in proton's rest frame) where p and q are proton and electron's momentum respectively, M is proton's mass. For elastic scattering, $W^2=M^2(x=1)$. In parton model, at large Q^2, for spin $\frac{1}{2}$ partons, $F_2(x)=2xF_1$ and $F_L=F_2-2xF_1=0$. For point like parton, Bjorken scaling occurs, structure function do not depend on Q^2. But scaling violations are found to occur in $(e-p)$ DIS processes, as x decreases, which means that structure function F_2^{ep} depends on Q^2 also. Thus the proton no longer consists of point like partons only, but has a dynamic structure deep inside, which can be explained via QCD evolution equations in leading log Q^2 approximation (LLQ^2), known as DGLAP equations [93]. In $(e-p)$ DIS, in the next to leading order, scaling violations occur through gluon bremsstrahlung from quarks and quark pair creation from gluons. At small $x<10^{-2}$, the latter process dominates the scaling violations. This property can be exploited to extract gluon density from the slope $\frac{dF_2}{dlnQ^2}$ of the proton structure function. The general equations [87] describing the Q^2 evolution of the quark density and gluon density respectively are

$$\frac{dq^i(x,t)}{dt}=\frac{\alpha(t)}{2\pi}\int_x^1\frac{dy}{y}[\sum_{j=1}^{2f}q^j(y,t)P_{qq}(\frac{x}{y})+G(y,t)P_{qG}(\frac{x}{y})], \tag{3.3}$$

$$\frac{dG(x,t)}{dt} = \frac{\alpha(t)}{2\pi}\int_x^1 \frac{dy}{y}[\sum_{j=1}^{2f} q^j(y,t)P_{Gq}(\frac{x}{y}) + G(y,t)P_{GG}(\frac{x}{y})], \tag{3.4}$$

where $P_{qq}(\frac{x}{y}), P_{qG}(\frac{x}{y}), P_{Gq}(\frac{x}{y}), P_{GG}(\frac{x}{y})$ are the splitting functions and $t = ln\frac{Q^2}{Q_0^2}$. Assuming that the quark densities are negligible and the non-singlet contribution F_2^{NS} can be ignored safely at small x in DGLAP equation, for F_2, the equation becomes

$$\frac{dF_2(x,Q^2)}{dlnQ^2} = \frac{10\alpha_s}{9\pi}\int_x^1 dx^{'} P_{qG}(x^{'})\frac{x}{x^{'}}g(\frac{x}{x^{'}},Q^2). \tag{3.5}$$

Here $xg(x,Q^2) = G(x,Q^2)$ is the gluon momentum density and $g(x,Q^2)$ is the gluon number density of the proton and $\frac{x}{x^{'}} = \frac{x}{y}$. Rearranging Eq (3.5) we have

$$\frac{dF_2(x,Q^2)}{dlnQ^2} = \frac{5\alpha_s}{9\pi}\int_x^1 dy\frac{x}{y}g(y,Q^2)\frac{1}{y^2}[x^2+(y-x)^2]. \tag{3.6}$$

Substituting $y = \frac{x}{1-z}$ we can write RHS of Eq (3.6) as

$$\frac{5\alpha_s}{9\pi}\int_0^{1-x} dzG(\frac{x}{1-z},Q^2)[z^2+(1-z)^2]. \tag{3.7}$$

Expanding $G(\frac{x}{1-z},Q^2)$ about $z = \frac{1-x}{2}$ and keeping terms upto the first derivative of G in the expansion we have

$$G(\frac{x}{1-z},Q^2) = G(\frac{2x}{1+x},Q^2) + (z-\frac{1-x}{2})\frac{4x}{(1+x)^2}\frac{dG(x^{''},Q^2)}{dx^{''}}\bigg|_{x^{''}=\frac{2x}{1+x}}. \tag{3.8}$$

When this expansion is used in Eq (3.6) we get

$$\frac{dF_2(x,Q^2)}{dlnQ^2} = \frac{5\alpha}{9\pi}\frac{(A+Ax+2B)^2}{(1+x)(A+Ax+4B)}G(y^{'},Q^2), \tag{3.9}$$

where $y^{'} = [\frac{2x}{1+x}\frac{(A+Ax+4B)}{(A+Ax+2B)}]$, $A = [\frac{2(1-x)^3}{3} - (1-x)^2 + (1-x)]$ and $B = [\frac{(1-x)^4-(1-x)^3}{6}]$. In the limit $x \to 0$, Eq (3.9) reduces to

$$\frac{dF_2(x,Q^2)}{dlnQ^2} = \frac{10\alpha_s}{9\pi}\frac{(1-x)^2}{(1-1.5x)}G(2x\frac{(1-1.5x)}{(1-x^2)},Q^2). \tag{3.10}$$

Using the above double asymptotic expression [94] for F_2 in small x and large Q^2 (DAL) limit, we can write

$$F_2^p \sim \frac{exp\sqrt{\frac{144}{33-2n_f}\xi ln(\frac{1}{x_1})}}{(\frac{144}{33-2n_f}\xi ln(\frac{1}{x_1}))^{\frac{1}{4}}}, \tag{3.11}$$

with $\xi = ln(\frac{ln\frac{Q^2}{\Lambda^2}}{ln\frac{Q_0^2}{\Lambda^2}})$, $x_1 = \frac{2x-3x^2}{1-x^2}$, n_f is the number of flavors, Q_0^2 is the value at which the input parton parameterization is to be used and Λ is the QCD mass scale. F_2^p in Eq (3.11) in DAL can be parametrized as

$$F_2^p \sim x^{-\lambda(Q^2)}, \tag{3.12}$$

which can be viewed as of dynamic pomeron type.

3.4 Total charged and neutral current neutrino nucleon cross section at UHE

The total charged and neutral current (CC and NC) cross section for neutrino nucleon scattering [91], for an isoscalar nucleon N = $\frac{n+p}{2}$, can be written as

$$\sigma_{CC}^{\nu N}(E_\nu) = \int_{Q^2_{min}}^{s} dQ^2 \int_{\frac{Q^2}{s}}^{1} dx \frac{d^2\sigma_{CC}}{dxdQ^2}(E_\nu, Q^2, x)$$

$$= \frac{G_F^2}{4\pi}\int_{Q^2_{min}=1}^{2mE_\nu} dQ^2 (\frac{M_W^2}{Q^2+M_W^2})^2 \int_{\frac{Q^2}{2mE_\nu}}^{1} \frac{dx}{x}\left[F_2^\nu + xF_3^\nu + (F_2^\nu - xF_3^\nu)\left(1-\frac{Q^2}{xs}\right)^2 - \left(\frac{Q^2}{xs}\right)^2 F_L^\nu\right], \tag{3.13}$$

where F_2^ν is the neutrino-nucleon structure function, $s = 2mE_\nu$, s is the Mandelstam variable which is the total energy in the centre of mass frame, m is the nucleon mass, G_F is the Fermi constant and M_W^2 is the squared mass of intermediate W-boson, Q^2 is the four momentum square of virtual photon. Here xF_3 is a measure of difference of quarks and antiquarks PDFs, and so is sensitive to the valence quark distribution function. We neglect valence quark contribution in our analysis, as at small x, structure of proton is dominated by gluons only [94]. Therefore, contributions of F_3^ν to νN scattering is sub dominant only and hence neglected in our analysis. Similar expression can be obtained for neutral current cross section by replacing M_W by M_Z in Eq (3.13). For the flavour-symmetric $(q\bar{q})$N interaction at small $x < 0.1$, the neutrino-nucleon structure function, $F_2^\nu(x, Q^2)$ can be related to electromagnetic

structure function, $F_2^{ep}(x,Q^2)$ (see [96]) as

$$F_2^{\nu}(x,Q^2) = \frac{n_f}{\sum_q^{n_f} Q_q^2} F_2^p(x,Q^2), \tag{3.14}$$

where n_f is the number of flavors and Q_q is the quark charge. Thus for $10^9 < E_\nu < 10^{12}$ GeV, x lies in the range $10^{-5} < x < 10^{-8}$. Here $\sigma_{CC,NC}^{\nu N}$, is the neutrino nucleon cross section - to leading order in weak coupling G_F and all orders in strong hadronic interaction.
Minimum value of Q^2 is consistant with application of pQCD, we have used $Q^2_{min} = 1\ GeV^2$ in our computation. Now using DAL value of F_2^{ep} from Eq (3.12) in Eq (3.13), we obtain the expression for total neutrino-nucleon cross sections as

$$\sigma_{CC}^{\nu N}(E_\nu) \approx \frac{G_F^2}{4\pi} \int_{Q^2_{min}=1}^{2mE_\nu \times 10^{-2}} dQ^2 (\frac{M_W^2}{Q^2+M_W^2})^2 \int_{\frac{Q^2}{2mE_\nu}}^1 \frac{dx}{x} (x^{-\lambda(Q^2)}), \tag{3.15}$$

where $\lambda(Q^2) = a - b.e^{-cQ^2}$ and the values of constants are found to be as $a = 0.486, b = 0.272$ and $c = 0.002$. Solving Eq (3.15), we get

$$\sigma_{CC}^{\nu N}(E_\nu) = A\frac{G_F^2}{4\pi} \int_{Q^2_{min}=1}^{2mE_\nu \times 10^{-2}} \frac{dQ^2}{-\lambda(Q^2)} (\frac{M_W^2}{Q^2+M_W^2})^2 x^{-\lambda(Q^2)} \Big|_{\frac{Q^2}{2mE_\nu}}^1$$

$$= -A\frac{G_F^2}{4\pi} \int_{Q^2_{min}=1}^{2mE_\nu \times 10^{-2}} \frac{dQ^2}{\lambda(Q^2)} (\frac{M_W^2}{Q^2+M_W^2})^2 \{1 - (\frac{Q^2}{2mE_\nu})^{-\lambda(Q^2)}\} \tag{3.16}$$

$$= A\frac{G_F^2 M_W^4}{4\pi} \int_{Q^2_{min}=1}^{2mE_\nu \times 10^{-2}} \frac{dQ^2}{\lambda(Q^2)} (\frac{1}{Q^2+M_W^2})^2 \{(\frac{Q^2}{2mE_\nu})^{-\lambda(Q^2)} - 1\}, \tag{3.17}$$

in low x and high Q^2 regime. Here A is normalisation constant.
The corresponding total neutral current cross section $\sigma_{NC}^{\nu N}(E_\nu)$ is obtained by replacing M_W by squared mass of intermediate Z boson M_Z that is

$$\sigma_{NC}^{\nu N}(E_\nu) = A\frac{G_F^2 M_Z^4}{4\pi} \int_{Q^2_{min}=1}^{2mE_\nu \times 10^{-2}} \frac{dQ^2}{\lambda(Q^2)} (\frac{1}{Q^2+M_Z^2})^2 \{(\frac{Q^2}{2mE_\nu})^{-\lambda(Q^2)} - 1\}. \tag{3.18}$$

3.5 Results and Discussion

We have computed $\sigma_{CC}^{\nu N}$ and $\sigma_{NC}^{\nu N}$ by carrying out the integration in Eq (3.17) and Eq (3.18) using our own computation (Monte Carlo integration technique) and have presented the results in Fig 3.2. We find that the behaviour of $\sigma_{CC}^{\nu N}$ and $\sigma_{NC}^{\nu N}$ is similar to that available in literature. The values of our total cross section both for charged and neutral current are

organised in tabular form (Tables 3.1 and 3.2) along with other cross section values that are available in literature. We then make a fit to the CC and NC $\nu - N$ cross sections to obtain the analytic forms of the following types in the energy range $10^9 GeV \leq E_\nu \leq 10^{12} GeV$:

$$\sigma_{CC}^{\nu N} = (2.00921 \pm 0.0113361) \times (lnE_\nu)^2 + (-4.45714 \pm 0.035448) \times (lnE_\nu) + (-32.2999 \pm 0.062563), \tag{3.19}$$

$$\sigma_{NC}^{\nu N} = (2.0157 \pm 0.010493) \times (lnE_\nu)^2 + (-4.46797 \pm 0.032813) \times (lnE_\nu) + (-32.3876 \pm 0.057913). \tag{3.20}$$

This can be viewed as a Reggeon exchange-type behaviour of the cross section at UHE. Here we would like to emphasize that, a dynamic pomeron type form of F_2^{ep} Eq (3.1), of the strong interactions, gives a Reggeon exchange-type behaviour of Eq (3.19) and Eq (3.20) total cross section of weak interactions.

3.6 Summary

In this work, we have calculated total neutrino-nucleon cross section $\sigma_{\nu N}^{CC}$ for CC and $\sigma_{\nu N}^{NC}$ for NC interactions using the Double Asymptotic Limit of F_2^{ep} of DIS $(e-p)$ scattering, found earlier by one of us [94]. In [88–91], they used standard sets of parton distribution functions available in literature at that times, to obtain total cross sections at UHE, but we have used our own parameterization for F_2^{ep} (within 10 % error) in DAL, using input PDFs at Q^2_{min}. We found that though the overall behaviour of our calculated νN cross sections is similar to the above mentioned works, our values are slightly smaller, in the low energy range, while larger in the high energy range. This difference could be attributed to different assumptions in input parameterization of PDFs used in F_2^{ep}, and due to the fact that we have used our own analytic form of F_2^{ep} in low x and large Q^2 regime obtained from DGLAP equation. We note that with the use of screening corrections in the evolution of proton structure function, these results can be improved, and will be done in future work. We used Monte Carlo integration technique in our computation to obtain these cross-sections in the energy range $10^9 \leq E_\nu \leq 10^{12}$ GeV. Then we did a parameter fitting of these cross-sections, to obtain their analytical form (Eq (3.19) and Eq (3.20)). The dynamical pomeron-type behaviour of F_2^{ep} give rise to a Reggeon exchange-type behaviour of total cross-section [95] in UHE regime. This could hint to some interplay between strong (F_2^{ep}) and weak ($\sigma^{\nu N}$) dynamics. The future measurements of $\sigma^{\nu N}$ in this regime would provide a test to the ideas presented in the work.

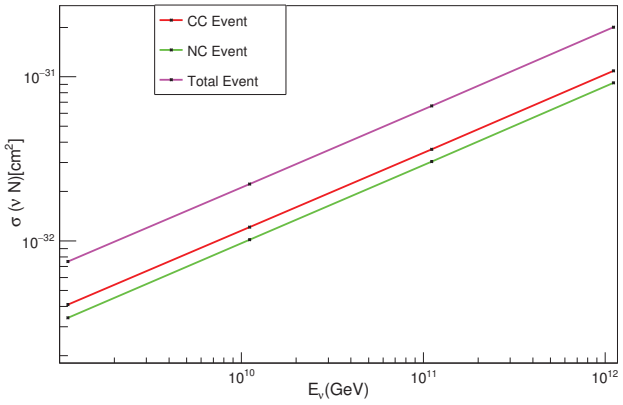

Fig. 3.2 Variation of neutrino-nucleon charged current, neutral current and total current cross sections with neutrino energy (from our calculation).

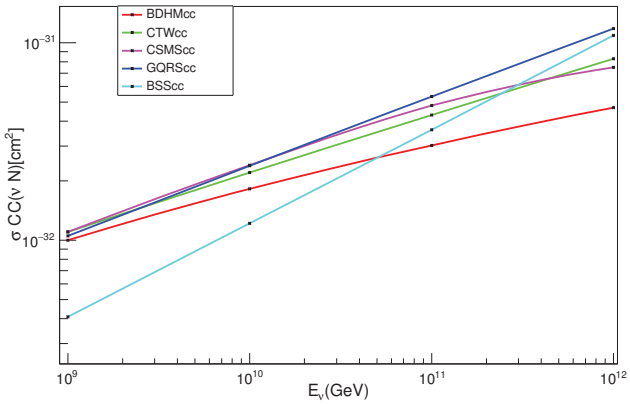

Fig. 3.3 Comparison of charged current νN cross sections, in cm^2 as a function of E_ν.

E_ν (GeV)	$\sigma_{BDHM}(cm^2)$	$\sigma_{CTW}(cm^2)$	$\sigma_{CSMS}(cm^2)$	$\sigma_{GQRS}(cm^2)$	$\sigma_{BSS}(cm^2)$
10^9	1.00×10^{-32}	1.1×10^{-32}	1.1×10^{-32}	1.05×10^{-32}	4.09×10^{-33}
10^{10}	1.82×10^{-32}	2.2×10^{-32}	2.4×10^{-32}	2.38×10^{-32}	1.21×10^{-32}
10^{11}	3.02×10^{-32}	4.3×10^{-32}	4.8×10^{-32}	5.34×10^{-32}	3.62×10^{-32}
10^{12}	4.69×10^{-32}	8.3×10^{-32}	7.5×10^{-32}	1.18×10^{-31}	1.08×10^{-31}

Table 3.1 Charged current νN cross sections, in cm^2 as a function of E_ν are listed. Here BDHM refers to the work done by Martin M.Block, et al. [91], CTW refers to A. Connolly, et al. [89], CSMS refers to A. Cooper-Sarkar, et al. [90], GQRS refers to R. Gandhi, et al. [88] and BSS refers our work in this chapter.

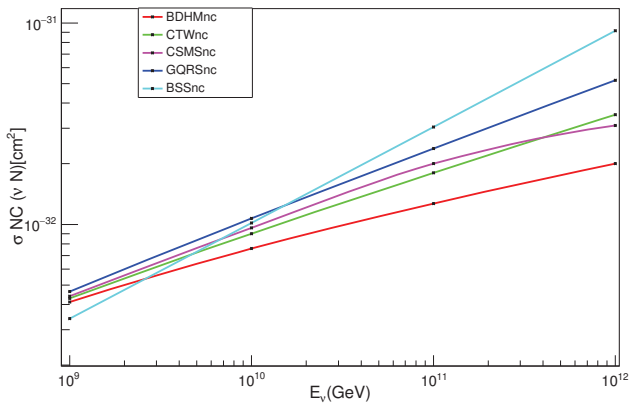

Fig. 3.4 Comparison of neutral current νN cross sections, in cm^2 as a function of E_ν.

E_ν (GeV)	$\sigma_{BDHM}(cm^2)$	$\sigma_{CTW}(cm^2)$	$\sigma_{CSMS}(cm^2)$	$\sigma_{GQRS}(cm^2)$	$\sigma_{BSS}(cm^2)$
10^9	4.12×10^{-33}	4.3×10^{-33}	4.4×10^{-33}	4.64×10^{-33}	3.40×10^{-33}
10^{10}	7.58×10^{-33}	9.0×10^{-33}	9.6×10^{-33}	1.07×10^{-32}	1.016×10^{-32}
10^{11}	1.27×10^{-32}	1.8×10^{-32}	2.0×10^{-32}	2.38×10^{-32}	3.042×10^{-32}
10^{12}	2.00×10^{-32}	3.5×10^{-32}	3.1×10^{-32}	5.20×10^{-32}	9.16×10^{-32}

Table 3.2 Neutral current νN cross sections, in cm^2 as a function of E_ν are listed. Here BDHM refers to the work done by Martin M.Block, et al. [91], CTW refers to A. Connolly, et al. [89], CSMS refers to A. Cooper-Sarkar, et al. [90], GQRS refers to R. Gandhi, et al. [88] and BSS refers our work in this chapter.

4

Compatibility of A_4 Flavour Symmetric Minimal Extended Seesaw with $(3+1)$ Neutrino Data

In Chapters 2 and 3, we have discussed neutrino carbon scattering at low three momentum transfer in quasi-elastic regime and neutrino nucleon scattering cross section in ultra high energy regime respectively. In this chapter, we have studied some application of neutrino scattering cross section, focussing on sterile neutrino sector.

4.1 Introduction

Non-zero neutrino masses and large leptonic mixing have now become a well established fact, thanks to a series of results from several experiments [97–102] over the last twenty years. While the solar and atmospheric mixing angles plus mass squared difference measurements have become more precise with time, the evidence for a non-zero reactor mixing angle emerged with the relatively recent experiments like MINOS [103], T2K [104], NOνA [105], Double ChooZ [106], Daya-Bay [107] and RENO [108]. Apart from the currently unknown issues in the neutrino sector, like mass hierarchy, Dirac CP violating phase as the global

fit data suggest [109], another interesting question in the neutrino sector is the possibility of additional neutrino species with eV scale mass. In fact, this has turned out to be not just a speculation, but has gathered considerable attention in the last two decades following some anomalies reported by a few experiments. The first such anomaly was reported by the Liquid Scintillator Neutrino Detector (LSND) experiment in their anti-neutrino flux measurements [110, 111]. The LSND experiment searched for $\bar{\nu}_\mu \to \bar{\nu}_e$ oscillations in the appearance mode and reported an excess of $\bar{\nu}_e$ interactions that could be explained by incorporating at least one additional light neutrino with mass in the eV range. This result was supported by the subsequent measurements at the MiniBooNE experiment [112]. Similar anomalies have also been observed at reactor neutrino experiments [113] as well as gallium solar neutrino experiments [114, 115]. These anomalies received renewed attention recently after the MiniBooNE collaboration reported their new analysis incorporating twice the size data sample than before [116], confirming the anomaly at 4.8σ significance level which becomes $> 6\sigma$ effect if combined with LSND. Although an eV scale neutrino can explain this anomaly, such a neutrino can not have gauge interactions in the standard model (SM) from the requirement of being in agreement with precision measurement of Z boson decay width at LEP experiment [117]. Hence such a neutrinos is often referred to as a sterile neutrino while the usual light neutrinos are known as active neutrinos. Status of this framework with three active and one sterile or $3+1$ framework with respect to such short baseline neutrino anomalies can be found in several global fit studies [118–121]. It is worth mentioning that the latest cosmology results from the Planck collaboration [122] constrains the effective number of relativistic degrees of freedom $N_{\rm eff} = 2.99 \pm 0.17$ at 68% confidence level (CL), which is consistent with the SM prediction $N_{\rm eff} = 3.046$ for three light neutrinos. Similarly, the constraint on the sum of absolute neutrino masses $\sum_i |m_i| < 0.12$ eV [122] (at 95% CL) does not leave any room for an additional light neutrino with mass in eV order. Although this latest bound from the Planck experiment can not accommodate one additional light sterile neutrino at eV scale within the standard ΛCDM model of cosmology, one can evade these tight bounds by considering the presence of some new physics beyond the standard model (BSM). For example, additional gauge interactions in order to suppress the production of sterile neutrinos through flavour oscillations were studied recently by the authors of [123].

Such experimental indications of an eV scale sterile neutrino having non-trivial mixing with active neutrinos have led to several BSM proposals that can account for the same. While the usual seesaw mechanisms like type I [124–128], type II [129–135] and type III [136] explaining the lightness of active neutrinos were studied in details for a long time, their extensions to the $3+1$ case was not very straightforward primarily due to the gauge singlet

nature of the sterile neutrino. Yet, there have been several proposals to generate a 4×4 light neutrino mass matrix within different seesaw frameworks in recent times [137–149, 62, 150]. Here we adopt a minimal framework known as the minimal extended seesaw proposed in the $3+1$ neutrino context by [138, 139] and study different possible realisations within the framework of non-abelian discrete flavour symmetry A_4. Flavour symmetry is needed to explain the observed flavour structure of different particles of the standard model. In the original proposal [139] also, the A_4 flavour symmetry was utilised but within the limited discussion the issue of non-zero reactor mixing angle as well as different A_4 vacuum alignments were not addressed. In another recent work based on the same model with A_4 flavour symmetry [151], some details of the associated neutrino phenomenology was discussed by sticking to the effective 3×3 active neutrino mass matrix which can be generated by integrating out the sterile neutrino. In our present work, we consider the full 4×4 mass matrix and do not integrate out the sterile neutrino as its mass may not lie far above the active ones always, as hinted by experiments mentioned above. We also classify different possible textures of the 4×4 neutrino mass matrix based on generic A_4 vacuum alignments for triplet flavons. Similar but not texture specific work in three neutrino cases to constrain different A_4 vacuum alignments from three neutrino data was done by the authors of [152] which was further constrained from successful leptogenesis in [153]. Here we extend such studies to the $3+1$ neutrino cases. Texture zeros in $3+1$ neutrino scenarios were discussed in different contexts earlier using flavour symmetries like $Z_N, U(1)$ etc. [147, 149, 62] but here we show that some of these textures can be realised (upto a few more constraints) just from the vacuum alignment of A_4 triplet flavons. We first make the classifications for allowed and disallowed textures based on already known texture results in $3+1$ neutrino frameworks [154–157, 147, 149] and then numerically analyse some of the textures which have not been studied before. To be more specific, we categorise our textures based on $\mu-\tau$ symmetric cases, texture zero cases, hybrid cases and disallowed ones. Out of them, we numerically analyse all the textures belonging to $\mu-\tau$ symmetric and texture zero cases leaving the discussion on hybrid textures to future works. It should be noted that, although the discovery of non-zero reactor mixing angle has ruled out $\mu-\tau$ symmetry in the three neutrino scenarios, it is possible to retain it in a $3+1$ scenario where the 3×3 neutrino block retains this symmetry while the active-sterile sector breaks it. This interesting but much less explored idea to generate non-zero θ_{13} by allowing the mixing of three active neutrinos with a eV scale sterile neutrino was proposed earlier in [158–161] and was also studied in details recently in [150]. We find that many of the textures belonging to these categories are already ruled out by neutrino data while the ones which are allowed give interesting cor-

relations between neutrino parameters which can be tested at ongoing and future experiments.

This chapter is organised as follows. In Section 4.2 we discuss the details of the model followed by the classification of different textures in Section 4.3. In Section 4.4 we discuss the numerical analysis adopted in our work followed by results and discussions in Section 4.5. We finally summarise in Section 4.6.

4.2 The Model

As mentioned before, here we adopt the model first proposed in [139] but discuss it from a more general perspective taking all the allowed terms in the Lagrangian and all possible generic vacuum alignments of A_4 triplets. Here we note that the discrete non-abelian group A_4 is the group of even permutations of four objects or the symmetry group of a tetrahedron. It has twelve elements and four irreducible representations with dimensions n_i such that $\sum_i n_i^2 = 12$. These four representations are denoted by $\mathbf{1}, \mathbf{1}', \mathbf{1}''$ and $\mathbf{3}$ respectively. The product rules for these representations are given in Appendix A.
The particle content of the model along with their transformations under the symmetries of the model are shown in table 4.1. Apart from the SM gauge symmetry and A_4 flavour symmetry, an additional discrete symmetry Z_4 is also chosen in order to forbid certain unwanted terms. For example, the chosen Z_4 charge of the singlet neutrino S keeps a bare mass term away from the Lagrangian. This is important because a bare mass term will be typically large, at least of electroweak scale and hence will not help us generate a 4×4 light neutrino mass matrix with all terms at or below the eV scale. To have a seesaw mechanism at place, three right handed neutrinos $\nu_{Ri}, i = 1,2,3$ are included into the model. Apart from the usual Higgs field H responsible for electroweak symmetry breaking, there are six flavon fields ϕ, $\phi^{'}$, $\phi^{''}$, ξ, $\xi^{'}$, χ responsible for spontaneous breaking of the flavour symmetries and generating the desired leptonic mass matrices. The leading order Lagrangian for the leptons can be written as

	l	e_R	μ_R	τ_R	H	ϕ	$\phi^{'}$	$\phi^{''}$	ξ	$\xi^{'}$	χ	ν_{R1}	ν_{R2}	ν_{R3}	S
$SU(2)_L$	2	1	1	1	2	1	1	1	1	1	1	1	1	1	1
A_4	3	1	$1^{''}$	$1^{'}$	1	3	3	3	1	$1^{'}$	1	1	$1^{'}$	1	1
Z_4	1	1	1	1	1	1	i	-1	1	-1	$-i$	1	$-i$	-1	i

Table 4.1 Fields and their transformations under the chosen symmetries.

$$\begin{aligned}\mathscr{L}_Y \supset & \frac{y_e}{\Lambda}(\bar{l}H\phi)_{\underline{1}}e_R + \frac{y_\mu}{\Lambda}(\bar{l}H\phi)_{\underline{1'}}\mu_R + \frac{y_\tau}{\Lambda}(\bar{l}H\phi)_{\underline{1''}}\tau_R + \frac{y_1}{\Lambda}(\bar{l}H\phi)_{\underline{1}}\nu_{R1} + \frac{y_2}{\Lambda}(\bar{l}H\phi')_{\underline{1''}}\nu_{R2} \\ & + \frac{y_3}{\Lambda}(\bar{l}H\phi'')_{\underline{1}}\nu_{R3} + \frac{1}{2}\lambda_1\xi\overline{\nu_{R1}^c}\nu_{R1} + \frac{1}{2}\lambda_2\xi'\overline{\nu_{R2}}^c\nu_{R2} + \frac{1}{2}\lambda_3\xi\overline{\nu_{R3}}^c\nu_{R3} \\ & + \frac{1}{2}\rho\chi\overline{S^c}\nu_{R1} + y_4\xi\overline{S^c}\nu_{R2} + y_5\chi^\dagger\overline{S^c}\nu_{R3} + \text{h.c.}\end{aligned} \tag{4.1}$$

where Λ is the cut-off scale of the theory, $y_e, y_\mu, y_\tau, y_1, y_2, y_3, y_4, y_5, \lambda_1, \lambda_2, \lambda_3, \rho$ are the dimensionless Yukawa couplings. It is worth noting that the last two terms were not included in the original model [139] although they are allowed by the chosen symmetry of the model. We include them here as they contribute non-trivially to the neutrino mass matrix as well as the generation of correct neutrino mixing.

We denote a generic vacuum alignment of the flavon fields as follows

$$\begin{gathered}\langle\phi\rangle = v(n_1,n_2,n_3), \quad \langle\phi'\rangle = v(n_4,n_5,n_6), \\ \langle\phi''\rangle = v(n_7,n_8,n_9), \quad \langle\xi\rangle = \langle\xi'\rangle = v, \quad \langle\chi\rangle = u\end{gathered} \tag{4.2}$$

where n_i, $i = 1-9$ are dimensionless numbers which we choose to take values as $n_i \in (-1,0,1)$, which are natural choices for alignments in such flavour symmetric models. Here v or u denotes the vacuum expectation value (VEV) of the flavon fields which typically characterises the scale of flavour symmetry breaking. Similar but more restricted alignments are chosen in the original proposal [139]. Using such VEV alignments and the A_4 product rules given in Appendix A, the charged lepton mass matrix can be written as

$$m_l = \frac{\langle H\rangle v}{\Lambda}\begin{pmatrix} n_1 y_e & n_2 y_\mu & n_3 y_\tau \\ n_3 y_e & n_1 y_\mu & n_2 y_\tau \\ n_2 y_e & n_3 y_\mu & n_1 y_\tau \end{pmatrix}. \tag{4.3}$$

The neutral fermion mass matrix in the basis (ν_L, ν_R, S) can be written as

$$\mathscr{M} = \begin{pmatrix} 0 & M_D & 0 \\ M_D^T & M_R & M_S^T \\ 0 & M_S & 0 \end{pmatrix} \tag{4.4}$$

where M_D, the Dirac neutrino mass matrix is

$$M_D = \frac{\langle H \rangle v}{\Lambda} \begin{pmatrix} y_1 n_1 & y_2 n_5 & y_3 n_7 \\ y_1 n_3 & y_2 n_4 & y_3 n_9 \\ y_1 n_2 & y_2 n_6 & y_3 n_8 \end{pmatrix} = \sqrt{A} \begin{pmatrix} y_1 n_1 & y_2 n_5 & y_3 n_7 \\ y_1 n_3 & y_2 n_4 & y_3 n_9 \\ y_1 n_2 & y_2 n_6 & y_3 n_8 \end{pmatrix} \tag{4.5}$$

with $A = \frac{\langle H \rangle^2 v^2}{\Lambda^2}$. The right-handed neutrino mass matrix takes the diagonal form

$$M_R = \begin{pmatrix} \lambda_1 v & 0 & 0 \\ 0 & \lambda_2 v & 0 \\ 0 & 0 & \lambda_3 v \end{pmatrix}, \tag{4.6}$$

and M_S in the basis (S, ν_R) is given by

$$M_S = (\rho u, y_4 v, y_5 u). \tag{4.7}$$

In the case where $M_R \gg M_S > M_D$, the effective 4×4 light neutrino mass matrix in the basis (ν_L, ν_s) can be written as [139]

$$M_\nu = - \begin{pmatrix} M_D M_R^{-1} M_D^T & M_D M_R^{-1} M_S^T \\ M_S (M_R^{-1})^T M_D^T & M_S M_R^{-1} M_S^T \end{pmatrix} \tag{4.8}$$

Using the expressions for M_D, M_R, M_S mentioned above, the 4×4 active-sterile mass matrix can be written as

$$m_\nu^{4\times4} = \begin{pmatrix} -Aa_7 & -Aa_8 & -Aa_9 & -\sqrt{A}a_1 \\ -Aa_{10} & -Aa_{11} & -Aa_{12} & -\sqrt{A}a_2 \\ -Aa_{13} & -Aa_{14} & -Aa_{15} & -\sqrt{A}a_3 \\ -\sqrt{A}a_4 & -\sqrt{A}a_5 & -\sqrt{A}a_6 & -a_0 \end{pmatrix} \tag{4.9}$$

where

$$a_0 = \left(\frac{\rho^2 u^2}{\lambda_1 v} + \frac{y_4^2 v}{\lambda_2} + \frac{y_5^2 u^2}{v \lambda_3}\right), \tag{4.10}$$

$$a_1 = a_4 = \left(\frac{\rho u y_1 n_1}{v \lambda_1} + \frac{y_4 y_2 n_5}{\lambda_2} + \frac{u y_5 y_3 n_7}{v \lambda_3}\right), \tag{4.11}$$

$$a_2 = a_5 = \left(\frac{\rho u y_1 n_3}{v \lambda_1} + \frac{y_4 y_2 n_4}{\lambda_2} + \frac{u y_5 y_3 n_9}{v \lambda_3}\right), \tag{4.12}$$

$$a_3 = a_6 = \left(\frac{\rho u y_1 n_2}{v \lambda_1} + \frac{y_4 y_2 n_6}{\lambda_2} + \frac{u y_5 y_3 n_8}{v \lambda_3}\right), \tag{4.13}$$

$$a_7 = (\frac{y_1^2 n_1^2}{v\lambda_1} + \frac{y_2^2 n_5^2}{v\lambda_2} + \frac{y_3^2 n_7^2}{v\lambda_3}), \tag{4.14}$$

$$a_8 = a_{10} = (\frac{y_1^2 n_3 n_1}{v\lambda_1} + \frac{y_2^2 n_4 n_5}{v\lambda_2} + \frac{y_3^2 n_7 n_9}{v\lambda_3}), \tag{4.15}$$

$$a_9 = a_{13} = (\frac{y_1^2 n_1 n_2}{v\lambda_1} + \frac{y_2^2 n_5 n_6}{v\lambda_2} + \frac{y_3^2 n_7 n_8}{v\lambda_3}), \tag{4.16}$$

$$a_{11} = (\frac{y_1^2 n_3^2}{v\lambda_1} + \frac{y_2^2 n_4^2}{v\lambda_2} + \frac{y_3^2 n_9^2}{v\lambda_3}), \tag{4.17}$$

$$a_{12} = a_{14} = (\frac{y_1^2 n_2 n_3}{v\lambda_1} + \frac{y_2^2 n_4 n_6}{v\lambda_2} + \frac{y_3^2 n_8 n_9}{v\lambda_3}), \tag{4.18}$$

$$a_{15} = (\frac{y_1^2 n_2^2}{v\lambda_1} + \frac{y_2^2 n_6^2}{v\lambda_2} + \frac{y_3^2 n_8^2}{v\lambda_3}). \tag{4.19}$$

This is a 4×4 complex symmetric mass matrix, in general having ten independent elements. However, depending upon the vacuum alignments or the specific values of $n_i \in (-1, 0, 1)$, the mass matrix can have interesting textures which we discuss in details in the next section.

The choice of vacuum alignment of the flavon fields required to achieve the desired structures of lepton mass matrices can be realised only when additional driving fields are incorporated as discussed in [162] for usual three neutrino scenarios. For similar discussion in a $3+1$ neutrino scenario, please refer to [150]. Since these driving fields do not affect the general structure of the mass matrices, we have not incorporated them in the discussion above. The non-trivial vacuum alignment of the ϕ, $\phi^{'}$, $\phi^{''}$ fields required to produce the specific structure of the charged lepton mass matrix and the 4×4 block of the light neutrino mass matrix is realised by introducing three additional driving fields. As shown in such works discussing the vacuum alignment of A_4 flavons, $n_i \in (-1, 0, 1)$ corresponds to generic alignments which can be naturally realised from the minimisation of the scalar potential (superpotential in supersymmetric scenarios). For illustrative purposes, we show the scalar potential for triplet flavons in Appendix B and minimise the parts for one triplet flavon. By solving the minimisation equations, we get several minima which belong to the above mentioned general class. Analysis of the full scalar potential is beyond the scope of the present work and one can refer to dedicated studies of vacuum alignment in supersymmetric [163] as well as non-supersymmetric A_4 models [164]. It should be noted that additional driving fields are needed sometimes to get the desired alignment and depending upon the combinations of such driving fields, it may be possible to get vacuum alignment different from the above mentioned class. However, we stick to the minimal class as mentioned above for our studies.

4.3 Classification of Textures

We choose to work in the basis where the charged lepton mass matrix is diagonal. This allows the leptonic mixing matrix to be directly related to the diagonalising matrix of the light neutrino mass matrix. As discussed in the previous section, this corresponds to the VEV of the flavon field ϕ to be $\langle\phi\rangle = v(n_1, n_2, n_3)$, with $n_1 = 1$, $n_2 = n_3 = 0$. In the most general case of the vacuum alignments of the flavon fields ϕ' and ϕ'', each of $n_4, n_5, n_6, n_7, n_8, n_9$ can take 3 values, i.e. $0, 1, -1$. Therefore we have $3^6 = 729$ possible cases of different vacuum alignments, which will generate 729 different 4×4 neutrino mass matrices. These 729 vacuum alignments are presented in Appendix C and Appendix D. We also note that many of the vacuum alignments give rise to light neutrino mass matrices having the same set of constraints and hence predict same correlations among neutrino parameters. We point out these alignments for the allowed cases (to be found in our numerical analysis below) in Appendix E.

We first single out the disallowed textures based on the known results from previous analysis [154–157, 147–149]. They are given as follows.

Disallowed cases:

1. Texture zero in entire second row and column. Total number of such textures is 71.
2. Texture zero in entire third row and column. Total number of such textures is 73.
3. Texture zero in entire second and third rows and columns. Total number of such textures is 9.
4. $\mu - \tau$ symmetry in the entire 4×4 block. Total number of such textures is 72.

Total no of such disallowed mass matrices is 225. While the first three categories are inconsistent with the $3+1$ global fit neutrino data (see for example, [165]), the last category is ruled out as it gives rise to vanishing reactor mixing angle.

The textures which are not disallowed from the results of previous analysis can be categorised spontaneous breaking of flavour symmetries as follows.

Allowed cases:

1. $\mu - \tau$ symmetry in 3×3 active neutrino block. Total number of such textures is 40.
2. One zero texture mass matrix. Total number of such textures is 96.
3. Two zero texture mass matrix. Total number of such textures is 64.
4. Three zero texture mass matrix. Total number of such textures is 8.

5. Hybrid texture mass matrix with no zeros but some constraints relating different elements. Total number of such textures is 296.

Total number of such allowed mass matrices is 504. We further classify each of these allowed categories into different sub-categories based on the the constraints relating different elements of the light neutrino mass matrix.

4.3.1 Classification of Allowed Textures

$(\mu-\tau)$ symmetric textures

The 40 $\mu-\tau$ symmetric textures can be classified into 4 sub-categories depending upon the constraints that they satisfy. For representative purpose, we also mention one such VEV alignment and the corresponding mass matrix.
(i) 16 matrices with 5 complex constraints:

$$M_{e\mu}=0,\quad M_{e\tau}=0,\quad M_{\mu\mu}=M_{\tau\tau},M_{\mu\tau}=-M_{\tau\tau},\quad M_{\mu s}=-M_{\tau s}$$

- $n_1=1;n_2=0;n_3=0;n_4=1;n_5=0;n_6=-1;n_7=0;\ n_8=1;n_9=-1;$

$$\begin{pmatrix} -\frac{H^2vy_1^2}{\Lambda^2\lambda_1} & 0 & 0 & -\frac{u\sqrt{\frac{H^2v^2}{\Lambda^2}}\rho y_1}{v\lambda_1} \\ 0 & -\frac{H^2v^2\left(\frac{y_2^2}{v\lambda_2}+\frac{y_3^2}{v\lambda_3}\right)}{\Lambda^2} & -\frac{H^2v^2\left(-\frac{y_2^2}{v\lambda_2}-\frac{y_3^2}{v\lambda_3}\right)}{\Lambda^2} & -\sqrt{\frac{H^2v^2}{\Lambda^2}}\left(\frac{y_2y_4}{\lambda_2}-\frac{uy_3y_5}{v\lambda_3}\right) \\ 0 & -\frac{H^2v^2\left(-\frac{y_2^2}{v\lambda_2}-\frac{y_3^2}{v\lambda_3}\right)}{\Lambda^2} & -\frac{H^2v^2\left(\frac{y_2^2}{v\lambda_2}+\frac{y_3^2}{v\lambda_3}\right)}{\Lambda^2} & -\sqrt{\frac{H^2v^2}{\Lambda^2}}\left(-\frac{y_2y_4}{\lambda_2}+\frac{uy_3y_5}{v\lambda_3}\right) \\ -\frac{u\sqrt{\frac{H^2v^2}{\Lambda^2}}\rho y_1}{v\lambda_1} & -\sqrt{\frac{H^2v^2}{\Lambda^2}}\left(\frac{y_2y_4}{\lambda_2}-\frac{uy_3y_5}{v\lambda_3}\right) & -\sqrt{\frac{H^2v^2}{\Lambda^2}}\left(-\frac{y_2y_4}{\lambda_2}+\frac{uy_3y_5}{v\lambda_3}\right) & -\frac{u^2\rho^2}{v\lambda_1}-\frac{vy_4^2}{\lambda_2}-\frac{u^2y_5^2}{v\lambda_3} \end{pmatrix}$$

(ii) 8 matrices with 3 complex constraints:

$$M_{e\mu}=0,\quad M_{e\tau}=0,\quad M_{\mu\mu}=M_{\tau\tau}$$

- $n_1=1;n_2=0;\ n_3=0;n_4=1;n_5=0;\ n_6=1;n_7=0;\ n_8=1;\ n_9=-1;$

$$\begin{pmatrix} -\frac{H^2vy_1^2}{\Lambda^2\lambda_1} & 0 & 0 & -\frac{u\sqrt{\frac{H^2v^2}{\Lambda^2}}\rho y_1}{v\lambda_1} \\ 0 & -\frac{H^2v^2\left(\frac{y_2^2}{v\lambda_2}+\frac{y_3^2}{v\lambda_3}\right)}{\Lambda^2} & -\frac{H^2v^2\left(\frac{y_2^2}{v\lambda_2}-\frac{y_3^2}{v\lambda_3}\right)}{\Lambda^2} & -\sqrt{\frac{H^2v^2}{\Lambda^2}}\left(\frac{y_2y_4}{\lambda_2}-\frac{uy_3y_5}{v\lambda_3}\right) \\ 0 & -\frac{H^2v^2\left(\frac{y_2^2}{v\lambda_2}-\frac{y_3^2}{v\lambda_3}\right)}{\Lambda^2} & -\frac{H^2v^2\left(\frac{y_2^2}{v\lambda_2}+\frac{y_3^2}{v\lambda_3}\right)}{\Lambda^2} & -\sqrt{\frac{H^2v^2}{\Lambda^2}}\left(\frac{y_2y_4}{\lambda_2}+\frac{uy_3y_5}{v\lambda_3}\right) \\ -\frac{u\sqrt{\frac{H^2v^2}{\Lambda^2}}\rho y_1}{v\lambda_1} & -\sqrt{\frac{H^2v^2}{\Lambda^2}}\left(\frac{y_2y_4}{\lambda_2}-\frac{uy_3y_5}{v\lambda_3}\right) & -\sqrt{\frac{H^2v^2}{\Lambda^2}}\left(\frac{y_2y_4}{\lambda_2}+\frac{uy_3y_5}{v\lambda_3}\right) & -\frac{u^2\rho^2}{v\lambda_1}-\frac{vy_4^2}{\lambda_2}-\frac{u^2y_5^2}{v\lambda_3} \end{pmatrix}$$

(iii) 8 matrices with 3 complex constraints:

$$M_{e\mu} = M_{e\tau}, \quad M_{\mu\mu} = M_{\tau\tau}, \quad M_{\tau\tau} + M_{\mu\tau} = 2M_{e\tau}$$

• $n_1 = 1; n_2 = 0;\ n_3 = 0; n_4 = 1; n_5 = 0;\ n_6 = -1; n_7 = 1; n_8 = 1;\ n_9 = 1;$

$$\begin{pmatrix} -\frac{H^2v^2\left(\frac{y_1^2}{v\lambda_1}+\frac{y_3^2}{v\lambda_3}\right)}{\Lambda^2} & -\frac{H^2vy_3^2}{\Lambda^2\lambda_3} & -\frac{H^2vy_3^2}{\Lambda^2\lambda_3} & -\sqrt{\frac{H^2v^2}{\Lambda^2}}\left(\frac{u\rho y_1}{v\lambda_1}+\frac{uy_3y_5}{v\lambda_3}\right) \\ -\frac{H^2vy_3^2}{\Lambda^2\lambda_3} & -\frac{H^2v^2\left(\frac{y_2^2}{v\lambda_2}+\frac{y_3^2}{v\lambda_3}\right)}{\Lambda^2} & -\frac{H^2v^2\left(-\frac{y_2^2}{v\lambda_2}+\frac{y_3^2}{v\lambda_3}\right)}{\Lambda^2} & -\sqrt{\frac{H^2v^2}{\Lambda^2}}\left(\frac{y_2y_4}{\lambda_2}+\frac{uy_3y_5}{v\lambda_3}\right) \\ -\frac{H^2vy_3^2}{\Lambda^2\lambda_3} & -\frac{H^2v^2\left(-\frac{y_2^2}{v\lambda_2}+\frac{y_3^2}{v\lambda_3}\right)}{\Lambda^2} & -\frac{H^2v^2\left(\frac{y_2^2}{v\lambda_2}+\frac{y_3^2}{v\lambda_3}\right)}{\Lambda^2} & -\sqrt{\frac{H^2v^2}{\Lambda^2}}\left(-\frac{y_2y_4}{\lambda_2}+\frac{uy_3y_5}{v\lambda_3}\right) \\ -\sqrt{\frac{H^2v^2}{\Lambda^2}}\left(\frac{u\rho y_1}{v\lambda_1}+\frac{uy_3y_5}{v\lambda_3}\right) & -\sqrt{\frac{H^2v^2}{\Lambda^2}}\left(\frac{y_2y_4}{\lambda_2}+\frac{uy_3y_5}{v\lambda_3}\right) & -\sqrt{\frac{H^2v^2}{\Lambda^2}}\left(-\frac{y_2y_4}{\lambda_2}+\frac{uy_3y_5}{v\lambda_3}\right) & -\frac{u^2\rho^2}{v\lambda_1}-\frac{vy_4^2}{\lambda_2}-\frac{u^2y_5^2}{v\lambda_3} \end{pmatrix}$$

(iv) 8 matrices with 3 complex constraints:

$$M_{e\mu} = M_{e\tau}, \quad M_{\mu\mu} = M_{\tau\tau}, \quad M_{\tau\tau} + M_{\mu\tau} = -2M_{e\tau}$$

• $n_1 = 1; n_2 = 0;\ n_3 = 0; n_4 = 1; n_5 = 0;\ n_6 = -1; n_7 = 1; n_8 = -1;\ n_9 = -1;$

$$\begin{pmatrix} -\frac{H^2v^2\left(\frac{y_1^2}{v\lambda_1}+\frac{y_3^2}{v\lambda_3}\right)}{\Lambda^2} & \frac{H^2vy_3^2}{\Lambda^2\lambda_3} & \frac{H^2vy_3^2}{\Lambda^2\lambda_3} & -\sqrt{\frac{H^2v^2}{\Lambda^2}}\left(\frac{u\rho y_1}{v\lambda_1}+\frac{uy_3y_5}{v\lambda_3}\right) \\ \frac{H^2vy_3^2}{\Lambda^2\lambda_3} & -\frac{H^2v^2\left(\frac{y_2^2}{v\lambda_2}+\frac{y_3^2}{v\lambda_3}\right)}{\Lambda^2} & -\frac{H^2v^2\left(-\frac{y_2^2}{v\lambda_2}+\frac{y_3^2}{v\lambda_3}\right)}{\Lambda^2} & -\sqrt{\frac{H^2v^2}{\Lambda^2}}\left(\frac{y_2y_4}{\lambda_2}-\frac{uy_3y_5}{v\lambda_3}\right) \\ \frac{H^2vy_3^2}{\Lambda^2\lambda_3} & -\frac{H^2v^2\left(-\frac{y_2^2}{v\lambda_2}+\frac{y_3^2}{v\lambda_3}\right)}{\Lambda^2} & -\frac{H^2v^2\left(\frac{y_2^2}{v\lambda_2}+\frac{y_3^2}{v\lambda_3}\right)}{\Lambda^2} & -\sqrt{\frac{H^2v^2}{\Lambda^2}}\left(-\frac{y_2y_4}{\lambda_2}-\frac{uy_3y_5}{v\lambda_3}\right) \\ -\sqrt{\frac{H^2v^2}{\Lambda^2}}\left(\frac{u\rho y_1}{v\lambda_1}+\frac{uy_3y_5}{v\lambda_3}\right) & -\sqrt{\frac{H^2v^2}{\Lambda^2}}\left(\frac{y_2y_4}{\lambda_2}-\frac{uy_3y_5}{v\lambda_3}\right) & -\sqrt{\frac{H^2v^2}{\Lambda^2}}\left(-\frac{y_2y_4}{\lambda_2}-\frac{uy_3y_5}{v\lambda_3}\right) & -\frac{u^2\rho^2}{v\lambda_1}-\frac{vy_4^2}{\lambda_2}-\frac{u^2y_5^2}{v\lambda_3} \end{pmatrix}$$

Texture 1 zero case

All 96 texture 1 zero cases can be classified into 12 categories depending upon constraints satisfied by them. For representative purpose, we also mention one such VEV alignment and the corresponding mass matrix.

(i) 8 matrices with 3 complex constraints:

$$M_{e\mu} = 0, \quad M_{\mu\mu} = -M_{\mu\tau}, \quad M_{e\tau} + M_{\mu\tau} = -M_{\tau\tau}$$

• $n_1=1; n_2=0; n_3=0; n_4=0; n_5=1; n_6=-1; n_7=0; n_8=1; n_9=-1;$

$$\begin{pmatrix} -\frac{H^2v^2\left(\frac{y_1^2}{v\lambda_1}+\frac{y_2^2}{v\lambda_2}\right)}{\Lambda^2} & 0 & \frac{H^2vy_2^2}{\Lambda^2\lambda_2} & -\sqrt{\frac{H^2v^2}{\Lambda^2}}\left(\frac{u\rho y_1}{v\lambda_1}+\frac{y_2y_4}{\lambda_2}\right) \\ 0 & -\frac{H^2vy_3^2}{\Lambda^2\lambda_3} & \frac{H^2vy_3^2}{\Lambda^2\lambda_3} & \frac{u\sqrt{\frac{H^2v^2}{\Lambda^2}}y_3y_5}{v\lambda_3} \\ \frac{H^2vy_2^2}{\Lambda^2\lambda_2} & \frac{H^2vy_3^2}{\Lambda^2\lambda_3} & -\frac{H^2v^2\left(\frac{y_2^2}{v\lambda_2}+\frac{y_3^2}{v\lambda_3}\right)}{\Lambda^2} & -\sqrt{\frac{H^2v^2}{\Lambda^2}}\left(-\frac{y_2y_4}{\lambda_2}+\frac{uy_3y_5}{v\lambda_3}\right) \\ -\sqrt{\frac{H^2v^2}{\Lambda^2}}\left(\frac{u\rho y_1}{v\lambda_1}+\frac{y_2y_4}{\lambda_2}\right) & \frac{u\sqrt{\frac{H^2v^2}{\Lambda^2}}y_3y_5}{v\lambda_3} & -\sqrt{\frac{H^2v^2}{\Lambda^2}}\left(-\frac{y_2y_4}{\lambda_2}+\frac{uy_3y_5}{v\lambda_3}\right) & -\frac{u^2\rho^2}{v\lambda_1}-\frac{vy_4^2}{\lambda_2}-\frac{u^2y_5^2}{v\lambda_3} \end{pmatrix}$$

(ii) 8 matrices with 3 complex constraints:

$$M_{e\tau}=0, \quad M_{\tau\tau}=-M_{\mu\tau}, \quad M_{e\mu}+M_{\mu\tau}=-M_{\mu\mu}$$

• $n_1=1; n_2=0; {}_3=0; n_4=1; n_5=0; n_6=-1; n_7=1; n_8=0; n_9=-1;$

$$\begin{pmatrix} -\frac{H^2v^2\left(\frac{y_1^2}{v\lambda_1}+\frac{y_3^2}{v\lambda_3}\right)}{\Lambda^2} & \frac{H^2vy_3^2}{\Lambda^2\lambda_3} & 0 & -\sqrt{\frac{H^2v^2}{\Lambda^2}}\left(\frac{u\rho y_1}{v\lambda_1}+\frac{uy_3y_5}{v\lambda_3}\right) \\ \frac{H^2vy_3^2}{\Lambda^2\lambda_3} & -\frac{H^2v^2\left(\frac{y_2^2}{v\lambda_2}+\frac{y_3^2}{v\lambda_3}\right)}{\Lambda^2} & \frac{H^2vy_2^2}{\Lambda^2\lambda_2} & -\sqrt{\frac{H^2v^2}{\Lambda^2}}\left(\frac{y_2y_4}{\lambda_2}-\frac{uy_3y_5}{v\lambda_3}\right) \\ 0 & \frac{H^2vy_2^2}{\Lambda^2\lambda_2} & -\frac{H^2vy_2^2}{\Lambda^2\lambda_2} & \frac{\sqrt{\frac{H^2v^2}{\Lambda^2}}y_2y_4}{\lambda_2} \\ -\sqrt{\frac{H^2v^2}{\Lambda^2}}\left(\frac{u\rho y_1}{v\lambda_1}+\frac{uy_3y_5}{v\lambda_3}\right) & -\sqrt{\frac{H^2v^2}{\Lambda^2}}\left(\frac{y_2y_4}{\lambda_2}-\frac{uy_3y_5}{v\lambda_3}\right) & \frac{\sqrt{\frac{H^2v^2}{\Lambda^2}}y_2y_4}{\lambda_2} & -\frac{u^2\rho^2}{v\lambda_1}-\frac{vy_4^2}{\lambda_2}-\frac{u^2y_5^2}{v\lambda_3} \end{pmatrix}$$

(iii) 8 matrices with 3 complex constraints:

$$M_{e\mu}=0, \quad M_{\mu\mu}=M_{\mu\tau}, \quad M_{e\tau}+M_{\mu\tau}=M_{\tau\tau}$$

• $n_1=1; n_2=0;\ n_3=0; n_4=0; n_5=1;\ n_6=1; n_7=0; n_8=1;\ n_9=1;$

$$\begin{pmatrix} -\frac{H^2v^2\left(\frac{y_1^2}{v\lambda_1}+\frac{y_2^2}{v\lambda_2}\right)}{\Lambda^2} & 0 & -\frac{H^2vy_2^2}{\Lambda^2\lambda_2} & -\sqrt{\frac{H^2v^2}{\Lambda^2}}\left(\frac{u\rho y_1}{v\lambda_1}+\frac{y_2y_4}{\lambda_2}\right) \\ 0 & -\frac{H^2vy_3^2}{\Lambda^2\lambda_3} & -\frac{H^2vy_3^2}{\Lambda^2\lambda_3} & -\frac{u\sqrt{\frac{H^2v^2}{\Lambda^2}}y_3y_5}{v\lambda_3} \\ -\frac{H^2vy_2^2}{\Lambda^2\lambda_2} & -\frac{H^2vy_3^2}{\Lambda^2\lambda_3} & -\frac{H^2v^2\left(\frac{y_2^2}{v\lambda_2}+\frac{y_3^2}{v\lambda_3}\right)}{\Lambda^2} & -\sqrt{\frac{H^2v^2}{\Lambda^2}}\left(\frac{y_2y_4}{\lambda_2}+\frac{uy_3y_5}{v\lambda_3}\right) \\ -\sqrt{\frac{H^2v^2}{\Lambda^2}}\left(\frac{u\rho y_1}{v\lambda_1}+\frac{y_2y_4}{\lambda_2}\right) & -\frac{u\sqrt{\frac{H^2v^2}{\Lambda^2}}y_3y_5}{v\lambda_3} & -\sqrt{\frac{H^2v^2}{\Lambda^2}}\left(\frac{y_2y_4}{\lambda_2}+\frac{uy_3y_5}{v\lambda_3}\right) & -\frac{u^2\rho^2}{v\lambda_1}-\frac{vy_4^2}{\lambda_2}-\frac{u^2y_5^2}{v\lambda_3} \end{pmatrix}$$

(iv) 8 matrices with 3 complex constraints:

$$M_{e\mu}=0, \quad M_{\mu\mu}=-M_{\mu\tau}, \quad M_{e\tau}-M_{\mu\tau}=M_{\tau\tau}$$

• $n_1 = 1; n_2 = 0;\ n_3 = 0; n_4 = 0; n_5 = 1;\ n_6 = 1; n_7 = 0; n_8 = 1;\ n_9 = -1;$

$$\begin{pmatrix} -\frac{H^2v^2\left(\frac{y_1^2}{v\lambda_1}+\frac{y_2^2}{v\lambda_2}\right)}{\Lambda^2} & 0 & -\frac{H^2vy_2^2}{\Lambda^2\lambda_2} & -\sqrt{\frac{H^2v^2}{\Lambda^2}}\left(\frac{u\rho y_1}{v\lambda_1}+\frac{y_2y_4}{\lambda_2}\right) \\ 0 & -\frac{H^2vy_3^2}{\Lambda^2\lambda_3} & \frac{H^2vy_3^2}{\Lambda^2\lambda_3} & \frac{u\sqrt{\frac{H^2v^2}{\Lambda^2}}y_3y_5}{v\lambda_3} \\ -\frac{H^2vy_2^2}{\Lambda^2\lambda_2} & \frac{H^2vy_3^2}{\Lambda^2\lambda_3} & -\frac{H^2v^2\left(\frac{y_2^2}{v\lambda_2}+\frac{y_3^2}{v\lambda_3}\right)}{\Lambda^2} & -\sqrt{\frac{H^2v^2}{\Lambda^2}}\left(\frac{y_2y_4}{\lambda_2}+\frac{uy_3y_5}{v\lambda_3}\right) \\ -\sqrt{\frac{H^2v^2}{\Lambda^2}}\left(\frac{u\rho y_1}{v\lambda_1}+\frac{y_2y_4}{\lambda_2}\right) & \frac{u\sqrt{\frac{H^2v^2}{\Lambda^2}}y_3y_5}{v\lambda_3} & -\sqrt{\frac{H^2v^2}{\Lambda^2}}\left(\frac{y_2y_4}{\lambda_2}+\frac{uy_3y_5}{v\lambda_3}\right) & -\frac{u^2\rho^2}{v\lambda_1}-\frac{vy_4^2}{\lambda_2}-\frac{u^2y_5^2}{v\lambda_3} \end{pmatrix}$$

(v) 8 matrices with 3 complex constraints:

$$M_{e\mu} = 0, \quad M_{\mu\mu} = M_{\mu\tau}, \quad M_{e\tau} - M_{\mu\tau} = -M_{\tau\tau}$$

• $n_1 = 1; n_2 = 0;\ n_3 = 0; n_4 = 0; n_5 = 1;\ n_6 = -1; n_7 = 0; n_8 = 1;\ n_9 = 1;$

$$\begin{pmatrix} -\frac{H^2v^2\left(\frac{y_1^2}{v\lambda_1}+\frac{y_2^2}{v\lambda_2}\right)}{\Lambda^2} & 0 & \frac{H^2vy_2^2}{\Lambda^2\lambda_2} & -\sqrt{\frac{H^2v^2}{\Lambda^2}}\left(\frac{u\rho y_1}{v\lambda_1}+\frac{y_2y_4}{\lambda_2}\right) \\ 0 & -\frac{H^2vy_3^2}{\Lambda^2\lambda_3} & -\frac{H^2vy_3^2}{\Lambda^2\lambda_3} & -\frac{u\sqrt{\frac{H^2v^2}{\Lambda^2}}y_3y_5}{v\lambda_3} \\ \frac{H^2vy_2^2}{\Lambda^2\lambda_2} & -\frac{H^2vy_3^2}{\Lambda^2\lambda_3} & -\frac{H^2v^2\left(\frac{y_2^2}{v\lambda_2}+\frac{y_3^2}{v\lambda_3}\right)}{\Lambda^2} & -\sqrt{\frac{H^2v^2}{\Lambda^2}}\left(-\frac{y_2y_4}{\lambda_2}+\frac{uy_3y_5}{v\lambda_3}\right) \\ -\sqrt{\frac{H^2v^2}{\Lambda^2}}\left(\frac{u\rho y_1}{v\lambda_1}+\frac{y_2y_4}{\lambda_2}\right) & -\frac{u\sqrt{\frac{H^2v^2}{\Lambda^2}}y_3y_5}{v\lambda_3} & -\sqrt{\frac{H^2v^2}{\Lambda^2}}\left(-\frac{y_2y_4}{\lambda_2}+\frac{uy_3y_5}{v\lambda_3}\right) & -\frac{u^2\rho^2}{v\lambda_1}-\frac{vy_4^2}{\lambda_2}-\frac{u^2y_5^2}{v\lambda_3} \end{pmatrix}$$

(vi) 8 matrices with 3 complex constraints:

$$M_{e\tau} = 0, \quad M_{\tau\tau} = M_{\mu\tau}, \quad M_{e\mu} + M_{\mu\tau} = M_{\mu\mu}$$

• $n_1 = 1; n_2 = 0;\ n_3 = 0; n_4 = 1; n_5 = 0;\ n_6 = 1; n_7 = 1; n_8 = 0;\ n_9 = 1;$

$$\begin{pmatrix} -\frac{H^2v^2\left(\frac{y_1^2}{v\lambda_1}+\frac{y_3^2}{v\lambda_3}\right)}{\Lambda^2} & -\frac{H^2vy_3^2}{\Lambda^2\lambda_3} & 0 & -\sqrt{\frac{H^2v^2}{\Lambda^2}}\left(\frac{u\rho y_1}{v\lambda_1}+\frac{uy_3y_5}{v\lambda_3}\right) \\ -\frac{H^2vy_3^2}{\Lambda^2\lambda_3} & -\frac{H^2v^2\left(\frac{y_2^2}{v\lambda_2}+\frac{y_3^2}{v\lambda_3}\right)}{\Lambda^2} & -\frac{H^2vy_2^2}{\Lambda^2\lambda_2} & -\sqrt{\frac{H^2v^2}{\Lambda^2}}\left(\frac{y_2y_4}{\lambda_2}+\frac{uy_3y_5}{v\lambda_3}\right) \\ 0 & -\frac{H^2vy_2^2}{\Lambda^2\lambda_2} & -\frac{H^2vy_2^2}{\Lambda^2\lambda_2} & -\frac{\sqrt{\frac{H^2v^2}{\Lambda^2}}y_2y_4}{\lambda_2} \\ -\sqrt{\frac{H^2v^2}{\Lambda^2}}\left(\frac{u\rho y_1}{v\lambda_1}+\frac{uy_3y_5}{v\lambda_3}\right) & -\sqrt{\frac{H^2v^2}{\Lambda^2}}\left(\frac{y_2y_4}{\lambda_2}+\frac{uy_3y_5}{v\lambda_3}\right) & -\frac{\sqrt{\frac{H^2v^2}{\Lambda^2}}y_2y_4}{\lambda_2} & -\frac{u^2\rho^2}{v\lambda_1}-\frac{vy_4^2}{\lambda_2}-\frac{u^2y_5^2}{v\lambda_3} \end{pmatrix}$$

(vii) 7 matrices with 3 complex constraints:

$$M_{e\tau} = 0, \quad M_{\tau\tau} = M_{\mu\tau}, \quad M_{e\mu} - M_{\mu\tau} = -M_{\mu\mu}$$

• $n_1 = 1; n_2 = 0;\ n_3 = 0; n_4 = 1; n_5 = 0;\ n_6 = 1; n_7 = 1; n_8 = 0;\ n_9 = -1;$

$$\begin{pmatrix} -\frac{H^2v^2\left(\frac{y_1^2}{v\lambda_1}+\frac{y_3^2}{v\lambda_3}\right)}{\Lambda^2} & \frac{H^2vy_3^2}{\Lambda^2\lambda_3} & 0 & -\sqrt{\frac{H^2v^2}{\Lambda^2}}\left(\frac{u\rho y_1}{v\lambda_1}+\frac{uy_3y_5}{v\lambda_3}\right) \\ \frac{H^2vy_3^2}{\Lambda^2\lambda_3} & -\frac{H^2v^2\left(\frac{y_2^2}{v\lambda_2}+\frac{y_3^2}{v\lambda_3}\right)}{\Lambda^2} & -\frac{H^2vy_2^2}{\Lambda^2\lambda_2} & -\sqrt{\frac{H^2v^2}{\Lambda^2}}\left(\frac{y_2y_4}{\lambda_2}-\frac{uy_3y_5}{v\lambda_3}\right) \\ 0 & -\frac{H^2vy_2^2}{\Lambda^2\lambda_2} & -\frac{H^2vy_2^2}{\Lambda^2\lambda_2} & -\frac{\sqrt{\frac{H^2v^2}{\Lambda^2}}y_2y_4}{\lambda_2} \\ -\sqrt{\frac{H^2v^2}{\Lambda^2}}\left(\frac{u\rho y_1}{v\lambda_1}+\frac{uy_3y_5}{v\lambda_3}\right) & -\sqrt{\frac{H^2v^2}{\Lambda^2}}\left(\frac{y_2y_4}{\lambda_2}-\frac{uy_3y_5}{v\lambda_3}\right) & -\frac{\sqrt{\frac{H^2v^2}{\Lambda^2}}y_2y_4}{\lambda_2} & -\frac{u^2\rho^2}{v\lambda_1}-\frac{vy_4^2}{\lambda_2}-\frac{u^2y_5^2}{v\lambda_3} \end{pmatrix}$$

(viii) 8 matrices with 3 complex constraints:

$$M_{e\tau} = 0, \quad M_{\tau\tau} = -M_{\mu\tau}, \quad M_{e\mu} - M_{\mu\tau} = M_{\mu\mu}$$

• $n_1 = 1; n_2 = 0;\ n_3 = 0; n_4 = 1; n_5 = 0;\ n_6 = -1; n_7 = 1; n_8 = 0;\ n_9 = 1;$

$$\begin{pmatrix} -\frac{H^2v^2\left(\frac{y_1^2}{v\lambda_1}+\frac{y_3^2}{v\lambda_3}\right)}{\Lambda^2} & -\frac{H^2vy_3^2}{\Lambda^2\lambda_3} & 0 & -\sqrt{\frac{H^2v^2}{\Lambda^2}}\left(\frac{u\rho y_1}{v\lambda_1}+\frac{uy_3y_5}{v\lambda_3}\right) \\ -\frac{H^2vy_3^2}{\Lambda^2\lambda_3} & -\frac{H^2v^2\left(\frac{y_2^2}{v\lambda_2}+\frac{y_3^2}{v\lambda_3}\right)}{\Lambda^2} & \frac{H^2vy_2^2}{\Lambda^2\lambda_2} & -\sqrt{\frac{H^2v^2}{\Lambda^2}}\left(\frac{y_2y_4}{\lambda_2}+\frac{uy_3y_5}{v\lambda_3}\right) \\ 0 & \frac{H^2vy_2^2}{\Lambda^2\lambda_2} & -\frac{H^2vy_2^2}{\Lambda^2\lambda_2} & \frac{\sqrt{\frac{H^2v^2}{\Lambda^2}}y_2y_4}{\lambda_2} \\ -\sqrt{\frac{H^2v^2}{\Lambda^2}}\left(\frac{u\rho y_1}{v\lambda_1}+\frac{uy_3y_5}{v\lambda_3}\right) & -\sqrt{\frac{H^2v^2}{\Lambda^2}}\left(\frac{y_2y_4}{\lambda_2}+\frac{uy_3y_5}{v\lambda_3}\right) & \frac{\sqrt{\frac{H^2v^2}{\Lambda^2}}y_2y_4}{\lambda_2} & -\frac{u^2\rho^2}{v\lambda_1}-\frac{vy_4^2}{\lambda_2}-\frac{u^2y_5^2}{v\lambda_3} \end{pmatrix}$$

(ix) 8 matrices with 3 complex constraints:

$$M_{\mu\tau} = 0, \quad M_{e\mu} = -M_{\mu\mu}, \quad M_{e\tau} = -M_{\tau\tau}$$

• $n_1 = 1; n_2 = 0; n_3 = 0; n_4 = 1; n_5 = -1; n_6 = 0; n_7 = 1; n_8 = -1; n_9 = 0;$

$$\begin{pmatrix} -\frac{H^2v^2\left(\frac{y_1^2}{v\lambda_1}+\frac{y_2^2}{v\lambda_2}+\frac{y_3^2}{v\lambda_3}\right)}{\Lambda^2} & \frac{H^2vy_2^2}{\Lambda^2\lambda_2} & \frac{H^2vy_3^2}{\Lambda^2\lambda_3} & -\sqrt{\frac{H^2v^2}{\Lambda^2}}\left(\frac{u\rho y_1}{v\lambda_1}-\frac{y_2y_4}{\lambda_2}+\frac{uy_3y_5}{v\lambda_3}\right) \\ \frac{H^2vy_2^2}{\Lambda^2\lambda_2} & -\frac{H^2vy_2^2}{\Lambda^2\lambda_2} & 0 & -\frac{\sqrt{\frac{H^2v^2}{\Lambda^2}}y_2y_4}{\lambda_2} \\ \frac{H^2vy_3^2}{\Lambda^2\lambda_3} & 0 & -\frac{H^2vy_3^2}{\Lambda^2\lambda_3} & \frac{u\sqrt{\frac{H^2v^2}{\Lambda^2}}y_3y_5}{v\lambda_3} \\ -\sqrt{\frac{H^2v^2}{\Lambda^2}}\left(\frac{u\rho y_1}{v\lambda_1}-\frac{y_2y_4}{\lambda_2}+\frac{uy_3y_5}{v\lambda_3}\right) & -\frac{\sqrt{\frac{H^2v^2}{\Lambda^2}}y_2y_4}{\lambda_2} & \frac{u\sqrt{\frac{H^2v^2}{\Lambda^2}}y_3y_5}{v\lambda_3} & -\frac{u^2\rho^2}{v\lambda_1}-\frac{vy_4^2}{\lambda_2}-\frac{u^2y_5^2}{v\lambda_3} \end{pmatrix}$$

(x) 8 matrices with 3 complex constraints:

$$M_{\mu\tau} = 0, \quad M_{e\mu} = M_{\mu\mu}, \quad M_{e\tau} = M_{\tau\tau}$$

• $n_1 = 1; n_2 = 0;\ n_3 = 0; n_4 = 0; n_5 = 1;\ n_6 = 1; n_7 = 1; n_8 = 0;\ n_9 = 1;$

$$\begin{pmatrix} -\frac{H^2v^2\left(\frac{y_1^2}{v\lambda_1}+\frac{y_2^2}{v\lambda_2}+\frac{y_3^2}{v\lambda_3}\right)}{\Lambda^2} & -\frac{H^2vy_3^2}{\Lambda^2\lambda_3} & -\frac{H^2vy_2^2}{\Lambda^2\lambda_2} & -\sqrt{\frac{H^2v^2}{\Lambda^2}}\left(\frac{u\rho y_1}{v\lambda_1}+\frac{y_2y_4}{\lambda_2}+\frac{uy_3y_5}{v\lambda_3}\right) \\ -\frac{H^2vy_3^2}{\Lambda^2\lambda_3} & -\frac{H^2vy_3^2}{\Lambda^2\lambda_3} & 0 & -\frac{u\sqrt{\frac{H^2v^2}{\Lambda^2}}y_3y_5}{v\lambda_3} \\ -\frac{H^2vy_2^2}{\Lambda^2\lambda_2} & 0 & -\frac{H^2vy_2^2}{\Lambda^2\lambda_2} & -\frac{\sqrt{\frac{H^2v^2}{\Lambda^2}}y_2y_4}{\lambda_2} \\ -\sqrt{\frac{H^2v^2}{\Lambda^2}}\left(\frac{u\rho y_1}{v\lambda_1}+\frac{y_2y_4}{\lambda_2}+\frac{uy_3y_5}{v\lambda_3}\right) & -\frac{u\sqrt{\frac{H^2v^2}{\Lambda^2}}y_3y_5}{v\lambda_3} & -\frac{\sqrt{\frac{H^2v^2}{\Lambda^2}}y_2y_4}{\lambda_2} & -\frac{u^2\rho^2}{v\lambda_1}-\frac{vy_4^2}{\lambda_2}-\frac{u^2y_5^2}{v\lambda_3} \end{pmatrix}$$

(xi) 9 matrices with 3 complex constraints:

$$M_{\mu\tau} = 0, \quad M_{e\mu} = -M_{\mu\mu}, \quad M_{e\tau} = M_{\tau\tau}$$

• $n_1 = 1; n_2 = 0;\ n_3 = 0; n_4 = 0; n_5 = 1;\ n_6 = 1; n_7 = 1; n_8 = 0;\ n_9 = -1;$

$$\begin{pmatrix} -\frac{H^2v^2\left(\frac{y_1^2}{v\lambda_1}+\frac{y_2^2}{v\lambda_2}+\frac{y_3^2}{v\lambda_3}\right)}{\Lambda^2} & \frac{H^2vy_3^2}{\Lambda^2\lambda_3} & -\frac{H^2vy_2^2}{\Lambda^2\lambda_2} & -\sqrt{\frac{H^2v^2}{\Lambda^2}}\left(\frac{u\rho y_1}{v\lambda_1}+\frac{y_2y_4}{\lambda_2}+\frac{uy_3y_5}{v\lambda_3}\right) \\ \frac{H^2vy_3^2}{\Lambda^2\lambda_3} & -\frac{H^2vy_3^2}{\Lambda^2\lambda_3} & 0 & \frac{u\sqrt{\frac{H^2v^2}{\Lambda^2}}y_3y_5}{v\lambda_3} \\ -\frac{H^2vy_2^2}{\Lambda^2\lambda_2} & 0 & -\frac{H^2vy_2^2}{\Lambda^2\lambda_2} & -\frac{\sqrt{\frac{H^2v^2}{\Lambda^2}}y_2y_4}{\lambda_2} \\ -\sqrt{\frac{H^2v^2}{\Lambda^2}}\left(\frac{u\rho y_1}{v\lambda_1}+\frac{y_2y_4}{\lambda_2}+\frac{uy_3y_5}{v\lambda_3}\right) & \frac{u\sqrt{\frac{H^2v^2}{\Lambda^2}}y_3y_5}{v\lambda_3} & -\frac{\sqrt{\frac{H^2v^2}{\Lambda^2}}y_2y_4}{\lambda_2} & -\frac{u^2\rho^2}{v\lambda_1}-\frac{vy_4^2}{\lambda_2}-\frac{u^2y_5^2}{v\lambda_3} \end{pmatrix}$$

(xii) 8 matrices with 3 complex constraints:

$$M_{\mu\tau} = 0, \quad M_{e\mu} = M_{\mu\mu}, \quad M_{e\tau} = -M_{\tau\tau}$$

• $n_1 = 1; n_2 = 0;\ n_3 = 0; n_4 = 0; n_5 = 1;\ n_6 = -1; n_7 = 1; n_8 = 0;\ n_9 = 1;$

$$\begin{pmatrix} -\frac{H^2v^2\left(\frac{y_1^2}{v\lambda_1}+\frac{y_2^2}{v\lambda_2}+\frac{y_3^2}{v\lambda_3}\right)}{\Lambda^2} & -\frac{H^2vy_3^2}{\Lambda^2\lambda_3} & \frac{H^2vy_2^2}{\Lambda^2\lambda_2} & -\sqrt{\frac{H^2v^2}{\Lambda^2}}\left(\frac{u\rho y_1}{v\lambda_1}+\frac{y_2y_4}{\lambda_2}+\frac{uy_3y_5}{v\lambda_3}\right) \\ -\frac{H^2vy_3^2}{\Lambda^2\lambda_3} & -\frac{H^2vy_3^2}{\Lambda^2\lambda_3} & 0 & -\frac{u\sqrt{\frac{H^2v^2}{\Lambda^2}}y_3y_5}{v\lambda_3} \\ \frac{H^2vy_2^2}{\Lambda^2\lambda_2} & 0 & -\frac{H^2vy_2^2}{\Lambda^2\lambda_2} & \frac{\sqrt{\frac{H^2v^2}{\Lambda^2}}y_2y_4}{\lambda_2} \\ -\sqrt{\frac{H^2v^2}{\Lambda^2}}\left(\frac{u\rho y_1}{v\lambda_1}+\frac{y_2y_4}{\lambda_2}+\frac{uy_3y_5}{v\lambda_3}\right) & -\frac{u\sqrt{\frac{H^2v^2}{\Lambda^2}}y_3y_5}{v\lambda_3} & \frac{\sqrt{\frac{H^2v^2}{\Lambda^2}}y_2y_4}{\lambda_2} & -\frac{u^2\rho^2}{v\lambda_1}-\frac{vy_4^2}{\lambda_2}-\frac{u^2y_5^2}{v\lambda_3} \end{pmatrix}$$

Texture 2 zero case

All 64 texture 2 zero cases can be classified into following categories. For representative purpose, we also mention one such VEV alignment and the corresponding mass matrix.
(i) 8 matrices with 3 complex constraints:

$$M_{e\mu} = 0, \quad M_{e\tau} = 0, \quad M_{\mu\mu} = M_{\mu\tau}$$

• $n_1 = 1; n_2 = 0;\ n_3 = 0; n_4 = 0; n_5 = 0;\ n_6 = 1; n_7 = 0; n_8 = 1;\ n_9 = 1;$

$$\begin{pmatrix} -\frac{H^2 v y_1^2}{\Lambda^2 \lambda_1} & 0 & 0 & -\frac{u\sqrt{\frac{H^2v^2}{\Lambda^2}}\rho y_1}{v\lambda_1} \\ 0 & -\frac{H^2 v y_3^2}{\Lambda^2 \lambda_3} & -\frac{H^2 v y_3^2}{\Lambda^2 \lambda_3} & -\frac{u\sqrt{\frac{H^2v^2}{\Lambda^2}} y_3 y_5}{v\lambda_3} \\ 0 & -\frac{H^2 v y_3^2}{\Lambda^2 \lambda_3} & -\frac{H^2 v^2 \left(\frac{y_2^2}{v\lambda_2}+\frac{y_3^2}{v\lambda_3}\right)}{\Lambda^2} & -\sqrt{\frac{H^2v^2}{\Lambda^2}}\left(\frac{y_2 y_4}{\lambda_2}+\frac{u y_3 y_5}{v\lambda_3}\right) \\ -\frac{u\sqrt{\frac{H^2v^2}{\Lambda^2}}\rho y_1}{v\lambda_1} & -\frac{u\sqrt{\frac{H^2v^2}{\Lambda^2}} y_3 y_5}{v\lambda_3} & -\sqrt{\frac{H^2v^2}{\Lambda^2}}\left(\frac{y_2 y_4}{\lambda_2}+\frac{u y_3 y_5}{v\lambda_3}\right) & -\frac{u^2\rho^2}{v\lambda_1}-\frac{v y_4^2}{\lambda_2}-\frac{u^2 y_5^2}{v\lambda_3} \end{pmatrix}$$

(ii) 8 matrices with 3 complex constraints:

$$M_{e\mu} = 0, \quad M_{e\tau} = 0, \quad M_{\mu\mu} = -M_{\mu\tau}$$

• $n_1 = 1; n_2 = 0;\ n_3 = 0; n_4 = 0; n_5 = 0;\ n_6 = 1; n_7 = 0; n_8 = 1;\ n_9 = -1;$

$$\begin{pmatrix} -\frac{H^2 v y_1^2}{\Lambda^2 \lambda_1} & 0 & 0 & -\frac{u\sqrt{\frac{H^2v^2}{\Lambda^2}}\rho y_1}{v\lambda_1} \\ 0 & -\frac{H^2 v y_3^2}{\Lambda^2 \lambda_3} & \frac{H^2 v y_3^2}{\Lambda^2 \lambda_3} & \frac{u\sqrt{\frac{H^2v^2}{\Lambda^2}} y_3 y_5}{v\lambda_3} \\ 0 & \frac{H^2 v y_3^2}{\Lambda^2 \lambda_3} & -\frac{H^2 v^2 \left(\frac{y_2^2}{v\lambda_2}+\frac{y_3^2}{v\lambda_3}\right)}{\Lambda^2} & -\sqrt{\frac{H^2v^2}{\Lambda^2}}\left(\frac{y_2 y_4}{\lambda_2}+\frac{u y_3 y_5}{v\lambda_3}\right) \\ -\frac{u\sqrt{\frac{H^2v^2}{\Lambda^2}}\rho y_1}{v\lambda_1} & \frac{u\sqrt{\frac{H^2v^2}{\Lambda^2}} y_3 y_5}{v\lambda_3} & -\sqrt{\frac{H^2v^2}{\Lambda^2}}\left(\frac{y_2 y_4}{\lambda_2}+\frac{u y_3 y_5}{v\lambda_3}\right) & -\frac{u^2\rho^2}{v\lambda_1}-\frac{v y_4^2}{\lambda_2}-\frac{u^2 y_5^2}{v\lambda_3} \end{pmatrix}$$

(iii) 8 matrices with 3 complex constraints:

$$M_{e\tau} = 0, \quad M_{\mu\tau} = 0, \quad M_{e\mu} = -M_{\mu\mu}$$

• $n_1 = 1; n_2 = 0;\ n_3 = 0; n_4 = 0; n_5 = 0;\ n_6 = 1; n_7 = 1; n_8 = 0;\ n_9 = -1;$

$$\begin{pmatrix} -\frac{H^2 v^2 \left(\frac{y_1^2}{v\lambda_1}+\frac{y_3^2}{v\lambda_3}\right)}{\Lambda^2} & \frac{H^2 v y_3^2}{\Lambda^2 \lambda_3} & 0 & -\sqrt{\frac{H^2v^2}{\Lambda^2}}\left(\frac{u\rho y_1}{v\lambda_1}+\frac{u y_3 y_5}{v\lambda_3}\right) \\ \frac{H^2 v y_3^2}{\Lambda^2 \lambda_3} & -\frac{H^2 v y_3^2}{\Lambda^2 \lambda_3} & 0 & \frac{u\sqrt{\frac{H^2v^2}{\Lambda^2}} y_3 y_5}{v\lambda_3} \\ 0 & 0 & -\frac{H^2 v y_2^2}{\Lambda^2 \lambda_2} & -\frac{\sqrt{\frac{H^2v^2}{\Lambda^2}} y_2 y_4}{\lambda_2} \\ -\sqrt{\frac{H^2v^2}{\Lambda^2}}\left(\frac{u\rho y_1}{v\lambda_1}+\frac{u y_3 y_5}{v\lambda_3}\right) & \frac{u\sqrt{\frac{H^2v^2}{\Lambda^2}} y_3 y_5}{v\lambda_3} & -\frac{\sqrt{\frac{H^2v^2}{\Lambda^2}} y_2 y_4}{\lambda_2} & -\frac{u^2\rho^2}{v\lambda_1}-\frac{v y_4^2}{\lambda_2}-\frac{u^2 y_5^2}{v\lambda_3} \end{pmatrix}$$

(iv) 8 matrices with 3 complex constraints:

$$M_{e\tau}=0,\quad M_{\mu\tau}=0,\quad M_{e\mu}=M_{\mu\mu}$$

• $n_1=1; n_2=0;\ n_3=0; n_4=0; n_5=0;\ n_6=1; n_7=1; n_8=0;\ n_9=1;$

$$\begin{pmatrix} -\frac{H^2v^2\left(\frac{y_1^2}{v\lambda_1}+\frac{y_3^2}{v\lambda_3}\right)}{\Lambda^2} & -\frac{H^2vy_3^2}{\Lambda^2\lambda_3} & 0 & -\sqrt{\frac{H^2v^2}{\Lambda^2}}\left(\frac{u\rho y_1}{v\lambda_1}+\frac{uy_3y_5}{v\lambda_3}\right) \\ -\frac{H^2vy_3^2}{\Lambda^2\lambda_3} & -\frac{H^2vy_3^2}{\Lambda^2\lambda_3} & 0 & -\frac{u\sqrt{\frac{H^2v^2}{\Lambda^2}}y_3y_5}{v\lambda_3} \\ 0 & 0 & -\frac{H^2vy_2^2}{\Lambda^2\lambda_2} & -\frac{\sqrt{\frac{H^2v^2}{\Lambda^2}}y_2y_4}{\lambda_2} \\ -\sqrt{\frac{H^2v^2}{\Lambda^2}}\left(\frac{u\rho y_1}{v\lambda_1}+\frac{uy_3y_5}{v\lambda_3}\right) & -\frac{u\sqrt{\frac{H^2v^2}{\Lambda^2}}y_3y_5}{v\lambda_3} & -\frac{\sqrt{\frac{H^2v^2}{\Lambda^2}}y_2y_4}{\lambda_2} & -\frac{u^2\rho^2}{v\lambda_1}-\frac{vy_4^2}{\lambda_2}-\frac{u^2y_5^2}{v\lambda_3} \end{pmatrix}$$

(v) 8 matrices with 3 complex constraints:

$$M_{e\mu}=0,\quad M_{\mu\tau}=0,\quad M_{e\tau}=M_{\tau\tau}$$

• $n_1=1; n_2=0;\ n_3=0; n_4=0; n_5=1;\ n_6=1; n_7=0; n_8=0;\ n_9=-1;$

$$\begin{pmatrix} -\frac{H^2v^2\left(\frac{y_1^2}{v\lambda_1}+\frac{y_2^2}{v\lambda_2}\right)}{\Lambda^2} & 0 & -\frac{H^2vy_2^2}{\Lambda^2\lambda_2} & -\sqrt{\frac{H^2v^2}{\Lambda^2}}\left(\frac{u\rho y_1}{v\lambda_1}+\frac{y_2y_4}{\lambda_2}\right) \\ 0 & -\frac{H^2vy_3^2}{\Lambda^2\lambda_3} & 0 & \frac{u\sqrt{\frac{H^2v^2}{\Lambda^2}}y_3y_5}{v\lambda_3} \\ -\frac{H^2vy_2^2}{\Lambda^2\lambda_2} & 0 & -\frac{H^2vy_2^2}{\Lambda^2\lambda_2} & -\frac{\sqrt{\frac{H^2v^2}{\Lambda^2}}y_2y_4}{\lambda_2} \\ -\sqrt{\frac{H^2v^2}{\Lambda^2}}\left(\frac{u\rho y_1}{v\lambda_1}+\frac{y_2y_4}{\lambda_2}\right) & \frac{u\sqrt{\frac{H^2v^2}{\Lambda^2}}y_3y_5}{v\lambda_3} & -\frac{\sqrt{\frac{H^2v^2}{\Lambda^2}}y_2y_4}{\lambda_2} & -\frac{u^2\rho^2}{v\lambda_1}-\frac{vy_4^2}{\lambda_2}-\frac{u^2y_5^2}{v\lambda_3} \end{pmatrix}$$

(vi) 8 matrices with 3 complex constraints:

$$M_{e\mu}=0,\quad M_{\mu\tau}=0,\quad M_{e\tau}=-M_{\tau\tau}$$

• $n_1=1; n_2=0;\ n_3=0; n_4=0; n_5=1;\ n_6=-1; n_7=0; n_8=0;\ n_9=1;$

$$\begin{pmatrix} -\frac{H^2v^2\left(\frac{y_1^2}{v\lambda_1}+\frac{y_2^2}{v\lambda_2}\right)}{\Lambda^2} & 0 & \frac{H^2vy_2^2}{\Lambda^2\lambda_2} & -\sqrt{\frac{H^2v^2}{\Lambda^2}}\left(\frac{u\rho y_1}{v\lambda_1}+\frac{y_2y_4}{\lambda_2}\right) \\ 0 & -\frac{H^2vy_3^2}{\Lambda^2\lambda_3} & 0 & -\frac{u\sqrt{\frac{H^2v^2}{\Lambda^2}}y_3y_5}{v\lambda_3} \\ \frac{H^2vy_2^2}{\Lambda^2\lambda_2} & 0 & -\frac{H^2vy_2^2}{\Lambda^2\lambda_2} & \frac{\sqrt{\frac{H^2v^2}{\Lambda^2}}y_2y_4}{\lambda_2} \\ -\sqrt{\frac{H^2v^2}{\Lambda^2}}\left(\frac{u\rho y_1}{v\lambda_1}+\frac{y_2y_4}{\lambda_2}\right) & -\frac{u\sqrt{\frac{H^2v^2}{\Lambda^2}}y_3y_5}{v\lambda_3} & \frac{\sqrt{\frac{H^2v^2}{\Lambda^2}}y_2y_4}{\lambda_2} & -\frac{u^2\rho^2}{v\lambda_1}-\frac{vy_4^2}{\lambda_2}-\frac{u^2y_5^2}{v\lambda_3} \end{pmatrix}$$

(vii) 9 matrices with 3 complex constraints:

$$M_{e\mu}=0,\quad M_{e\tau}=0,\quad M_{\mu\tau}=M_{\tau\tau}$$

• $n_1=1; n_2=0;\ n_3=0; n_4=1; n_5=0;\ n_6=0; n_7=0; n_8=1;\ n_9=1;$

$$\begin{pmatrix} -\frac{H^2 v y_1^2}{\Lambda^2\lambda_1} & 0 & 0 & -\frac{u\sqrt{\frac{H^2v^2}{\Lambda^2}}\rho y_1}{v\lambda_1} \\ 0 & -\frac{H^2v^2\left(\frac{y_2^2}{v\lambda_2}+\frac{y_3^2}{v\lambda_3}\right)}{\Lambda^2} & -\frac{H^2 v y_3^2}{\Lambda^2\lambda_3} & -\sqrt{\frac{H^2v^2}{\Lambda^2}}\left(\frac{y_2y_4}{\lambda_2}+\frac{uy_3y_5}{v\lambda_3}\right) \\ 0 & -\frac{H^2 v y_3^2}{\Lambda^2\lambda_3} & -\frac{H^2 v y_3^2}{\Lambda^2\lambda_3} & -\frac{u\sqrt{\frac{H^2v^2}{\Lambda^2}}y_3y_5}{v\lambda_3} \\ -\frac{u\sqrt{\frac{H^2v^2}{\Lambda^2}}\rho y_1}{v\lambda_1} & -\sqrt{\frac{H^2v^2}{\Lambda^2}}\left(\frac{y_2y_4}{\lambda_2}+\frac{uy_3y_5}{v\lambda_3}\right) & -\frac{u\sqrt{\frac{H^2v^2}{\Lambda^2}}y_3y_5}{v\lambda_3} & -\frac{u^2\rho^2}{v\lambda_1}-\frac{vy_4^2}{\lambda_2}-\frac{u^2y_5^2}{v\lambda_3} \end{pmatrix}$$

(viii) 7 matrices with 3 complex constraints:

$$M_{e\mu}=0,\quad M_{e\tau}=0,\quad M_{\mu\tau}=-M_{\tau\tau}$$

• $n_1=1; n_2=0;\ n_3=0; n_4=1; n_5=0;\ n_6=0; n_7=0; n_8=-1;\ n_9=1;$

$$\begin{pmatrix} -\frac{H^2 v y_1^2}{\Lambda^2\lambda_1} & 0 & 0 & -\frac{u\sqrt{\frac{H^2v^2}{\Lambda^2}}\rho y_1}{v\lambda_1} \\ 0 & -\frac{H^2v^2\left(\frac{y_2^2}{v\lambda_2}+\frac{y_3^2}{v\lambda_3}\right)}{\Lambda^2} & \frac{H^2 v y_3^2}{\Lambda^2\lambda_3} & -\sqrt{\frac{H^2v^2}{\Lambda^2}}\left(\frac{y_2y_4}{\lambda_2}+\frac{uy_3y_5}{v\lambda_3}\right) \\ 0 & \frac{H^2 v y_3^2}{\Lambda^2\lambda_3} & -\frac{H^2 v y_3^2}{\Lambda^2\lambda_3} & \frac{u\sqrt{\frac{H^2v^2}{\Lambda^2}}y_3y_5}{v\lambda_3} \\ -\frac{u\sqrt{\frac{H^2v^2}{\Lambda^2}}\rho y_1}{v\lambda_1} & -\sqrt{\frac{H^2v^2}{\Lambda^2}}\left(\frac{y_2y_4}{\lambda_2}+\frac{uy_3y_5}{v\lambda_3}\right) & \frac{u\sqrt{\frac{H^2v^2}{\Lambda^2}}y_3y_5}{v\lambda_3} & -\frac{u^2\rho^2}{v\lambda_1}-\frac{vy_4^2}{\lambda_2}-\frac{u^2y_5^2}{v\lambda_3} \end{pmatrix}$$

Texture 3 zero case

All 8 texture 3 zero cases can be classified into the following category. For representative purpose, we mention the VEV alignment and the corresponding mass matrix.
(i) 8 matrices with 3 complex constraints:

$$M_{e\mu}=0,\quad M_{e\tau}=0,\quad M_{\mu\tau}=0$$

• $n_1=1; n_2=0;\ n_3=0; n_4=0; n_5=0;\ n_6=1; n_7=0; n_8=0;\ v_9=-1;$

$$\begin{pmatrix} -\frac{H^2 v y_1^2}{\Lambda^2 \lambda_1} & 0 & 0 & -\frac{u\sqrt{\frac{H^2v^2}{\Lambda^2}}\rho y_1}{v\lambda_1} \\ 0 & -\frac{H^2 v y_3^2}{\Lambda^2 \lambda_3} & 0 & \frac{u\sqrt{\frac{H^2v^2}{\Lambda^2}} y_3 y_5}{v\lambda_3} \\ 0 & 0 & -\frac{H^2 v y_2^2}{\Lambda^2 \lambda_2} & -\frac{\sqrt{\frac{H^2v^2}{\Lambda^2}} y_2 y_4}{\lambda_2} \\ -\frac{u\sqrt{\frac{H^2v^2}{\Lambda^2}}\rho y_1}{v\lambda_1} & \frac{u\sqrt{\frac{H^2v^2}{\Lambda^2}} y_3 y_5}{v\lambda_3} & -\frac{\sqrt{\frac{H^2v^2}{\Lambda^2}} y_2 y_4}{\lambda_2} & -\frac{u^2\rho^2}{v\lambda_1} - \frac{v y_4^2}{\lambda_2} - \frac{u^2 y_5^2}{v\lambda_3} \end{pmatrix}$$

Hybrid texture case

All 296 hybrid textures can be classified into following categories depending upon constraints satisfied by them.

(i) 12 matrices with 6 complex constraints:

$$M_{e\mu} = -M_{e\tau}, \quad M_{\mu\mu} = M_{\tau\tau}, \quad M_{e\tau} = M_{\tau\tau}, \quad M_{e\mu} = M_{\mu\tau},$$
$$M_{e\mu} + M_{e\tau} = M_{\mu\mu} + M_{\mu\tau}, \quad M_{\mu s} = -M_{\tau s}$$

(ii) 6 matrices with 6 complex constraints:

$$M_{e\mu} = -M_{e\tau}, \quad M_{\mu\mu} = M_{\tau\tau}\,, \quad M_{e\tau} = M_{\mu\tau}\,, \quad M_{e\mu} = M_{\tau\tau}\,,$$
$$M_{e\mu} + M_{e\tau} = M_{\mu\mu} + M_{\mu\tau}, \quad M_{\mu s} = -M_{\tau s}$$

(iii) 6 matrices with 6 complex constraints:

$$M_{e\mu} = -M_{e\tau}, \quad M_{\mu\mu} = M_{\tau\tau}, \quad M_{e\tau} = M_{\mu\tau}, \quad M_{e\mu} = M_{\mu\mu},$$
$$M_{e\mu} + M_{e\tau} = M_{\mu\mu} + M_{\mu\tau}, \quad M_{\mu s} = -M_{\tau s}$$

(iv) 8 matrices with 3 complex constraints:

$$M_{e\mu} = M_{e\tau}, \quad M_{\mu\mu} = M_{\mu\tau}, \quad M_{e\mu} = M_{\mu\tau}$$

(v) 8 matrices with 4 complex constraints:

$$M_{e\mu} = M_{\mu\tau}, \quad M_{e\tau} = M_{\mu\mu}, \quad M_{e\mu} = -M_{e\tau}, \quad M_{\mu\mu} = -M_{\tau\tau}$$

(vi) 8 matrices with 3 complex constraints:

$$M_{e\mu} = -M_{e\tau}, \quad M_{e\mu} = M_{\mu\mu}, \quad M_{e\tau} = M_{\mu\tau}$$

(vii) 8 matrices with 4 complex constraints:

$$M_{e\mu} = M_{e\tau}, \quad M_{\mu\mu} = M_{\mu\tau}, \quad M_{e\mu} = -M_{\mu\tau}, \quad M_{e\mu} = -M_{\mu\mu}$$

(viii) 8 matrices with 3 complex constraints:

$$M_{\mu\mu} = M_{\mu\tau}, \quad M_{e\mu} = M_{\mu\tau}, \quad M_{e\tau} = M_{\tau\tau}$$

(ix) 8 matrices with 3 complex constraints:

$$M_{e\mu} = M_{\mu\tau}, \quad M_{e\mu} = -M_{\mu\mu}, \quad M_{e\tau} = M_{\tau\tau}$$

(x) 8 matrices with 3 complex constraints:

$$M_{e\mu} = M_{\mu\mu}, \quad M_{e\mu} = -M_{\mu\tau} \quad M_{e\mu} + M_{e\tau} = M_{\mu\tau} + M_{\tau\tau}$$

(xi) 8 matrices with 3 complex constraints:

$$M_{\mu\mu} = M_{\mu\tau}, \quad M_{e\mu} = -M_{\mu\mu}\ , \quad M_{e\tau} + M_{\mu\mu} = M_{e\mu} + M_{\tau\tau}$$

(xii) 7 matrices with 2 complex constraints:

$$M_{e\mu} = M_{\mu\mu}, \quad M_{e\mu} = M_{\mu\tau}$$

(xiii) 8 matrices with 3 complex constraints:

$$M_{\mu\mu} - M_{e\tau} = M_{\mu\tau} + M_{\tau\tau}\ , \quad M_{\mu\mu} = -M_{\mu\tau}\ , \quad M_{e\mu} = M_{\mu\tau}$$

(xiv) 8 matrices with 3 complex constraints:

$$M_{e\mu} = M_{\mu\mu}, \quad M_{e\mu} = -M_{\mu\tau}, \quad M_{e\tau} = -M_{\tau\tau}$$

(xv) 8 matrices with 3 complex constraints:

$$M_{\mu\mu} = M_{\mu\tau}, \quad M_{e\mu} = -M_{\mu\mu}, \quad M_{\tau\tau} = -M_{e\tau}$$

(xvi) 8 matrices with 3 complex constraints:

$$M_{e\mu} = M_{e\tau}, \quad M_{e\tau} = M_{\mu\tau}, \quad M_{e\tau} = M_{\tau\tau}$$

(xvii) 8 matrices with 3 complex constraints:

$$M_{e\mu} = M_{\mu\tau}, \quad M_{e\tau} = M_{\tau\tau}, \quad M_{e\mu} = -M_{e\tau}$$

(xviii) 8 matrices with 4 complex constraints:

$$M_{e\mu} = -M_{e\tau}, \quad M_{e\mu} = -M_{\mu\tau}, \quad M_{\mu\tau} = -M_{\tau\tau}, \quad M_{e\mu} = M_{\tau\tau}$$

(xix) 8 matrices with 3 complex constraints:

$$M_{e\mu} = M_{e\tau}, \quad M_{\mu\tau} = M_{\tau\tau}, \quad M_{e\mu} = -M_{\mu\tau}$$

(xx) 16 matrices with 3 complex constraints:

$$M_{e\mu} = -M_{e\tau}, \quad M_{\mu\mu} = M_{\tau\tau}\,, \quad 2M_{e\mu} + M_{\mu\mu} - M_{\mu\tau} = 0$$

(xxi) 16 matrices with 4 complex constraints:

$$M_{e\mu} = -M_{e\tau}, \quad M_{\mu\mu} = M_{\tau\tau}, \quad M_{\mu s} = -M_{\tau s}, \quad M_{\mu\tau} = -M_{\tau\tau}$$

(xxii) 8 matrices with 4 complex constraints:

$$M_{e\mu} = -M_{\mu\mu}, \quad M_{e\tau} = M_{\mu\tau}, \quad M_{e\tau} = M_{\tau\tau}\,, \quad M_{e\mu} - M_{\mu\mu} + M_{e\tau} + M_{\mu\tau} - 2M_{\tau\tau} = 0$$

(xxiii) 8 matrices with 3 complex constraints:

$$M_{e\tau} = M_{\tau\tau}, \quad M_{e\tau} = -M_{\mu\tau}, \quad M_{e\mu} - M_{\mu\mu} - 2M_{\mu\tau} = 0$$

(xxiv) 8 matrices with 3 complex constraints:

$$M_{e\mu} = M_{\mu\mu}\,, \quad M_{e\tau} = -M_{\tau\tau}\,, \quad M_{e\tau} = M_{\mu\tau}$$

(xxv) 8 matrices with 3 complex constraints:

$$M_{e\mu} = M_{\mu\mu}, \quad M_{\mu\mu} = M_{\tau\tau}, \quad M_{e\tau} = M_{\mu\tau}$$

(xxvi) 8 matrices with 3 complex constraints:

$$M_{e\tau} = -M_{\tau\tau}, \quad M_{e\tau} = -M_{\mu\tau}\,, \quad M_{e\mu} - M_{\mu\mu} - 2M_{e\tau} = 0$$

(xxvii) 3 matrices with 3 complex constraints:

$$M_{e\tau} = M_{\tau\tau}\,, \quad M_{e\tau} = M_{\mu\tau}, \quad M_{e\mu} - M_{\mu\mu} + M_{\mu\tau} + M_{\tau\tau} = 0$$

(xxviii) 1 matrix with 5 complex constraints:

$$M_{e\tau} = M_{\tau\tau}, \quad M_{\mu\mu} = M_{\tau\tau},$$
$$M_{\mu s} = -M_{\tau s}, \quad M_{e\mu} = M_{\mu\mu}, \quad M_{e\mu} + M_{\mu\mu} = M_{e\tau} + M_{\mu\tau}$$

(xxix) 2 matrices with 3 complex constraints:

$$M_{e\tau} = M_{\mu\tau}, \quad M_{\mu\tau} = -M_{\tau\tau}, \quad M_{e\mu} + M_{\mu\mu} - 2M_{e\tau} = 0$$

(xxx) 6 matrices with 3 complex constraints:

$$M_{e\tau} = M_{\mu\tau}, \quad M_{e\tau} = -M_{\tau\tau}, \quad M_{e\mu} + M_{\mu\mu} - 2M_{\tau\tau} = 0$$

(xxxi) 5 matrices with 3 complex constraints:

$$M_{e\tau} = M_{\mu\tau}\,, \quad M_{e\tau} = M_{\tau\tau}\,, \quad M_{e\mu} + M_{\mu\mu} - 2M_{e\tau} = 0$$

(xxxii) 8 matrices with 3 complex constraints:

$$M_{e\tau} = -M_{\mu\tau}, \quad M_{e\tau} = M_{\tau\tau}, \quad M_{e\mu} + M_{\mu\mu} = 0$$

(xxxiii) 7 matrices with 3 complex constraints:

$$M_{e\tau} = M_{\tau\tau}\,, \quad M_{\mu\mu} = M_{\tau\tau}, \quad M_{e\mu} = M_{\mu\tau}$$

(xxxiv) 4 matrices with 5 complex constraints:

$$M_{e\mu} = M_{\mu\mu}, \quad M_{e\tau} = M_{\mu\tau}, \quad M_{e\mu} = M_{\tau\tau}, \quad M_{\mu s} + M_{\tau s} = 0, \quad M_{e\tau} + M_{\mu\mu} = 0$$

(xxxv) 8 matrices with 4 complex constraints:

$$M_{\mu\mu} = M_{\tau\tau}\,, \quad M_{e\mu} + M_{\mu\tau} = 0\,, \quad M_{\mu\mu} + M_{e\tau} = 0\,, \quad M_{e\tau} + M_{\tau\tau} = 0$$

(xxxvi) 4 matrices with 4 complex constraints:

$$M_{\mu\mu} = M_{\tau\tau}, \quad M_{e\mu} = M_{\mu\tau}, \quad M_{e\tau} = M_{\mu\mu}, \quad M_{e\mu} + M_{e\tau} = 0$$

(xxxvii) 8 matrices with 4 complex constraints:

$$M_{\mu\mu} = M_{\tau\tau}\,, \quad M_{\mu s} + M_{\tau s} = 0\,,$$
$$M_{\mu\mu} = -M_{\mu\tau}\,, \quad M_{e\mu} + M_{\mu\mu} = M_{\tau\tau} - M_{e\tau}$$

(xxxviii) 8 matrices with 3 complex constraints:

$$M_{\mu\mu} = M_{\tau\tau}\,, \quad M_{e\tau} = -M_{\mu\tau}\,, \quad M_{e\mu} = -M_{\tau\tau}$$

(xxxix) 8 matrices with 3 complex constraints:

$$M_{e\tau} = -M_{\tau\tau}, \quad M_{e\tau} = -M_{\mu\tau}\,, \quad M_{e\mu} + M_{\mu\mu} = 0$$

(xxxx) 1 matrix with 3 complex constraints:

$$M_{\mu\mu} = M_{\mu\tau}, \quad M_{e\mu} = M_{\mu\tau}\,, \quad M_{e\tau} - M_{\mu\mu} = M_{\mu\tau} - M_{\tau\tau}$$

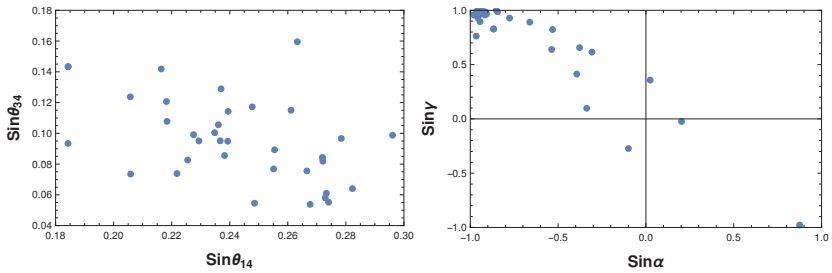

Fig. 4.1 Neutrino oscillation parameters in active-sterile sector for case (ii) from $\mu-\tau$ symmetric category for NH.

4.4 Numerical analysis

In this section, we present the method adopted for numerical analysis for $(\mu-\tau)$ symmetric textures, texture 1, texture 2 and texture 3 zero cases, in order to check their consistency with $3+1$ neutrino data. It is well known that 4×4 unitary mixing matrix can be parametrised as [159]

$$U = R_{34}\tilde{R}_{24}\tilde{R}_{14}R_{23}\tilde{R}_{13}R_{12}P \tag{4.20}$$

where

$$R_{34} = \begin{pmatrix} 1 & 0 & 0 & 0 \\ 0 & 1 & 0 & 0 \\ 0 & 0 & c_{34} & s_{34} \\ 0 & 0 & -s_{34} & c_{34} \end{pmatrix} \tag{4.21}$$

$$\tilde{R}_{14} = \begin{pmatrix} c_{14} & 0 & 0 & s_{14}e^{-i\delta_{14}} \\ 0 & 1 & 0 & 0 \\ 0 & 0 & 1 & 0 \\ -s_{14}e^{i\delta_{14}} & 0 & 0 & c_{14} \end{pmatrix} \tag{4.22}$$

with $c_{ij}=\cos\theta_{ij}$, $s_{ij}=\sin\theta_{ij}$, δ_{ij} being the Dirac CP phases, and

$$P = \mathrm{diag}(1, e^{-i\frac{\alpha}{2}}, e^{-i(\frac{\beta}{2}-\delta_{13})}, e^{-i(\frac{\gamma}{2}-\delta_{14})})$$

is the diagonal phase matrix containing the three Majorana phases α,β,γ. In this parametrisation, the six CP phases vary from $-\pi$ to π. Using the above form of mixing matrix, the 4×4 complex symmetric Majorana light neutrino mass matrix can be written as

$$M_\nu = UM_\nu^{\mathrm{diag}}U^T \tag{4.23}$$

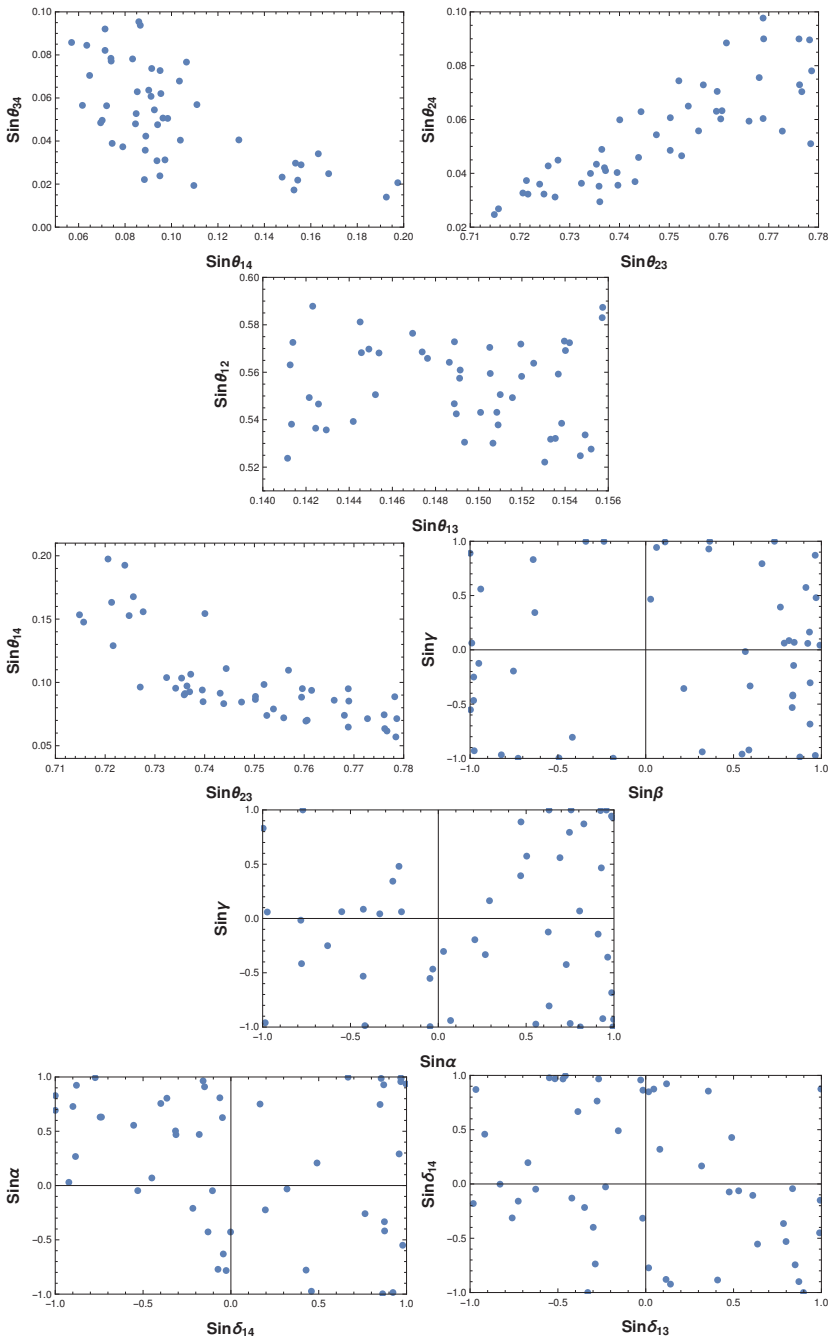

Fig. 4.2 Neutrino oscillation parameters in active-sterile sector for case (iii) from $\mu - \tau$ symmetric category for NH.

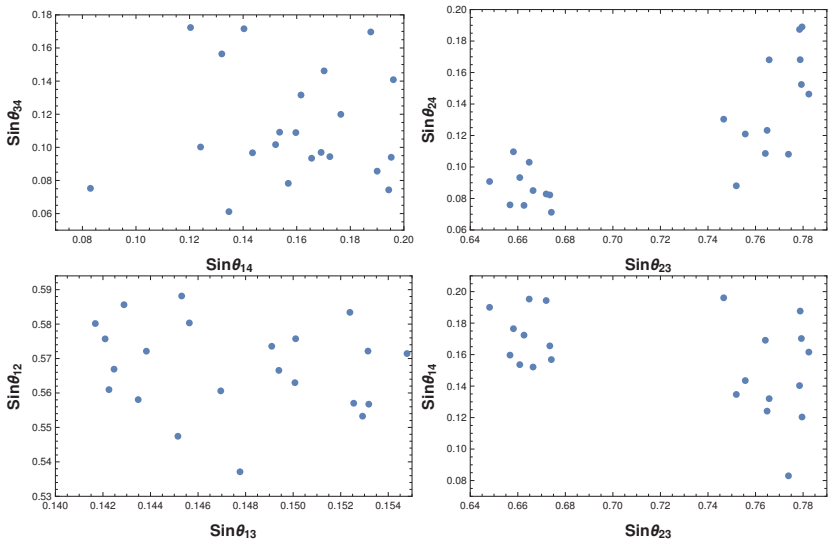

Fig. 4.3 Neutrino oscillation parameters in active-sterile sector for case (iv) from $\mu - \tau$ symmetric category for NH

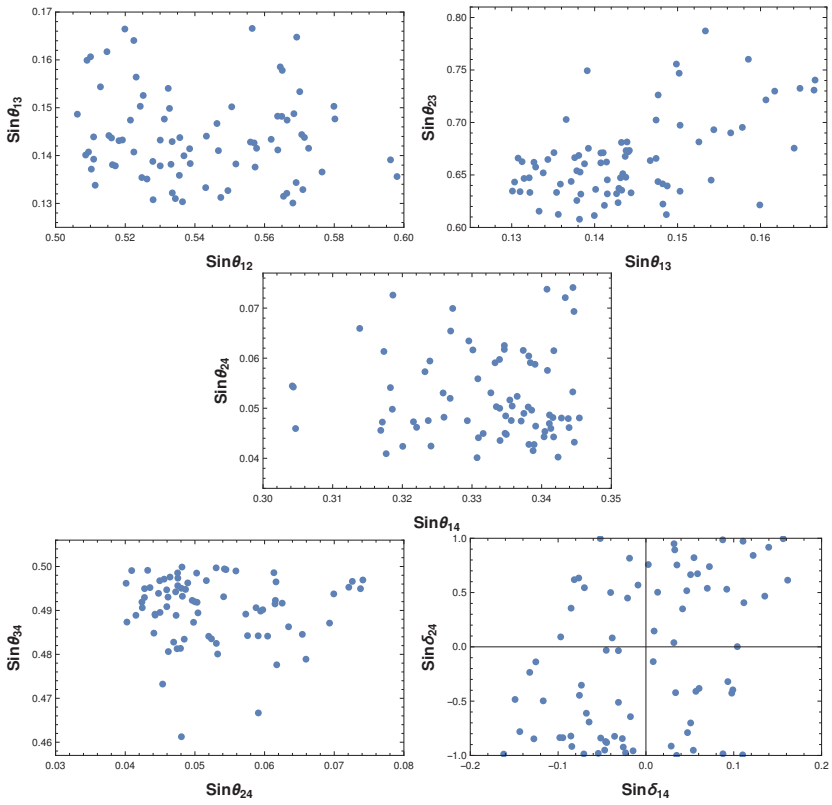

Fig. 4.4 Neutrino oscillation parameters in active-sterile sector for case (ix) from texture 1 zero category for NH.

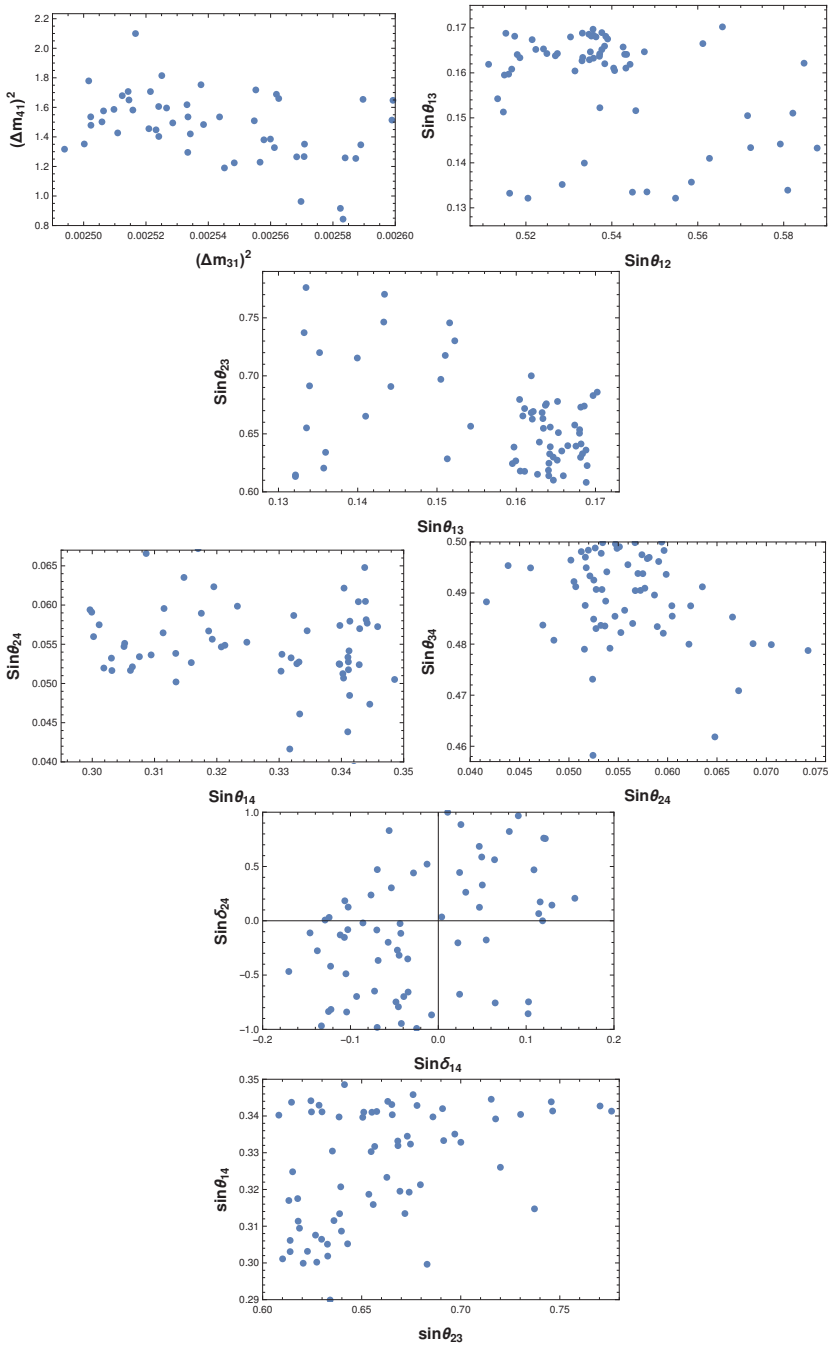

Fig. 4.5 Neutrino oscillation parameters in active-sterile sector for case (x) from texture 1 zero category for NH.

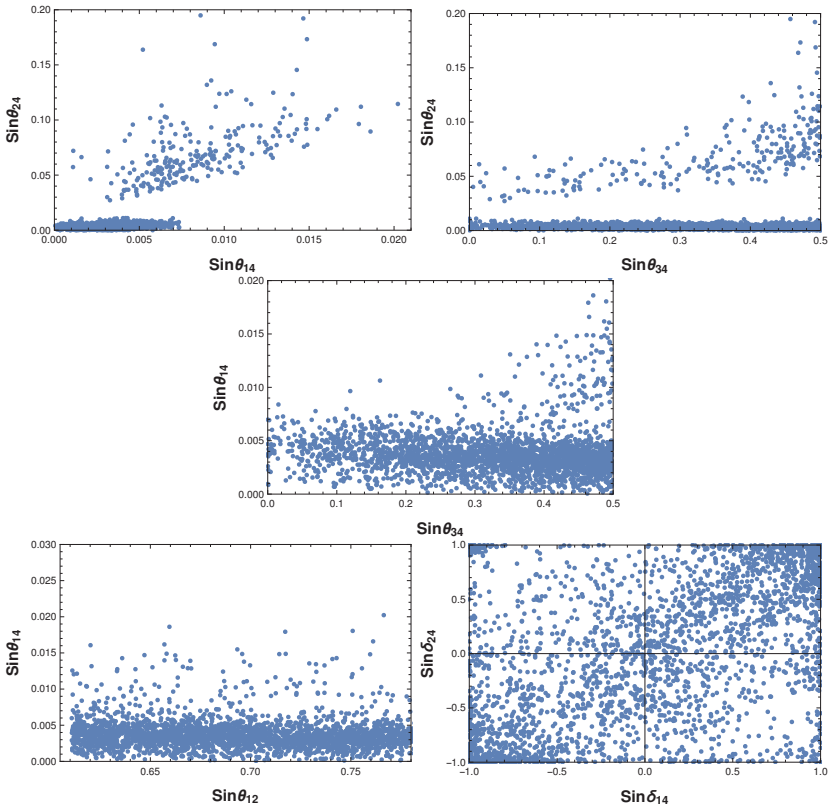

Fig. 4.6 Neutrino oscillation parameters in active-sterile sector for case (i) from texture 2 zero category for NH.

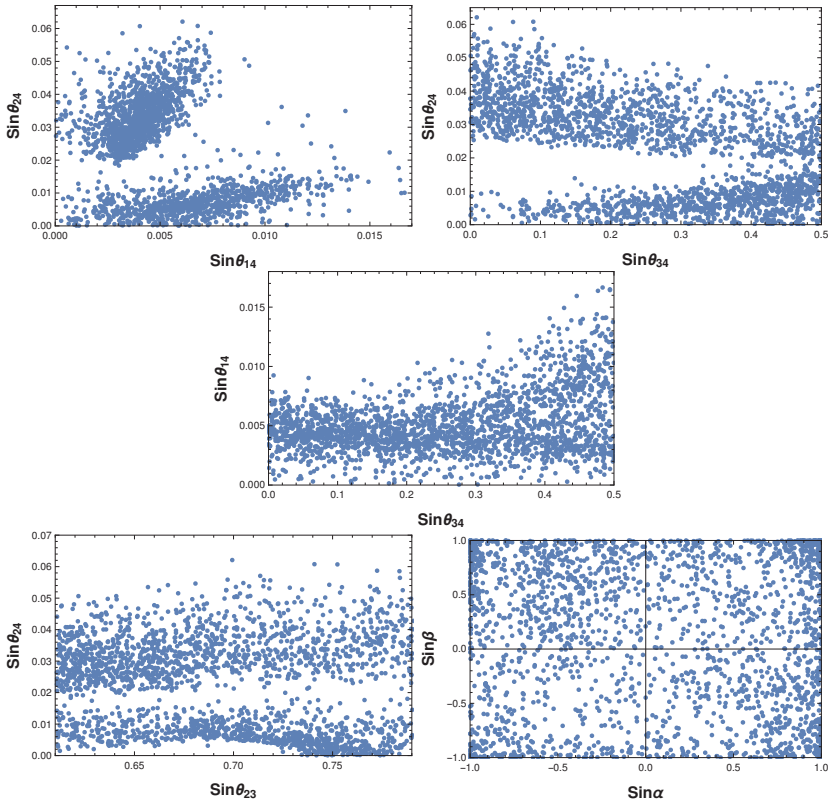

Fig. 4.7 Neutrino oscillation parameters in active-sterile sector for case (ii) from texture 2 zero category for NH.

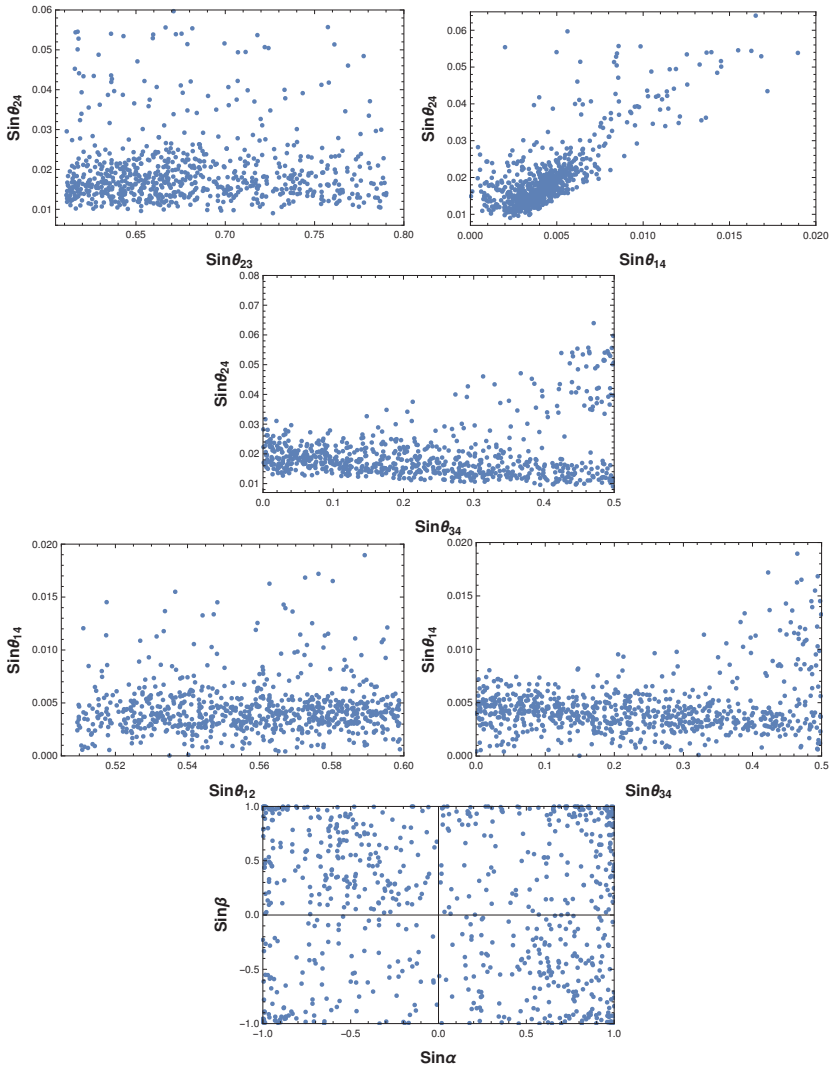

Fig. 4.8 Neutrino oscillation parameters in active-sterile sector for texture 3 zero case for NH.

$$= \begin{pmatrix} m_{ee} & m_{e\mu} & m_{e\tau} & m_{es} \\ m_{\mu e} & m_{\mu\mu} & m_{\mu\tau} & m_{\mu s} \\ m_{\tau e} & m_{\tau\mu} & m_{\tau\tau} & m_{\tau s} \\ m_{se} & m_{s\mu} & m_{s\tau} & m_{ss} \end{pmatrix}, \tag{4.24}$$

where $M_\nu^{diag} = \text{diag}(m_1, m_2, m_3, m_4)$ is the diagonal light neutrino mass matrix. For normal hierarchy (NH) of active neutrinos i.e., $m_4 > m_3 > m_2 > m_1$, the neutrino mass eigenvalues can be written in terms of the lightest neutrino mass m_1 as
$m_2 = \sqrt{m_1^2 + \Delta m_{21}^2}$, $m_3 = \sqrt{m_1^2 + \Delta m_{31}^2}$, $m_4 = \sqrt{m_1^2 + \Delta m_{41}^2}$.
Similarly for inverted hierarchy (IH) of active neutrinos i.e., $m_4 > m_2 > m_1 > m_3$, the neutrino mass eigenvalues can be written in terms of the lightest neutrino mass m_3 as
$m_1 = \sqrt{m_3^2 - \Delta m_{32}^2 - \Delta m_{21}^2}$, $m_2 = \sqrt{m_3^2 - \Delta m_{32}^2}$, $m_4 = \sqrt{m_3^2 + \Delta m_{43}^2}$.
Using these, one can analytically write down the 4×4 light neutrino mass matrix in terms of three mass squared differences, lightest neutrino mass $m_1(m_3)$, six mixing angles i.e., θ_{13}, θ_{12}, θ_{23}, θ_{14}, θ_{24}, θ_{34}, three Dirac type CP phases i.e., δ_{13}, δ_{14}, δ_{24} and three Majorana type CP phases i.e., α, β, γ. The analytical expressions of the 4×4 light neutrino mass matrix elements are given in Appendix F.

For each class of neutrino mass matrix with textures that we analyse, there exists several constraints relating the mass matrix elements or equating some of them to zero. Since the mass matrix is complex symmetric, each such constraint gives rise to two real equations that can be solved for two unknown parameters. Depending upon the number of constraints, we choose the set of input parameters and solve for the remaining ones. We have varied our input parameters for the usual three neutrino part in the 3σ allowed range as given in the global analysis of the world neutrino data [109, 166, 167] and varied Δm^2_{LSND} from 0.7 eV^2 to 2.5 eV^2. If the output of θ_{14}, θ_{24} and θ_{34} falls between 0° to 20°, 0° to 11.5° and 0° to 30° respectively [118, 168, 169] with the condition $m_1(m_3) = 0$ (as the model predicts vanishing lightest neutrino mass), then we say this texture is allowed in NH (IH). Note that according to the global analysis of the short-baseline data [118] we have $6^\circ < \theta_{14} < 20^\circ$ and $3^\circ < \theta_{24} < 11.5^\circ$ at 3σ. However the Refs. [168, 169], give only an upper limit on θ_{14} and θ_{24} as they analyse stand-alone data. Thus for a conservative approach, in our analysis we have taken the upper limits of θ_{14} and θ_{24} from the global analysis and allowed them to have lower limits as zero.

4.5 Results and Discussion

Adopting the classifications of different textures in 4×4 mass matrix not ruled out from previous studies and the method of numerical analysis discussed in the previous section we have analysed all possible mass matrices either with texture zeros or with $\mu - \tau$ symmetry in the 3×3 block. Here we show some of the numerical results we have obtained for those textures which are found to be allowed in our analysis after taking into account the $3+1$ neutrino data.

We first show the results for $\mu - \tau$ symmetric textures. Out of four different classes belonging to this type of texture we found three of them to be allowed for NH of active neutrino masses. They are namely, the subclasses (ii), (iii), (iv) of $\mu - \tau$ symmetric textures discussed earlier. It is not surprising that the texture subclass (i) is not allowed due to too many constraints (5 complex and hence 10 real constraint equations) it has, which become difficult to be satisfied simultaneously while keeping all neutrino parameters in allowed range. For IH of active neutrino masses, none of these textures are allowed. We show some correlation plots between neutrino parameters for $\mu - \tau$ symmetric subclasses (ii), (iii), (iv) with NH in Fig 4.1, 4.2, 4.3 respectively. Fig 4.1 shows the correlations between active-sterile mixing angles $\theta_{34} - \theta_{14}$ and between Majorana CP phases $\alpha - \gamma$ after the constraint equations corresponding to $\mu - \tau$ symmetric subclass (ii) were solved for 1 million random points. The resulting acceptable number of solutions is only a handful, as can be seen from the plots. The same trend is repeated for the other two subclasses (iii), (iv) as well, the correlations for which are shown in Fig 4.2, 4.3 respectively.

Among the one zero texture category, only two subclasses namely (ix), (x) with NH are allowed. The subclass (ix) has three complex constraints $M_{\mu\tau} = 0, M_{e\mu} = -M_{\mu\mu}, M_{e\tau} = -M_{\tau\tau}$ which indeed give rise to six real equations. These six real equations are solved simultaneously for six unknown parameters: three active-sterile mixing angles $(\theta_{14}, \theta_{24}, \theta_{34})$ and three CP violating Majorana phases (α, β, γ). We took the lightest neutrino mass $m_{lightest} = m_1$ to be zero as before and varied the three active neutrino mixing angles $(\theta_{12}, \theta_{13},$
$\theta_{23})$, three mass squared differences $(\Delta m^2_{21}, \Delta m^2_{31}, \Delta m^2_{41})$ and three Dirac CP violating phases $(\delta_{13}, \delta_{14}, \delta_{24})$ in their respective 3σ global fit ranges. The solution of the six real equations obtained like this give rise to a few correlation plots which are shown in Fig 4.4. Now, for the subclass (x) under texture 1 zero category, we again have three complex constraints $M_{\mu\tau} = 0, M_{e\mu} = M_{\mu\mu}, M_{e\tau} = M_{\tau\tau}$ which give rise to six real equation s. The corresponding correlation plots obtained from the solutions of these equations are shown in Fig 4.5.

Similar numerical analysis was done for two zero and three zero texture subclasses as well. Among the two zero texture subclasses only two namely, (i), (ii) with NH were found to be allowed. The subclass (i) has three complex constraints $M_{e\mu} = 0, M_{e\tau} = 0, M_{\mu\mu} = M_{\mu\tau}$ while subclass (ii) has $M_{e\mu} = 0 \quad M_{e\tau} = 0 \quad M_{\mu\mu} = -M_{\mu\tau}$. The correlations corresponding to the solutions for subclass (i), (ii) are shown in Fig 4.6, 4.7 respectively. Similarly, the three zero texture has the three complex constraint equations $M_{e\mu} = 0, M_{e\tau} = 0, M_{\mu\tau} = 0$ and the corresponding correlations are shown in Fig 4.8. As can be seen from these plots, we get more allowed solutions for two zero and three zero texture cases out of one million iterations compared to what we had obtained for $\mu - \tau$ symmetric and one zero texture cases.

4.6 Summary

To summarise, we have studied the viability of different possible textures in light neutrino mass matrix within the framework of $3+1$ light neutrino scenario by considering a A_4 flavour symmetric minimal extended seesaw mechanism.

While the minimal extended seesaw mechanism naturally explains $3+1$ light neutrino scenario in an economical way predicting the lightest neutrino to be massless, presence of the A_4 flavour symmetry dictates the flavour structure of the 4×4 light neutrino mass matrix. In addition to that, an additional discrete symmetry Z_4 is also chosen in order to forbid certain unwanted terms from the Lagrangian. Considering generic A_4 flavon alignments where a triplet flavon acquires VEV like $\langle \phi \rangle = v(n_1, n_2, n_3), n_i \in (-1, 0, 1)$, we first consider all possible combinations of such alignments and find the analytical form of the light neutrino mass matrix for each such case. For two triplet flavons taking part in generating the light neutrino mass matrix, while the other triplet alignment is kept fixed for diagonal charged lepton mass matrix, we get $1 \times 27 \times 27 = 729$ possible cases. Based on previous studies on $3+1$ neutrino textures, we first point out the disallowed textures out of these 729 mass matrices and discarded these 225 mass matrices from our analysis. From the remaining cases, we classify 96 of them as one zero texture, 64 as two zero texture, 8 as three zero texture and 296 of them as hybrid textures (which do not contain any zeros). The remaining 40 mass matrices correspond to an interesting category where the 3×3 active neutrino block of the $3+1$ light neutrino mass matrix possess $\mu - \tau$ symmetry whereas the active-sterile block breaks it explicitly.

We then analyse the mass matrices with texture zeros and $\mu - \tau$ symmetry by numerically solving the constraint equations in each case and comparing the resulting solution with the

$3+1$ neutrino data for consistency. Although there are large number of mass matrices for each such cases, they belong to a smaller number of subclasses where each subclass is a group of mass matrices giving rise to the same set of constraint equations. The number of such subclasses is 4, 12, 8 and 1 for $\mu-\tau$ symmetric, one zero, two zero and three zero texture mass matrices respectively. We therefore numerically solved the constraint equations for these 25 cases in total. We find that only 8 out of these 25 subclasses are allowed by the $3+1$ global fit data and all of them have normal hierarchical pattern of light neutrino masses. Out of these 8 allowed subclasses, 3 belong to the $\mu-\tau$ symmetric category, 2 belong to the one zero texture category, 2 belong to the two zero texture category and 1 belong to the remaining three zero texture category. We also find interesting correlation plots between different light neutrino parameters for each of these allowed subclasses. In some cases, we find a more favoured region of parameter space (within 3 σ range only) in active sterile sector with more density of points and hence more likely to be supported by the model. These preferred regions are shown in the Table 4.2. We also show the summary of allowed and disallowed cases in Table 4.3. Compared to the usual texture zero scenarios discussed in previous works, the textures in the present scenario are more constrained due to additional constraints apart from texture zero conditions or $\mu-\tau$ symmetry alone and the requirement of vanishing lightest neutrino mass. This is reflected in our results of getting only 8 out of 25 subclasses studied numerically. As we can see from the summary table, all the cases with inverted hierarchy are disfavoured. The allowed cases, however do not prefer any specific values of CP phases. We also find interesting correlations between θ_{23} and active-sterile mixing angles for the $\mu-\tau$ symmetric case. As can be seen from Fig 4.3, maximal θ_{23} seems to be disfavoured in this case. Also, lower octant values of θ_{23} favour lower values of mixing angle θ_{24}, while higher octant values of θ_{23} favour large mixing angle θ_{24}. So octant degeneracy of θ_{23} present in long baseline neutrino experiments is found to be related to the value of mixing in active sterile sector, (i.e. in mixing angle θ_{24}). On the other hand lower octant of θ_{23} seem to favour high values of mixing angle θ_{14}.

While the fate of an additional light neutrino having mass around the eV scale is yet to be confirmed by other neutrino experiments, our analysis show how difficult it is to realise such a scenario in the minimal extended seesaw if A_4 flavour symmetry with generic vacuum alignment is present. If the existence of such light sterile neutrino gets well established later, the predictions for unknown neutrino parameters obtained in our analysis can be tested for further scrutiny of the model, in a way similar to [170] where the possibility of probing texture zeros in three neutrino scenarios at neutrino oscillation experiments was studied.

Sl no.	Case	Parameter space	Range of parameter
1.	$\mu-\tau$ symmetry Fig 4.2 (case iii)	$(\theta_{14},\theta_{34})$ $(\theta_{23},\theta_{24})$ $(\theta_{23},\theta_{14})$	$0.06<\sin\theta_{14}<0.15$, $0.02<\sin\theta_{34}<0.09$. higher octant of θ_{23} is favoured for $0.02<sin\theta_{24}<0.1$ higher octant of θ_{23} is favoured for $0.05<sin\theta_{14}<0.2$
2.	$\mu-\tau$ symmetry (Fig. 4.3) (case iv)	$(\theta_{23},\theta_{24})$ $(\theta_{23},\theta_{14})$	$(0.64<\sin\theta_{23}<0.68, 0.07<\sin\theta_{24}<0.11)$, $(0.74<\sin\theta_{23}<0.78, 0.09<\sin\theta_{24}<0.19)$ $(0.64<\sin\theta_{23}<0.68, 0.15<\sin\theta_{14}<0.2)$, $(0.74<\sin\theta_{23}<0.78, 0.12<\sin\theta_{14}<0.2)$
	Texture 1 zero (Fig. 4.4) (case ix)	$(\theta_{34},\theta_{24})$ $(\theta_{13},\theta_{23})$	$(0.48<\sin\theta_{34}<0.50, 0.04<\sin\theta_{24}<0.05)$ $(0.13<\sin\theta_{13}<0.145, 0.6<\sin\theta_{23}<0.65)$
3.	Texture 2 zero (Fig. 4.6) (case i)	$(\theta_{14},\theta_{24})$	$(0.002<\sin\theta_{14}<0.016$, $0.03<\sin\theta_{24}<0.15)$
		$(\theta_{34},\theta_{14})$	$\sin\theta_{14}<0.007$ more favoured for $\sin\theta_{34}<0.3$
4.		$(\theta_{12},\theta_{14})$	$\sin\theta_{14}<0.015$ more favoured for whole 3σ range of $\sin\theta_{12}$
5.	Texture 2 zero (Fig. 4.7) (case ii)	$(\theta_{14},\theta_{24})$	$(0.002<\sin\theta_{14}<0.007$, $0.02<\sin\theta_{24}<0.06$ $\sin\theta_{14}<0.014$, $\sin\theta_{24}<0.015)$
	Texture 3 zero (Fig. 4.8)	$(\theta_{23},\theta_{24})$	$\sin\theta_{24}<0.03$ more favoured for whole 3σ range of $\sin\theta_{23}$
		$(\theta_{14},\theta_{24})$	$\sin\theta_{14}<0.008$ and $0.01<\sin\theta_{24}<0.03$
		$(\theta_{34},\theta_{24})$	$\sin\theta_{24}<0.03$ more favoured for whole 3σ range of $\sin\theta_{34}$
		$(\theta_{12},\theta_{14})$	$\sin\theta_{14}<0.008$ more favoured for whole 3σ range of $\sin\theta_{12}$
6.		$(\theta_{34},\theta_{14})$	$\sin\theta_{14}<0.008$ more favoured for whole 3σ range of $\sin\theta_{34}$

Table 4.2 Favoured region of parameter space for active sterile neutrino mixing $(3+1)$ neutrino parameters.

Texture	Subclass	Normal Hierarchy	Inverted Hierarchy
$\mu-$ τ symmetric	(i)	$\times$	$\times$
	(ii)	$\surd$	$\times$
	(iii)	$\surd$	$\times$
	(iv)	$\surd$	$\times$
One zero	(i)	$\times$	$\times$
	(ii)	$\times$	$\times$
	(iii)	$\times$	$\times$
	(iv)	$\times$	$\times$
	(v)	$\times$	$\times$
	(vi)	$\times$	$\times$
	(vii)	$\times$	$\times$
	(viii)	$\times$	$\times$
	(ix)	$\surd$	$\times$
	(x)	$\surd$	$\times$
	(xi)	$\times$	$\times$
	(xii)	$\times$	$\times$
Two zero	(i)	$\surd$	$\times$
	(ii)	$\surd$	$\times$
	(iii)	$\times$	$\times$
	(iv)	$\times$	$\times$
	(v)	$\times$	$\times$
	(vi)	$\times$	$\times$
	(vii)	$\times$	$\times$
	(viii)	$\times$	$\times$
Three zero	(i)	$\surd$	$\times$

Table 4.3 Table showing allowed and disallowed texture subclasses which have been analysed numerically. Here $(\surd)$ indicates allowed cases and $(\times)$ indicates disallowed cases.

5

Summary, Outlook and Future prospects

5.1 Summary

To summarise, in **Chapter 1**, we presented a brief review of historical background of neutrino oscillation and various processes for detection, experimental status of neutrino oscillation and neutrino cross section measurements etc.

In **Chapter 2**, we studied the importance of nuclear effects in neutrino nucleus interactions at low three momentum transfer, in quasi-elastic regime ($2 < E_\nu < 6$) GeV of neutrino energies. Various nuclear effects include Fermi motion and binding energy, Pauli blocking, random phase approximation (RPA), multi-nucleon effects, final state interaction (FSI) effect. This study was done with reference to the data taken by MINERνA experiment. We calculated double differential cross section for carbon target for some interaction channels like 2p2h/MEC and default process (QE). Since the theoretical results produced using the event generator GENIE [39], are found to show some discrepancies with the data, we used another neutrino event generator - GiBUU version 2016. We then compared our results with the data and with those reported in [39]. We find that our results are in better agreement with the MINERνA data.

In **Chapter 3**, we calculated neutrino nucleon cross section both for charged current and neutral current processes in ultra high energy regime in the energy range of $10^9 GeV \leq E_\nu \leq 10^{12} GeV$. We made use of double asymptotic limit of F_2^{ep} proton structure function of DIS (e-p) scattering in order to calculate the total cross sections $\sigma_{\nu N}^{CC}$ and $\sigma_{\nu N}^{NC}$ at UHE. Though some softwares are available for calculation of neutrino scattering cross section, we made our own computation program for this purpose. The dynamical pomeron-type behaviour of F_2^{ep} gives rise to a Reggeon exchange-type behaviour of total neutrino cross-section in UHE regime. Our results are in reasonably good agreement with other works available in literature.

In **Chapter 4**, we studied the viability of different possible textures in light neutrino mass matrix within the framework of $3+1$ light neutrino scenario by considering a A_4 flavour symmetric minimal extended seesaw mechanism. We considered A_4 flavon alignments where a triplet flavon acquires VEV like $\langle \phi \rangle = v(n_1, n_2, n_3), n_i \in (-1, 0, 1)$. We then considered all possible combinations of such alignments and found the analytical form of the light neutrino mass matrix for each such case. One of the triplet alignment is kept fixed while the other two triplet flavons take part in generating the light neutrino mass matrix, as a result we get $1 \times 27 \times 27 = 729$ possible cases. Out of the 729 cases, we discarded 225 mass matrices from our analysis (as they did not gave results within the global best fit values of the light neutrino oscillation parameters), remaining cases were classified as - one zero, two zero, three zero and hybrid textures i.e. total of 504 cases. In (3+1) neutrino scenario, texture zeros were discussed in different contexts earlier using flavour symmetries, but in this thesis we have shown that some of these textures can be realised (upto a few more constraints) just from the general vacuum alignment of A_4 triplet flavons. We then numerically analysed all the textures belonging to $(\mu - \tau)$ symmetric and texture 1, texture 2 and texture 3 zero cases by taking into account latest (3+1) neutrino data. We presented our results as correlation plots among the neutrino oscillation parameters for the allowed cases, within 3σ range of their global best fit values. We also performed same analysis for inverted hierarchy and found that none of our textures are allowed for IH. These results can be tested in future, when more data becomes available from sterile neutrino measurements.

5.2 Outlook and Conclusions of the thesis

5.2.1 Main features of the thesis

1. In Chapter 2, we made use of double asymptotic limit of the proton structure function, to estimate the neutrino-nucleon scattering cross section.
2. In Chapter 3, we used effects of nuclear environment, to study neutrino-carbon scattering in quasi-elastic range, with reference to MINERνA data, using the event generator GiBUU.
3. In Chapter 4, we studied compatibility of 3+1 scenario of neutrinos, in presence of an eV scale sterile neutrino, with A_4 discrete flavour symmetry group, and general VEV alignments of the triplet flavour field.

5.2.2 Highlights of the results

1. Chapter 2 - We presented predictions on $\nu - N$ scattering cross section in UHE range, which can be tested in future, when the data becomes available from the experiments worldwide (as stated in Chapter 1).
2. Chapter 3 - From the analysis of results of Chapter 3, we can say that including the nuclear effects (through GiBUU) improves agreement between our theoretical values and the data (in low momentum transfer region) on double differential cross section of MINERνA experiment, for neutrino scattering off Carbon target.
3. From the results presented in Chapter 4, we can pinpoint, which flavon VEV alignments are more favourable to explain the data on light neutrino mass oscillation parameters, in presence of an eV scale sterile neutrino (3+1 scenario), if A_4 group is assumed to explain the flavour structure of the fermions. This would help us gain a deeper understanding of the flavour structure, and favourable VEV alignments of the flavon field.

5.2.3 Relevance

From the highlights of the results presented above, we conclude that all the results obtained in this thesis are testable in future neutrino experiments. We addressed some important and contemporary issues in neutrino physics in this thesis - to reduce uncertainties in $\nu - N$ scattering cross section in QE regime, prediction on these cross section in UHE regime, and to build model for eV scale sterile neutrino in presence of discrete flavour symmetry. This can further help us improve our understanding of nuclear effects in $\nu - N$ scattering, which in turn could be applied in future precision measurements of unknown neutrino oscillation parameters, along with a better understanding of theories for existence of light sterile neutrino

and flavour structure of fermions. The UHE $\nu - N$ cross sections would help us gain insights into nature of fundamental interactions at energy scales which otherwise cannot be reached in terresterial experiments.

5.3 Future prospects

1. As future prospects of the work done in this thesis, we would like to continue work of Chapter 3, on ultra high energy cross section calculation. Though we found that the overall behaviour of our calculated νN cross sections both for CC and NC processes are similar to the other works available in literature, our values are slightly smaller, in the low energy range, while larger in the high energy range. With the use of screening corrections in the evolution of proton structure function, these results can be improved.
Shadowing correction to the evolution of the singlet quark distribution [171] can be written as

$$\frac{\partial xq(x,Q^2)}{\partial lnQ^2} = \frac{\partial xq(x,Q^2)}{\partial lnQ^2}\Big|_{DGLAP} - \frac{27}{160}\frac{\alpha_s^2}{R^2Q^2}[xg(x,Q^2)]^2, \tag{5.1}$$

which can be written as

$$\frac{\partial F_2(x,Q^2)}{\partial lnQ^2} = \frac{\partial F_2(x,Q^2)}{\partial lnQ^2}\Big|_{DGLAP} - \frac{5}{18}\frac{27\alpha_s^2}{R^2Q^2}[xg(x,Q^2)]^2, \tag{5.2}$$

where the first term is the standard DGLAP evolution equation and the value of R is the correlation radius between two interacting gluons. Putting Eq (3.10) in Eq (5.2) we get

$$\frac{\partial F_2(x,Q^2)}{\partial lnQ^2} = \frac{10\alpha_s}{9\pi}\frac{(1-x)^2}{(1-1.5x)}G(2x\frac{(1-1.5x)}{(1-x^2)},Q^2) - \frac{5}{18}\frac{27\alpha_s^2}{R^2Q^2}[G(x,Q_2)]^2, \tag{5.3}$$

here $q(x,Q_2)$ is the quark density and $g(x,Q_2)$ is the gluon density distribution functions. Here, the representation for the gluon distribution $G(x,Q_2) = xg(x,Q_2)$ is used.
Integrating above Eq (5.3), we get

$$\int dF_2(x,Q^2) = \int [\frac{10\alpha_s}{9\pi}\frac{(1-x)^2}{(1-1.5x)}G(2x\frac{(1-1.5x)}{(1-x^2)},Q^2) - \frac{5}{18}\frac{27\alpha_s^2}{R^2Q^2}[G(x,Q_2)]^2]dlnQ^2. \tag{5.4}$$

Once the value of $F_2(x,Q^2)$ is found out from above equation, the total $\nu - N$ scattering cross section can be calculated from Eq (3.13). We expect that inclusion of screening corrections in proton structure function $F_2(x,Q^2)$ will improve the results both for CC and NC process $\nu - N$ cross section.

2. We also aim to continue our work on Chapter 2, where we would calculate double differential cross section for neutrino carbon interaction using random phase approximation (RPA) effects with 2p2h/ MEC process. Using such nuclear effects we expect that our double differential cross section results would be in good agreement with the available MINERνA experimental data. We would do such analysis using both the generators i.e. GENIE and GiBUU.

References

[1] Corey Adams et al., (LBNE Collaboration) BNL-101354-2014-JA, FERMILAB-PUB-14-022, LA-UR-14-20881, arxiv: 1307.7335.

[2] Kenneth S. Krane, *Introductory Nuclear Physics* (John Wiley and Sons).

[3] S.L. Kakani and Shubra Kakani, *Nuclear and Particle Physics* (Viva Books).

[4] Carlo Guinti and Chung W. Kim, *Fundamental of Neutrino Physics and Astrophysics* (Oxford University Press).

[5] David Griffiths, *Introduction to Elementary Particles* (Willey-VCH Verlag GmbH & Co. KGaA).

[6] K. Heyde, *Basic Ideas and Concepts in Nuclear Physics* (IOP Publishing Ltd).

[7] E. D. Commins and P. H. Bucksbaum, *Weak Interactions of leptons and quarks* (Cambridge University Press).

[8] R. Davis, J. C. Evans and B. Cleveland, Conference Proceedings, Purdue University, Lafayette, Ind, 1978.

[9] B. T. Cleveland et al., J. Astrophy., **496**, 505–526, (1998).

[10] J. N. Bahcall, M. H. Pinsonneault, and S. Basu, Astrophys. J., **555**, 990–1012, astro-ph/0010346 (2001).

[11] J. N. Bahcall, N. A. Bahcall and G. Shaviv, Phys. Rev. Lett., **20**, 1209–1212, (1968).

[12] Y. Fukuda et al. (Super-Kamiokande Collaboration), Phys.Rev.Lett. **81**, 1562 (1998).

[13] Q. R. Ahmad et al, (SNO Collaboration), Phys. Rev. Lett. **87**, 071301 (2001).

[14] K. Kodama et al, (DONOUT Collaboration), Phys. Lett. B**504**, 218 (2001).

[15] A. Aguilar et al., (LSND), Phys. Rev.D **64**, 112007 (2001).

[16] A. A. Aguilar-Arevalo et al., (MiniBooNE Collaboration), Phys. Rev.Lett.**110**, 161801 (2013).

[17] M. A. Acero, C. Guinti, M. Laveder, Phys.Rev.D **78**, 073009 (2008).

[18] C. Giunti, M. Laveder, Phys. Rev. C **83**, 065504 (2011).

[19] Takaaki Kajita, Advances in High Energy Physics Volume **2012**, Article ID 504715, 24 pages.

[20] T. P. Cheng and L. F. Li, *Gauge theory of elementary particle physics* (Oxford University Press).

[21] S. P. Mikheev, A. Yu. Smirnov, J. Nucl. Phys., **42**:913917, (1985).

[22] L. Wolfenstein, Phys. Rev., D**17**: 23692374, (1978).

[23] J.M. Conrad and M.H.Shaevitz, arXiv: 1609.07803v1.

[24] Kalpana Bora, Debajyoti Dutta and Pomita Ghoshal, JHEP **12** 025 (2012).

[25] Osamu Yasuda, arXiv: 1004.2388v1.

[26] G. Bellini et al. (Borexino Collaboration), Phys. Rev. D **82**, 033006 (2010).

[27] S. Abe et al. (KamLAND Collaboration), Phys. Rev. C **84**, 035804 (2011).

[28] M. Anderson et al., PRD **99**, 012012 (2019).

[29] Jen-Chieh Peng, Rep. Prog. Phys. **82** 036201 (2019).

[30] Feng Peng An et al., Phys. Rev. Lett., **116**(6):061801 (2016).

[31] F. An, et al., (Daya-Bay Collaboration), Phys. Rev. Lett. **108** 171803 (2012).

[32] Y. Abe, et al., (Double-Chooz Collaboration) Phys. Rev. Lett. **108** 131801 (2012).

[33] J. Ahn, et al., RENO Collaboration, Phys. Rev. Lett. **108** (2012) 191802 (2012).

[34] H.Zhang, Physics Letters B **714** 262-266 (2012).

[35] M.S. Atthar, Talk presented at Nu HoriZon 2016.

[36] J. A. Formaggio and G. P. Zeller, Rev. Mod. Phys. **84**, 1307 (2012).

[37] V. Lyubushkin, et al., Eur. Phys. J. C **63**, 355 (2009).

[38] Pilar Coloma et al., Phys. Rev. D **89**, 073015 (2014)

[39] P.A. Rodrigues et al., PRL **116**, 071802 (2016).

[40] Tappei Katori and Marco Martini, arXiv hep/ 1611.07770v1.

[41] M.G. Aartsen et al., Phys. Rev. Lett. **113**, 101101 (2014).

[42] M. G. Aartsen, R. Abbasi et al., IceCube Collaboration, Phys. Rev. Lett. **111**, 021103 (2013).

[43] K. Antipin, et al., Nucl. Phys. B, Proc. Suppl. **168** 296 (2007).

[44] V. Aynutdinov et al., in *Proceedings of the 3rd International Workshop on a Very Large Volume Neutrino Telescope for the Mediterranean Sea* Vol 14, pp. 602 (2009).

[45] E. Aslanides et al., (ANTARES), arXiv:astro-ph/9907432, (2009).

[46] A. Achterberg et al., Phys. Rev. D **75**, 102001 (2007).

[47] I. Kravchenko et al., Astropart. Phys. **20**, 195 (2003).

[48] S. W. Barwick et al., (ANITA) Phys. Rev. Lett. **96**, 171101 (2006).

[49] R. U. Abbasi et al. (High Resolution Flys Eye Collaboration) Phys. Rev. Lett.**92** 151101 (2004).

[50] P. W. Gorham et al., Phys. Rev. Lett. **93**, 041101 (2004).

[51] Teppei Katori, Journal of Physics: Conference Series **598** 012006 (2015), and references therein.

[52] S. K. Agarwalla, S. S. Chatterjee and Antonio Palazzo, JHEP **04** 091 (2018) .

[53] S. Choubey, D. Dutta and D. Pramanik, Phys. Rev. D **96**, 056026 (2017).

[54] K. Abe, R. Akutsu, A. Ali, (T2K Collaboration) arXiv: 1902.06529v1.

[55] Igor Krasnov, arXiv: 1902.06099v1.

[56] B. J. P. Jones Proceeding for the VLVNT2018 Conference (IceCube Collaboration), arXiv: 1902.06185.

[57] Carlo Giunti and Thierry Lasserre, Submitted for publication in the Annual Review of Nuclear and Particle Science, Volume 69, arXiv: 1901.08330.

[58] Alan M. Knee, Dagoberto Contreras, Douglas Scott, arxiv : 1812.02102v2.

[59] Susanne Mertens et al., arXiv: 1810.06711.

[60] P. Adamson et al., (MINOS+ Collaboration) Phys. Rev. Lett. **122**, 091803 (2019).

[61] F. Capozzi et al., Nucl. Phys. B **908** 218 (2016).

[62] N. Nath, M. Ghosh, S. Goswami and S. Gupta, JHEP **1703**, 075 (2017) [arXiv:1610.09090 [hep-ph]].

[63] Costas Andreopoulos et al., arXiv [hep-ph]/1510.05494v1.

[64] O. Buss et al., Physics Reports **512** 1-124 (2012).

[65] O. Buss et al. Phys.Rept. **512** 1 (2012).

[66] U. Mosel, Ann. Rev. Nuc. Part. Sci. **66** 1–26, (2016).

[67] Ulrich Mosel, Annual Review of Nuclear and Particle Science volume **66** (2016).

[68] Andrew Furmanski, Ph.D Thesis, The University of Warwick (2015).

[69] M. Betancourt et al., TENSIONS2016 report, arXiv: 1805.07378.

[70] D. Casper, Nucl. Phys. Proc. Suppl. **112**, 161 (2002).

[71] Y. Hayato, Acta Phys. Polon. B**40**, 2477 (2009).

[72] L. Alvarez-Ruso, Y. Hayato and J. Nieves, New J. Phys. 16 075015 (2014).

[73] C. H. Llewellyn Smith. *Neutrino reactions at accelerator energies* Physics Reports, **3**(5):261 – 379, (1972), ISSN 0370-1573.

[74] Teppei Katori, *Proceedings of the 8th International Workshop on Neutrino-Nucleus Interactions in the Few-GeV Region (NuInt12)* arXiv: 1304.6014 (2012).

[75] http://link.aps.org/supplemental/10.1103/PhysRevLett.**116**.071802.

[76] K. Gallmeister, U. Mosel, J. Weil, Phys. Rev. C **94**, 035502 (2016).

[77] A.D. Avrorin, et al., Astropart. Phys. **62** 12-20 (2015).

[78] S. Hoover, et al., (ANITA Collaboration), Journal of Physics: Conference Series **81** 012009 (2007).

[79] I. Kravchenko, et al., (RICE Collaboration), Phys. Rev. D**85** 062004 (2012).

[80] J. Ahrens, et al., (AMANDA Collaboration), Nucl. Inst. Meth. A**524** 169 (2004).

[81] R. Abbasi, et al., (HiRes Collaboration), Ap. J. **684** 790 (2008).

[82] A.Gleixner, et al., (ANTARES Collaboration), EPJ Web of Conferences **70** 00070 (2014).

[83] M. Aartsen, et al.,(IceCube Collaboration) Phys. Rev. Lett. **113**, 101101 (2014).

[84] P. Gorham, et al., (GLUE Collaboration), Phys. Rev. Lett. **93** (2004) 041101.

[85] A. Aab, et al., (Pierre Auger Collaboration), Phys. Rev. D**93** 072006 (2016).

[86] Stuart A. Kleinfelder (ARIANNA Collaboration) *Presented at the 2015 IEEE Nuclear Science Symposium*, arXiv: 1511.07525.

[87] Andreas Haungs, et al.,(JEM-EUSO collaboration), Journal of Physics: Conference Series, vol **632** 012092, arXiv : 1504.02593.

[88] R. Gandhi, et al., Phys. Rev. D**58** 093009 (1998).

[89] A. Connolly, et al., Phys. Rev. D**83** 113009 (2011), arXiv: 1102.0691.

[90] A. Cooper-Sarkar, et al., JHEP **08** 042 (2011), arXiv:1106.3723.

[91] Martin M. Block, et al., Phys. Rev. D**88** 013003 (2013), arXiv:1302.6127.

[92] Kalpana Bora, Neelakshi Sarma, *Springer Conference Proceedings* vol **174** 345-351 (2015).

[93] F. E. Close, *An Introduction to Quarks and Partons* (Academic Press) (1979).

[94] Kalpana Bora, PhD Thesis *Polarised and unpolarised structure functions of nucleons at low - x*, Gauhati University, (1998).

[95] P. D. B Collins, *Introduction to Regge Theory and High Energy Physics* (Cambridge University Press) (1977).

[96] M. Kuroda, D. Schildknecht, Phys. Rev. D**88** 053007 (2013) .

[97] S. Fukuda et al. (Super-Kamiokande), Phys. Rev. Lett. **86**, 5656 (2001), hep-ex/0103033.

[98] Q. R. Ahmad et al. (SNO), Phys. Rev. Lett. **89**, 011301 (2002), nucl-ex/0204008.

[99] Q. R. Ahmad et al. (SNO),Phys. Rev. Lett. **89**, 011302 (2002), nucl-ex/0204009.

[100] J. N. Bahcall and C. Pena-Garay, New J. Phys. **6**, 63 (2004), hep-ph/0404061.

[101] K. Nakamura et al., J. Phys. **G37**, 075021 (2010).

[102] S. Abe et al. (KamLAND Collaboration), Phys.Rev.Lett. **100**, 221803 (2008).

[103] P. Adamson et al. (MINOS), Phys.Rev.Lett. **110**, 171801 (2013)

[104] K. Abe et al. [T2K Collaboration], Phys. Rev. Lett. **107**, 041801 (2011), [arXiv:1106.2822 [hep-ex]].

[105] D. S. Ayres *et al.* [NOvA Collaboration], hep-ex/0503053.

[106] Y. Abe et al., Phys. Rev. Lett. **108**, 131801 (2012), [arXiv:1112.6353 [hep-ex]].

[107] F. P. An et al. [DAYA-BAY Collaboration], Phys. Rev. Lett. **108**, 171803 (2012), [arXiv:1203.1669 [hep-ex]].

[108] J. K. Ahn et al. [RENO Collaboration], Phys. Rev. Lett. **108**, 191802 (2012), [arXiv:1204.0626][hep-ex]].

[109] I. Esteban, M. C. Gonzalez-Garcia, M. Maltoni, I. Martinez-Soler and T. Schwetz, JHEP **01**, 087 (2017).

[110] C. Athanassopoulos *et al.* [LSND Collaboration], Phys. Rev. Lett. **77**, 3082 (1996) [nucl-ex/9605003].

[111] A. Aguilar-Arevalo *et al.* [LSND Collaboration], Phys. Rev. **D64**, 112007 (2001) [hep-ex/0104049].

[112] A. A. Aguilar-Arevalo *et al.* [MiniBooNE Collaboration], Phys. Rev. Lett. **110**, 161801 (2013) [arXiv:1303.2588 [hep-ex]].

[113] G. Mention, M. Fechner, T. Lasserre, T. A. Mueller, D. Lhuillier, M. Cribier and A. Letourneau, Phys. Rev. **D83**, 073006 (2011) [arXiv:1101.2755 [hep-ex]].

[114] M. A. Acero, C. Giunti and M. Laveder, Phys. Rev. **D78**, 073009 (2008) [arXiv:0711.4222 [hep-ph]].

[115] C. Giunti and M. Laveder, Phys. Rev. **C83**, 065504 (2011) [arXiv:1006.3244 [hep-ph]].

[116] A. A. Aguilar-Arevalo *et al.* [MiniBooNE Collaboration], [arXiv:1805.12028[hep-ex]].

[117] M. Tanabashi *et al.* [Particle Data Group], Phys. Rev. **D98**, 030001 (2018).

[118] J. Kopp, P. A. N. Machado, M. Maltoni and T. Schwetz, JHEP **1305**, 050 (2013) [arXiv:1303.3011 [hep-ph]].

[119] C. Giunti, M. Laveder, Y. F. Li and H. W. Long, Phys. Rev. **D88**, 073008 (2013) [arXiv:1308.5288 [hep-ph]].

[120] S. Gariazzo, C. Giunti, M. Laveder, Y. F. Li and E. M. Zavanin, J. Phys. **G43**, 033001 (2016) [arXiv:1507.08204 [hep-ph]].

[121] M. Dentler, A. Hernandez-Cabezudo, J. Kopp, P. A. N. Machado, M. Maltoni, I. Martinez-Soler and T. Schwetz, JHEP bf 08, 010 (2018), [arXiv:1803.10661[hep-ph]].

[122] N. Aghanim *et al.* [Planck Collaboration], [arXiv:1807.06209 [astro-ph.CO]].

[123] X. Chu, B. Dasgupta, M. Dentler, J. Kopp and N, Saviano, [arXiv:1806.10629 [hep-ph]].

[124] P. Minkowski, Phys. Lett. B **67**, 421 (1977).

[125] M. Gell-Mann, P. Ramond, and R. Slansky (1980), print-80-0576 (CERN).

[126] T. Yanagida (1979), in Proceedings of the Workshop on the Baryon Number of the Universe and Unified Theories, Tsukuba, Japan, 13-14 Feb 1979.

[127] R. N. Mohapatra and G. Senjanovic, Phys. Rev. Lett **44**, 912 (1980).

[128] J. Schechter and J. W. F. Valle, Phys. Rev. **D22**, 2227 (1980).

[129] R. N. Mohapatra and G. Senjanovic, Phys. Rev. D**23**, 165 (1981).

[130] G. Lazarides, Q. Shafi and C Wetterich, Nucl. Phys. B**181**, 287 (1981).

[131] C. Wetterich, Nucl. Phys. B**187**, 343 (1981).

[132] J. Schechter and J. W. F. Valle, Phys. Rev. D**25**, 774 (1982).

[133] B. Brahmachari and R. N. Mohapatra, Phys. Rev. D**58**, 015001 (1998).

[134] R. N. Mohapatra, Nucl. Phys. Proc. suppl. **138**, 257 (2005).

[135] S. Antusch and S. F. King, Phys. Lett. B**597**, (2), 199 (2004).

[136] R. Foot, H. Lew, X. G. He and G. C. Joshi, Z. Phys. C**44**, 441 (1989).

[137] A. Merle and V. Niro, JCAP **1107**, 023 (2011) [arXiv:1105.5136 [hep-ph]].

[138] J. Barry, W. Rodejohann and H. Zhang, JHEP **1107**, 091 (2011) [arXiv:1105.3911 [hep-ph]].

[139] H. Zhang, Phys. Lett. B**714**, 262 (2012) [arXiv:1110.6838 [hep-ph]].

[140] J. Barry, W. Rodejohann and H. Zhang, JCAP **1201**, 052 (2012) [arXiv:1110.6382 [hep-ph]].

[141] J. Heeck and H. Zhang, JHEP **1305**, 164 (2013) [arXiv:1211.0538 [hep-ph]].

[142] P. S. Bhupal Dev and A. Pilaftsis, Phys. Rev. D **87**, no. 5, 053007 (2013) [arXiv:1212.3808 [hep-ph]].

[143] Y. Zhang, X. Ji and R. N. Mohapatra, JHEP **1310**, 104 (2013) [arXiv:1307.6178 [hep-ph]].

[144] M. Frank and L. Selbuz, Phys. Rev. D **88**, 055003 (2013) [arXiv:1308.5243 [hep-ph]].

[145] D. Borah and R. Adhikari, Phys. Lett. B**729**, 143 (2014) [arXiv:1310.5419 [hep-ph]].

[146] R. Adhikari, D. Borah and E. Ma, Phys. Lett. B**755**, 414 (2016) [arXiv:1512.05491 [hep-ph]].

[147] D. Borah, M. Ghosh, S. Gupta, S. Prakash and S. K. Raut, Phys. Rev. **9D4**, no. 11, 113001 (2016) [arXiv:1606.02076 [hep-ph]].

[148] D. Borah, Phys. Rev. D**94**, 075024 (2016).

[149] D. Borah, M. Ghosh, S. Gupta and S. K. Raut, Phys. Rev. D **96**, no. 5, 055017 (20167) [arXiv:1706.02017 [hep-ph]].

[150] D. Borah, Phys. Rev. D**95**, 035016 (2017).

[151] P. Das, A. Mukherjee and M. K. Das, [arXiv:1805.09231[hep-ph]].

[152] M-C. Chen, J. Huang, J-M. O'Bryan, A. M. Wijangco and F. Yu, JHEP **1302**, 021 (2013).

[153] R. Kalita and D. Borah, Phys. Rev. D**92**, 055012 (2015).

[154] M. Ghosh, S. Goswami and S. Gupta, JHEP **1304**, 103 (2013) [arXiv:1211.0118 [hep-ph]].

[155] M. Ghosh, S. Goswami, S. Gupta and C. S. Kim, Phys. Rev. D**88**, no. 3, 033009 (2013) [arXiv:1305.0180 [hep-ph]].

[156] Y. Zhang, Phys. Rev. D**87**, no. 5, 053020 (2013) [arXiv:1301.7302 [hep-ph]].

[157] N. Nath, M. Ghosh and S. Gupta, Int. J. Mod. Phys. A**31**, no. 24, 1650132 (2016) [arXiv:1512.00635 [hep-ph]].

[158] R. N. Mohapatra, S. Nasri and H. -B. Yu, Phys. Rev. D**72**, 033007 (2005).

[159] J. Barry, W. Rodejohann and H. Zhang, JHEP **1107**, 091 (2011); J. Barry, W. Rodejohann and H. Zhang, JCAP **01**, 052 (2012).

[160] A. Merle, S. Morisi and W. Winter, JHEP **1407**, 039 (2014).

[161] D. C. Rivera-Agudelo and A. Perez-Lorenzana, Phys. Rev. D**92**, 073009 (2015).

[162] G. Altarelli and F. Feruglio, Nucl. Phys. B**741**, 215 (2006).

[163] F. Feruglio, C. Hagedorn and L. Merlo, JHEP **1003**, 084 (2010).

[164] M. Holthausen and M. A. Schmidt, JHEP **1201**, 126 (2012).

[165] S. Gariazzo C. Giunti, M. Laveder and Y.F. Li, JHEP **1706**, 135 (2017).

[166] D. V. Forero, M. Tortola and J. W. F. Valle, Phys. Rev. D**90**, no. 9, 093006 (2014) [arXiv:1405.7540 [hep-ph]].

[167] F. Capozzi, G. L. Fogli, E. Lisi, A. Marrone, D. Montanino and A. Palazzo, Phys. Rev. D**89**, 093018 (2014) [arXiv:1312.2878 [hep-ph]].

[168] F. P. An *et al.* [Daya Bay Collaboration], Phys. Rev. Lett. **113**, 141802 (2014) [arXiv:1407.7259 [hep-ex]].

[169] P. Adamson *et al.* [MINOS Collaboration], Phys. Rev. Lett. **107**, 011802 (2011) [arXiv:1104.3922 [hep-ex]].

[170] K. Bora, D. Borah and D. Dutta, Phys. Rev. D**96**, 075006 (2017).

[171] G. R. Boroun, Physical Review C **97**, 015206 (2018).

A

A_4 product rules

A_4, the symmetry group of a tetrahedron, is a discrete non-abelian group of even permutations of four objects. It has four irreducible representations: three one-dimensional and one three dimensional which are denoted by $\mathbf{1}, \mathbf{1}', \mathbf{1}''$ and $\mathbf{3}$ respectively, being consistent with the sum of square of the dimensions $\sum_i n_i^2 = 12$. Their product rules are given as

$$\mathbf{1} \otimes \mathbf{1} = \mathbf{1}$$

$$\mathbf{1}' \otimes \mathbf{1}' = \mathbf{1}''$$

$$\mathbf{1}' \otimes \mathbf{1}'' = \mathbf{1}$$

$$\mathbf{1}'' \otimes \mathbf{1}'' = \mathbf{1}'$$

$$\mathbf{3} \otimes \mathbf{3} = \mathbf{1} \oplus \mathbf{1}' \oplus \mathbf{1}'' \oplus \mathbf{3_a} \oplus \mathbf{3_s}$$

where a and s in the subscript corresponds to anti-symmetric and symmetric parts respectively. Denoting two triplets as (a_1, b_1, c_1) and (a_2, b_2, c_2) respectively, their direct product can be decomposed into the direct sum mentioned above as

$$\mathbf{1} \backsim \mathbf{a_1 a_2} + \mathbf{b_1 c_2} + \mathbf{c_1 b_2}$$

$$\mathbf{1}' \backsim \mathbf{c_1 c_2} + \mathbf{a_1 b_2} + \mathbf{b_1 a_2}$$

$$\mathbf{1}'' \backsim \mathbf{b_1 b_2} + \mathbf{c_1 a_2} + \mathbf{a_1 c_2}$$

$$\mathbf{3_s} \backsim (\mathbf{2a_1 a_2} - \mathbf{b_1 c_2} - \mathbf{c_1 b_2}, \mathbf{2c_1 c_2} - \mathbf{a_1 b_2} - \mathbf{b_1 a_2}, \mathbf{2b_1 b_2} - \mathbf{a_1 c_2} - \mathbf{c_1 a_2})$$

$$\mathbf{3_a} \backsim (\mathbf{b_1 c_2} - \mathbf{c_1 b_2}, \mathbf{a_1 b_2} - \mathbf{b_1 a_2}, \mathbf{c_1 a_2} - \mathbf{a_1 c_2})$$

B

Scalar Potential for Triplet Flavons ϕ, ϕ' ϕ''

The scalar potential for the most general case containing all the three triplet vevs, ϕ , ϕ' and ϕ'' can be written as

$$V = V(\phi) + V(\phi') + V(\phi'') + V_{\rm int}$$

where

$$V(\phi) = -\mu_1^2(\phi^\dagger\phi) + \lambda_1(\phi^\dagger\phi)^2,$$
$$V(\phi') = -\mu_2^2(\phi'^\dagger\phi') + \lambda_2(\phi'^\dagger\phi')^2,$$
$$V(\phi'') = -\mu_3^2(\phi''^\dagger\phi'') + \lambda_3(\phi''^\dagger\phi'')^2,$$

and the interaction among different triplet flavons are denoted as

$$V_{\rm int} = (\mu_4\phi'^2\phi'' + \mu_5\phi\phi''^2 + \text{h.c.}) + \lambda_4(\phi^\dagger\phi)(\phi'^\dagger\phi') + \lambda_5(\phi^\dagger\phi)(\phi''^\dagger\phi'') + \lambda_6(\phi'^\dagger\phi')(\phi''^\dagger\phi'') + \{\lambda_7(\phi\phi^{''})(\phi^{'}\phi^{'}) + \text{h.c.}\} \quad \text{(B.1)}$$

Expanding the triplet flavons in terms of components
$\phi = (\phi_1, \phi_2, \phi_3)$ $\quad \phi' = (\phi_1', \phi_2', \phi_3')$ $\quad \phi'' = (\phi_1'', \phi_2'', \phi_3'')$

we can write their products according to the A_4 product rules as

$$(\phi\phi^{''})_1 = (\phi_1\phi_1'' + \phi_2\phi_3'' + \phi_3\phi_2'')$$

$$(\phi'\phi^{'})_1 = (\phi_1'\phi_1' + \phi_2'\phi_3' + \phi_3'\phi_2')$$

$$(\phi\phi^{''})_{1'} = (\phi_3\phi_3'' + \phi_1\phi_2'' + \phi_2\phi_1'')$$

$$(\phi'\phi^{'})_{1''} = (\phi_2'\phi_2' + \phi_3'\phi_1' + \phi_1'\phi_3')$$

$$(\phi\phi'')_{3s} = (2\phi_1\phi_1'' - \phi_2\phi_3'' - \phi_3\phi_2'',\quad 2\phi_3\phi_3'' - \phi_1\phi_2'' - \phi_2\phi_1'',\quad 2\phi_2\phi_2'' - \phi_1\phi_3'' - \phi_3\phi_1'')$$

$$(\phi'\phi')_{3s} = (2\phi_1'\phi_1' - \phi_2'\phi_3' - \phi_3'\phi_2',\quad 2\phi_3'\phi_3' - \phi_1'\phi_2' - \phi_2'\phi_1',\quad 2\phi_2'\phi_2' - \phi_1'\phi_3' - \phi_3'\phi_1')$$

$$\begin{aligned}(\phi\phi'')_3 \times (\phi'\phi')_3 = {} & (2\phi_1\phi_1'' - \phi_2\phi_3'' - \phi_3\phi_2'') \times (2\phi_1'\phi_1' - \phi_2'\phi_3' - \phi_3'\phi_2') + \\ & (2\phi_3\phi_3'' - \phi_1\phi_2'' - \phi_2\phi_1'') \times (2\phi_2'\phi_2' - \phi_1'\phi_3' - \phi_3'\phi_1') \\ & + (2\phi_2\phi_2'' - \phi_1\phi_3'' - \phi_3\phi_1'') \times (2\phi_3'\phi_3' - \phi_1'\phi_2' - \phi_2'\phi_1'). \end{aligned} \tag{B.2}$$

The other products can similarly be written in component forms. For an illustrative purpose, we consider the minimisation of a single triplet flavon ϕ'. The potential for this flavon in component form can be written as

$$\begin{aligned} V(\phi') = {} & -\mu_2^2(\phi_1'^{\dagger}\phi_1' + \phi_2'^{\dagger}\phi_3' + \phi_3'^{\dagger}\phi_2') + \lambda_2[(\phi_1'^{\dagger}\phi_1' + \phi_2'^{\dagger}\phi_3' + \phi_3'^{\dagger}\phi_2')^2 + (\phi_3'^{\dagger}\phi_3' + \phi_1'^{\dagger}\phi_2' + \phi_2'^{\dagger}\phi_1') \\ & \times (\phi_2'^{\dagger}\phi_2' + \phi_3'^{\dagger}\phi_1' + \phi_1'^{\dagger}\phi_3') + (2\phi_1'^{\dagger}\phi_1' - \phi_2'^{\dagger}\phi_3' - \phi_3'^{\dagger}\phi_2')^2 + 2(2\phi_3'^{\dagger}\phi_3' - \phi_1'^{\dagger}\phi_2' - \phi_2'^{\dagger}\phi_1') \\ & \times (2\phi_2'^{\dagger}\phi_2' - \phi_1'^{\dagger}\phi_3' - \phi_3'^{\dagger}\phi_1')] \end{aligned} \tag{B.3}$$

The minimisation conditions are given as

$$\begin{aligned} \frac{\partial V(\phi')}{\partial \phi_1^{'}} = {} & -\mu_2^2\phi_1^{'\dagger} + \lambda_2[2\phi_1^{'\dagger}(\phi_1'^{\dagger}\phi_1' + \phi_2'^{\dagger}\phi_3' + \phi_3'^{\dagger}\phi_2') + \phi_2^{'\dagger}(\phi_2'^{\dagger}\phi_2' + \phi_3'^{\dagger}\phi_1' + \phi_1'^{\dagger}\phi_3') \\ & + \phi_3^{'\dagger}(\phi_3'^{\dagger}\phi_3' + \phi_1'^{\dagger}\phi_2' + \phi_2'^{\dagger}\phi_1') + 4\phi_1^{'\dagger}(2\phi_1'^{\dagger}\phi_1' - \phi_2'^{\dagger}\phi_3' - \phi_3'^{\dagger}\phi_2') - 2\phi_2^{'\dagger} \\ & (2\phi_2'^{\dagger}\phi_2' - \phi_1'^{\dagger}\phi_3' - \phi_3'^{\dagger}\phi_1') - 2\phi_3^{'\dagger}(2\phi_3'^{\dagger}\phi_3' - \phi_1'^{\dagger}\phi_2' - \phi_2'^{\dagger}\phi_1')] = 0 \end{aligned} \tag{B.4}$$

$$\begin{aligned} \frac{\partial V(\phi')}{\partial \phi_2^{'}} = {} & -\mu_2^2\phi_3^{'\dagger} + \lambda_2[2\phi_3^{'\dagger}(\phi_1'^{\dagger}\phi_1' + \phi_2'^{\dagger}\phi_3' + \phi_3'^{\dagger}\phi_2') + \phi_1^{'\dagger}(\phi_2'^{\dagger}\phi_2' + \phi_3'^{\dagger}\phi_1' + \phi_1'^{\dagger}\phi_3') \\ & + \phi_2^{'\dagger}(\phi_3'^{\dagger}\phi_3' + \phi_1'^{\dagger}\phi_2' + \phi_2'^{\dagger}\phi_1') - 2\phi_3^{'\dagger}(2\phi_1'^{\dagger}\phi_1' - \phi_2'^{\dagger}\phi_3' - \phi_3'^{\dagger}\phi_2') - 2\phi_1^{'\dagger} \\ & (2\phi_2'^{\dagger}\phi_2' - \phi_1'^{\dagger}\phi_3' - \phi_3'^{\dagger}\phi_1') + 4\phi_2^{'\dagger}(2\phi_3'^{\dagger}\phi_3' - \phi_1'^{\dagger}\phi_2' - \phi_2'^{\dagger}\phi_1')] = 0 \end{aligned} \tag{B.5}$$

$$\frac{\partial V(\phi')}{\partial \phi_3'} = -\mu_2^2 \phi_2'^{\dagger} + \lambda_2[2\phi_2'^{\dagger}(\phi_1'^{\dagger}\phi_1' + \phi_2'^{\dagger}\phi_3' + \phi_3'^{\dagger}\phi_2') + \phi_3'^{\dagger}(\phi_2'^{\dagger}\phi_2' + \phi_3'^{\dagger}\phi_1' + \phi_1'^{\dagger}\phi_3')$$
$$+ \phi_1'^{\dagger}(\phi_3'^{\dagger}\phi_3' + \phi_1'^{\dagger}\phi_2' + \phi_2'^{\dagger}\phi_1') - 2\phi_2'^{\dagger}(2\phi_1'^{\dagger}\phi_1' - \phi_2'^{\dagger}\phi_3' - \phi_3'^{\dagger}\phi_2') + 4\phi_3'^{\dagger}$$
$$(2\phi_2'^{\dagger}\phi_2' - \phi_1'^{\dagger}\phi_3' - \phi_3'^{\dagger}\phi_1') - 2\phi_1'^{\dagger}(2\phi_3'^{\dagger}\phi_3' - \phi_1'^{\dagger}\phi_2' - \phi_2'^{\dagger}\phi_1')] = 0 \quad \text{(B.6)}$$

A few of the solutions we obtained from the above minimisation conditions are as follows.

1) $\phi_1' \to 0, \phi_2' \to 0, \phi_3' \to 0$

2) $\phi_1' \to 0, \phi_2' \to -\frac{i\sqrt{\mu_2^2}}{\sqrt{17}\sqrt{\lambda_2}}, \phi_3' \to \frac{i\sqrt{\mu_2^2}}{\sqrt{17}\sqrt{\lambda_2}} \implies \phi' = -\frac{i\sqrt{\mu_2^2}}{\sqrt{17}\sqrt{\lambda_2}}(0,1,-1)$

3) $\phi_1' \to 0, \phi_2' \to \frac{i\sqrt{\mu_2^2}}{\sqrt{17}\sqrt{\lambda_2}}, \phi_3' \to -\frac{i\sqrt{\mu_2^2}}{\sqrt{17}\sqrt{\lambda_2}} \implies \phi' = -\frac{i\sqrt{\mu_2^2}}{\sqrt{17}\sqrt{\lambda_2}}(0,-1,1)$

4)$\phi_1' \to -\frac{\sqrt{\mu_2^2}}{2\sqrt{3}\sqrt{\lambda_2}}, \phi_2' \to -\frac{\sqrt{\mu_2^2}}{2\sqrt{3}\sqrt{\lambda_2}}, \phi_3' \to -\frac{\sqrt{\mu_2^2}}{2\sqrt{3}\sqrt{\lambda_2}} \implies \phi' = -\frac{\sqrt{\mu_2^2}}{2\sqrt{3}\sqrt{\lambda_2}}(1,1,1)$

5) $\phi_1' \to -\frac{\sqrt{\mu_2^2}}{\sqrt{10}\sqrt{\lambda_2}}, \phi_2' \to 0, \phi_3' \to 0 \implies \phi' = -\frac{\sqrt{\mu_2^2}}{\sqrt{10}\sqrt{\lambda_2}}(1,0,0)$

C

Vacuum alignment of flavon fields ϕ', ϕ'' of allowed cases

Sl no.	$\phi^{'}$	$\phi^{''}$
1.	$(0,1,-1)$	$(0,1,-1)$
2.	$(0,-1,1)$	$(0,-1,1)$
3.	$(1,0,-1)$	$(1,0,-1)$
4.	$(1,-1,0)$	$(1,-1,0)$
5.	$(-1,0,1)$	$(-1,0,1)$
6.	$(-1,1,0)$	$(-1,1,0)$
7.	$(0,1,-1)$	$(0,-1,1)$
8.	$(0,1,-1)$	$(1,0,-1)$
9.	$(0,1,-1)$	$(-1,0,1)$
10.	$(0,-1,1)$	$(0,1,-1)$
11.	$(0,-1,1)$	$(1,0,-1)$
12.	$(0,-1,1)$	$(-1,0,1)$

Table C.1 Texture one zero.

Sl no.	$\phi^{'}$	$\phi^{''}$
13.	$(1,0,-1)$	$(1,-1,0)$
14.	$(1,0,-1)$	$(-1,0,1)$
15.	$(1,0,-1)$	$(-1,1,0)$
16.	$(1,-1,0)$	$(0,1,-1)$
17.	$(1,-1,0)$	$(0,-1,1)$
18.	$(1,-1,0)$	$(-1,1,0)$
19.	$(-1,0,1)$	$(1,0,-1)$
20.	$(-1,0,1)$	$(1,-1,0)$
21.	$(-1,0,1)$	$(-1,1,0)$
22.	$(-1,1,0)$	$(0,1,-1)$
23.	$(-1,1,0)$	$(0,-1,1)$
24.	$(-1,1,0)$	$(1,-1,0)$

Table C.2 Texture one zero (contd).

Sl no.	$\phi^{'}$	$\phi^{''}$
25.	$(0,1,1)$	$(0,1,1)$
26.	$(0,1,1)$	$(0,1,-1)$
27.	$(0,1,1)$	$(0,-1,1)$
28.	$(0,1,1)$	$(0,-1,-1)$
29.	$(0,1,1)$	$(1,0,1)$
30.	$(0,1,1)$	$(1,0,-1)$
31.	$(0,1,1)$	$(-1,0,1)$
32.	$(0,1,1)$	$(-1,0,-1)$
33.	$(0,1,-1)$	$(0,1,1)$
34.	$(0,1,-1)$	$(0,-1,-1)$
35.	$(0,1,-1)$	$(1,0,1)$
36.	$(0,1,-1)$	$(-1,0,-1)$
37.	$(0,-1,1)$	$(0,1,1)$
38.	$(0,-1,1)$	$(0,-1,-1)$
39.	$(0,-1,1)$	$(1,0,1)$
40.	$(0,-1,-1)$	$(0,1,1)$
41.	$(0,-1,-1)$	$(0,1,-1)$
42.	$(0,-1,-1)$	$(0,-1,1)$
43.	$(0,-1,-1)$	$(0,-1,-1)$
44.	$(0,-1,-1)$	$(1,0,1)$
45.	$(0,-1,-1)$	$(1,0,-1)$
46.	$(0,-1,-1)$	$(-1,0,1)$
47.	$(0,-1,-1)$	$(-1,0,-1)$
48.	$(1,0,1)$	$(1,0,1)$
49.	$(1,0,1)$	$(1,0,-1)$
50.	$(1,0,1)$	$(1,1,0)$
51.	$(1,0,1)$	$(1,-1,0)$
52.	$(1,0,1)$	$(-1,0,1)$
53.	$(1,0,1)$	$(-1,1,0)$
54.	$(1,0,1)$	$(-1,-1,0)$
55.	$(1,0,1)$	$(-1,0,-1)$
56.	$(1,0,-1)$	$(1,0,1)$
57.	$(1,0,-1)$	$(1,1,0)$
58.	$(1,0,-1)$	$(-1,0,-1)$
59.	$(1,0,-1)$	$(-1,-1,0)$
60.	$(1,1,0)$	$(0,1,1)$

Table C.3 Texture one zero (contd).

Sl no.	$\phi^{'}$	$\phi^{''}$
61.	$(1,1,0)$	$(0,1,-1)$
62.	$(1,1,0)$	$(0,-1,1)$
63.	$(1,1,0)$	$(0,-1,-1)$
64.	$(1,1,0)$	$(1,1,0)$
65.	$(1,1,0)$	$(1,-1,0)$
66.	$(1,1,0)$	$(-1,1,0)$
67.	$(1,1,0)$	$(-1,-1,0)$
68.	$(1,-1,0)$	$(0,1,1)$
69.	$(1,-1,0)$	$(0,-1,-1)$
70.	$(1,-1,0)$	$(1,1,0)$
71.	$(-1,0,1)$	$(1,0,1)$
72.	$(-1,0,1)$	$(1,1,0)$
73.	$(-1,0,1)$	$(-1,0,-1)$
74.	$(-1,0,1)$	$(-1,-1,0)$
75.	$(-1,0,-1)$	$(1,0,1)$
76.	$(-1,0,-1)$	$(1,0,-1)$
77.	$(-1,0,-1)$	$(1,1,0)$
78.	$(-1,0,-1)$	$(1,-1,0)$
79.	$(-1,0,-1)$	$(-1,0,-1)$
80.	$(-1,0,-1)$	$(-1,1,0)$
81.	$(-1,0,-1)$	$(-1,-1,0)$
82.	$(-1,1,0)$	$(0,-1,-1)$
83.	$(-1,1,0)$	$(1,1,0)$
84.	$(-1,1,0)$	$(-1,-1,0)$
85.	$(-1,-1,0)$	$(0,1,1)$
86.	$(-1,-1,0)$	$(0,1,-1)$
87.	$(-1,-1,0)$	$(0,-1,1)$
88.	$(-1,-1,0)$	$(0,-1,-1)$
89.	$(-1,-1,0)$	$(-1,1,0)$
90.	$(-1,-1,0)$	$(-1,-1,0)$
91.	$(-1,-1,0)$	$(1,1,0)$
92.	$(-1,-1,0)$	$(1,-1,0)$
93.	$(-1,1,0)$	$(0,1,1)$
94.	$(0,-1,1)$	$(-1,0,-1)$
95.	$(1,-1,0)$	$(1,1,0)$
96	$(1,-1,0)$	$(-1,-1,0)$

Table C.4 Texture one zero.

Sl no.	$\phi^{'}$	$\phi^{''}$
1.	$(0,0,1)$	$(0,0,1)$
2.	$(0,0,1)$	$(0,0,-1)$
3.	$(0,0,-1)$	$(0,0,1)$
4.	$(0,0,-1)$	$(0,0,-1)$
5.	$(1,0,0)$	$(0,1,0)$
6.	$(1,0,0)$	$(0,-1,0)$
7.	$(-1,0,0)$	$(0,1,0)$
8.	$(-1,0,0)$	$(0,-1,0)$

Table C.5 Texture three zero.

Sl no.	$\phi^{'}$	$\phi^{''}$
1.	$(0,0,1)$	$(0,1,1)$
2.	$(0,0,1)$	$(0,1,-1)$
3.	$(0,0,1)$	$(0,-1,1)$
4.	$(0,0,1)$	$(0,-1,-1)$
5.	$(0,0,1)$	$(1,0,1)$
6.	$(0,0,1)$	$(1,0,-1)$
7.	$(0,0,1)$	$(-1,0,1)$
8.	$(0,0,1)$	$(-1,0,-1)$
9.	$(0,0,-1)$	$(0,1,1)$
10.	$(0,0,-1)$	$(0,1,-1)$
11.	$(0,0,-1)$	$(0,-1,1)$
12.	$(0,0,-1)$	$(0,-1,-1)$
13.	$(0,0,-1)$	$(1,0,1)$
14.	$(0,0,-1)$	$(1,0,-1)$
15.	$(0,0,-1)$	$(-1,0,1)$
16.	$(0,0,-1)$	$(-1,0,-1)$
17.	$(0,1,1)$	$(0,0,1)$
18.	$(0,1,1)$	$(0,0,-1)$
19.	$(0,1,-1)$	$(0,0,1)$
20.	$(0,1,-1)$	$(0,0,-1)$
21.	$(0,-1,1)$	$(0,0,1)$
22.	$(0,-1,1)$	$(0,0,-1)$
23.	$(0,-1,-1)$	$(0,0,1)$
24.	$(0,-1,-1)$	$(0,0,-1)$
25.	$(1,0,0)$	$(0,1,1)$
26.	$(1,0,0)$	$(0,1,-1)$
27.	$(1,0,0)$	$(0,-1,1)$
28.	$(1,0,0)$	$(0,-1,-1)$
29.	$(1,0,0)$	$(1,1,0)$
30.	$(1,0,0)$	$(1,-1,0)$
31.	$(1,0,0)$	$(-1,1,0)$
32.	$(1,0,0)$	$(-1,-1,0)$

Table C.6 Texture two zero.

Sl no.	$\phi^{'}$	$\phi^{''}$
33.	$(1,0,1)$	$(0,0,1)$
34.	$(1,0,1)$	$(0,0,-1)$
35.	$(1,0,1)$	$(0,1,0)$
36.	$(1,0,1)$	$(0,-1,0)$
37.	$(1,0,-1)$	$(0,0,1)$
38.	$(1,0,-1)$	$(0,0,-1)$
39.	$(1,0,-1)$	$(0,1,0)$
40.	$(1,0,-1)$	$(0,-1,0)$
41.	$(1,1,0)$	$(0,1,0)$
42.	$(1,1,0)$	$(0,-1,0)$
43.	$(1,-1,0)$	$(0,1,0)$
44.	$(1,-1,0)$	$(0,-1,0)$
45.	$(-1,0,0)$	$(0,1,1)$
46.	$(-1,0,0)$	$(0,1,-1)$
47.	$(-1,0,0)$	$(0,-1,1)$
48.	$(-1,0,0)$	$(0,-1,-1)$
49.	$(-1,0,0)$	$(1,1,0)$
50.	$(-1,0,0)$	$(1,-1,0)$
51.	$(-1,0,0)$	$(-1,1,0)$
52.	$(-1,0,0)$	$(-1,-1,0)$
53.	$(-1,0,1)$	$(0,0,1)$
54.	$(-1,0,1)$	$(0,0,-1)$
55.	$(-1,0,1)$	$(0,1,0)$
56.	$(-1,0,1)$	$(0,-1,0)$
57.	$(-1,0,-1)$	$(0,0,1)$
58.	$(-1,0,-1)$	$(0,0,-1)$
59.	$(-1,0,-1)$	$(0,1,0)$
60.	$(-1,0,-1)$	$(0,-1,0)$
61.	$(-1,1,0)$	$(0,1,0)$
62.	$(-1,1,0)$	$(0,-1,0)$
63.	$(-1,-1,0)$	$(0,1,0)$
64.	$(-1,-1,0)$	$(0,-1,0)$

Table C.7 Texture two zero (contd).

Sl no.	$\phi^{'}$	$\phi^{''}$
1.	$(1,0,-1)$	$(0,1,-1)$
2.	$(1,0,-1)$	$(0,-1,1)$
3.	$(-1,0,1)$	$(0,1,-1)$
4.	$(-1,0,1)$	$(0,-1,1)$
5.	$(0,0,0)$	$(0,1,-1)$
6.	$(0,0,0)$	$(0,-1,1)$
7.	$(0,1,0)$	$(0,1,-1)$
8.	$(0,1,0)$	$(0,-1,1)$
9.	$(0,-1,0)$	$(0,1,-1)$
10.	$(0,-1,0)$	$(0,-1,1)$
11.	$(1,0,1)$	$(0,1,-1)$
12.	$(1,0,1)$	$(0,-1,1)$
13.	$(1,0,-1)$	$(0,0,0)$
14.	$(1,0,-1)$	$(0,1,1)$
15.	$(1,0,-1)$	$(0,-1,-1)$
16.	$(1,0,-1)$	$(1,0,0)$
17.	$(1,0,-1)$	$(1,1,1)$
18.	$(1,0,-1)$	$(1,-1,-1)$
19.	$(1,0,-1)$	$(-1,0,0)$
20.	$(1,0,-1)$	$(-1,1,1)$
21.	$(1,0,-1)$	$(-1,-1,-1)$
22.	$(1,1,1)$	$(0,1,-1)$
23.	$(1,1,1)$	$(0,-1,1)$
24.	$(1,-1,1)$	$(0,1,-1)$
25.	$(1,-1,1)$	$(0,-1,1)$
26.	$(-1,0,1)$	$(0,0,0)$
27.	$(-1,0,1)$	$(0,1,1)$
28.	$(-1,0,1)$	$(0,-1,-1)$
29.	$(-1,0,1)$	$(1,0,0)$
30.	$(-1,0,1)$	$(1,1,1)$
31.	$(-1,0,1)$	$(1,-1,-1)$
32.	$(-1,0,1)$	$(-1,0,0)$
33.	$(-1,0,1)$	$(-1,1,1)$
34.	$(-1,0,1)$	$(-1,-1,-1)$
35.	$(-1,0,-1)$	$(0,1,-1)$
36.	$(-1,0,-1)$	$(0,-1,1)$
37.	$(-1,-1,-1)$	$(0,1,-1)$
38.	$(-1,1,-1)$	$(0,1,-1)$
39.	$(-1,1,-1)$	$(0,-1,1)$
40.	$(-1,-1,-1)$	$(0,-1,1)$

Table C.8 $(\mu-\tau)$ symmetry (in 3×3 block).

Sl no.	$\phi^{'}$	$\phi^{''}$
1.	$(0,0,0)$	$(1,1,-1)$
2.	$(0,0,0)$	$(1,-1,1)$
3.	$(0,0,0)$	$(-1,1,-1)$
4.	$(0,0,0)$	$(-1,-1,1)$
5.	$(0,0,1)$	$(1,1,1)$
6.	$(0,0,1)$	$(1,1,-1)$
7.	$(0,0,1)$	$(1,-1,1)$
8.	$(0,0,1)$	$(1,-1,-1)$
9.	$(0,0,1)$	$(-1,1,1)$
10.	$(0,0,1)$	$(-1,1,-1)$
11.	$(0,0,1)$	$(-1,-1,1)$
12.	$(0,0,1)$	$(-1,-1,-1)$
13.	$(0,0,-1)$	$(1,1,1)$
14.	$(0,0,-1)$	$(1,1,-1)$
15.	$(0,0,-1)$	$(1,-1,1)$
16.	$(0,0,-1)$	$(1,-1,-1)$
17.	$(0,0,-1)$	$(-1,1,1)$
18.	$(0,0,-1)$	$(-1,1,-1)$
19.	$(0,0,-1)$	$(-1,-1,1)$
20.	$(0,0,-1)$	$(-1,-1,-1)$
21.	$(0,1,0)$	$(1,1,-1)$
22.	$(0,1,0)$	$(1,-1,1)$
23.	$(0,1,0)$	$(-1,1,-1)$
24.	$(0,1,0)$	$(-1,-1,1)$
25.	$(0,1,1)$	$(1,1,1)$
26.	$(0,1,1)$	$(1,1,-1)$
27.	$(0,1,1)$	$(1,-1,1)$
28.	$(0,1,1)$	$(1,-1,-1)$
29.	$(0,1,1)$	$(-1,1,1)$
30.	$(0,1,1)$	$(-1,1,-1)$
31.	$(0,1,1)$	$(-1,-1,1)$
32.	$(0,1,1)$	$(-1,-1,-1)$
33.	$(0,1,-1)$	$(1,1,1)$
34.	$(0,1,-1)$	$(1,1,-1)$
35.	$(0,1,-1)$	$(1,-1,1)$
36.	$(0,1,-1)$	$(1,-1,-1)$
37.	$(0,1,-1)$	$(-1,1,1)$
38.	$(0,1,-1)$	$(-1,1,-1)$
39.	$(0,1,-1)$	$(-1,-1,1)$
40.	$(0,1,-1)$	$(-1,-1,-1)$

Table C.9 Hybrid texture.

Sl no.	$\phi^{'}$	$\phi^{''}$
41.	$(0,-1,0)$	$(1,1,-1)$
42.	$(0,-1,0)$	$(1,-1,1)$
43.	$(0,-1,0)$	$(-1,1,-1)$
44.	$(0,-1,0)$	$(-1,-1,1)$
45.	$(0,-1,1)$	$(1,1,1)$
46.	$(0,-1,1)$	$(1,1,-1)$
47.	$(0,-1,1)$	$(1,-1,1)$
48.	$(0,-1,1)$	$(1,-1,-1)$
49.	$(0,-1,1)$	$(-1,1,1)$
50.	$(0,-1,1)$	$(-1,1,-1)$
51.	$(0,-1,1)$	$(-1,-1,1)$
52.	$(0,-1,1)$	$(-1,-1,-1)$
53.	$(0,-1,-1)$	$(1,1,1)$
54.	$(0,-1,-1)$	$(1,1,-1)$
55.	$(0,-1,-1)$	$(1,-1,1)$
56.	$(0,-1,-1)$	$(1,-1,-1)$
57.	$(0,-1,-1)$	$(-1,1,1)$
58.	$(0,-1,-1)$	$(-1,1,-1)$
59.	$(0,-1,-1)$	$(-1,-1,1)$
60.	$(0,-1,-1)$	$(-1,-1,-1)$
61.	$(1,0,0)$	$(1,1,1)$
62.	$(1,0,0)$	$(1,1,-1)$
63.	$(1,0,0)$	$(1,-1,1)$
64.	$(1,0,0)$	$(1,-1,-1)$
65.	$(1,0,0)$	$(-1,1,1)$
66.	$(1,0,0)$	$(-1,1,-1)$
67.	$(1,0,0)$	$(-1,-1,1)$
68.	$(1,0,0)$	$(-1,-1,-1)$
69.	$(1,0,1)$	$(1,1,-1)$
70.	$(1,0,1)$	$(1,-1,1)$
71.	$(1,0,1)$	$(-1,1,-1)$
72.	$(1,0,1)$	$(-1,-1,1)$
73.	$(1,0,-1)$	$(1,1,-1)$
74.	$(1,0,-1)$	$(1,-1,1)$
75.	$(1,0,-1)$	$(-1,1,-1)$
76.	$(1,0,-1)$	$(-1,-1,1)$
77.	$(1,1,0)$	$(1,1,1)$
78.	$(1,1,0)$	$(1,1,-1)$
79.	$(1,1,0)$	$(1,-1,1)$
80.	$(1,1,0)$	$(1,-1,-1)$

Table C.10 Hybrid texture (contd).

Sl no.	$\phi^{'}$	$\phi^{''}$
81.	$(1,1,0)$	$(-1,1,1)$
82.	$(1,1,0)$	$(-1,1,-1)$
83.	$(1,1,0)$	$(-1,-1,1)$
84.	$(1,1,0)$	$(-1,-1,-1)$
85.	$(1,1,1)$	$(0,0,1)$
86.	$(1,1,1)$	$(0,0,-1)$
87.	$(1,1,1)$	$(0,1,0)$
88.	$(1,1,1)$	$(0,-1,0)$
89.	$(1,1,1)$	$(1,0,1)$
90.	$(1,1,1)$	$(1,0,-1)$
91.	$(1,1,1)$	$(1,1,0)$
92.	$(1,1,1)$	$(1,1,-1)$
93.	$(1,1,1)$	$(1,-1,0)$
94.	$(1,1,1)$	$(1,-1,1)$
95.	$(1,1,1)$	$(-1,0,1)$
96.	$(1,1,1)$	$(-1,0,-1)$
97.	$(1,1,1)$	$(-1,1,0)$
98.	$(1,1,1)$	$(-1,1,-1)$
99.	$(1,1,1)$	$(-1,-1,0)$
100.	$(1,1,1)$	$(-1,-1,1)$
101.	$(1,1,-1)$	$(0,0,0)$
102.	$(1,1,-1)$	$(0,0,1)$
103.	$(1,1,-1)$	$(0,0,-1)$
104.	$(1,1,-1)$	$(0,1,0)$
105.	$(1,1,-1)$	$(0,1,1)$
106.	$(1,1,-1)$	$(0,1,-1)$
107.	$(1,1,-1)$	$(0,-1,0)$
108.	$(1,1,-1)$	$(0,-1,1)$
109.	$(1,1,-1)$	$(0,-1,-1)$
110.	$(1,1,-1)$	$(1,0,0)$
111.	$(1,1,-1)$	$(1,0,1)$
112.	$(1,1,-1)$	$(1,0,-1)$
113.	$(1,1,-1)$	$(1,1,0)$
114.	$(1,1,-1)$	$(1,1,1)$
115.	$(1,1,-1)$	$(1,1,-1)$
116.	$(1,1,-1)$	$(1,-1,0)$
117.	$(1,1,-1)$	$(1,-1,1)$
118.	$(1,1,-1)$	$(1,-1,-1)$
119.	$(1,1,-1)$	$(-1,0,0)$
120.	$(1,1,-1)$	$(-1,0,1)$
121.	$(1,1,-1)$	$(-1,0,-1)$

Table C.11 Hybrid texture (contd).

Sl no.	$\phi^{'}$	$\phi^{''}$
122.	$(1,1,-1)$	$(-1,1,0)$
123.	$(1,1,-1)$	$(-1,1,1)$
124.	$(1,1,-1)$	$(-1,1,-1)$
125.	$(1,1,-1)$	$(-1,-1,0)$
126.	$(1,1,-1)$	$(-1,-1,1)$
127.	$(1,1,-1)$	$(-1,-1,-1)$
128.	$(1,-1,0)$	$(1,1,1)$
129.	$(1,-1,0)$	$(1,1,-1)$
130.	$(1,-1,0)$	$(1,-1,1)$
131.	$(1,-1,0)$	$(1,-1,-1)$
132.	$(1,-1,0)$	$(-1,1,1)$
133.	$(1,-1,0)$	$(-1,1,-1)$
134.	$(1,-1,0)$	$(-1,-1,1)$
135.	$(1,-1,0)$	$(-1,-1,-1)$
136.	$(1,-1,1)$	$(0,0,1)$
137.	$(1,-1,1)$	$(0,0,-1)$
138.	$(1,-1,1)$	$(0,1,0)$
139.	$(1,-1,1)$	$(0,-1,0)$
140.	$(1,-1,1)$	$(1,0,-1)$
141.	$(1,-1,1)$	$(1,1,0)$
142.	$(1,-1,1)$	$(1,-1,0)$
143.	$(1,-1,1)$	$(1,-1,1)$
144.	$(1,-1,1)$	$(1,1,-1)$
145.	$(1,-1,1)$	$(-1,0,1)$
146.	$(1,-1,1)$	$(-1,0,-1)$
147.	$(1,-1,1)$	$(-1,1,0)$
148.	$(1,-1,1)$	$(-1,1,-1)$
149.	$(1,-1,1)$	$(-1,-1,0)$
150.	$(1,-1,1)$	$(-1,-1,1)$
151.	$(1,-1,-1)$	$(0,0,0)$
152.	$(1,-1,-1)$	$(0,0,1)$
153.	$(1,-1,-1)$	$(0,0,-1)$
154.	$(1,-1,-1)$	$(0,1,0)$
155.	$(1,-1,-1)$	$(0,1,1)$
156.	$(1,-1,-1)$	$(0,1,-1)$
157.	$(1,-1,-1)$	$(0,-1,0)$
158.	$(1,-1,-1)$	$(0,-1,1)$
159.	$(1,-1,-1)$	$(0,-1,-1)$
160.	$(1,-1,-1)$	$(1,0,0)$
161.	$(1,-1,-1)$	$(1,0,1)$
162.	$(1,-1,-1)$	$(1,0,-1)$

Table C.12 Hybrid texture (contd).

Sl no.	ϕ'	ϕ''
163.	$(1,-1,-1)$	$(1,1,0)$
164.	$(1,-1,-1)$	$(1,1,1)$
165.	$(1,-1,-1)$	$(1,1,-1)$
166.	$(1,-1,-1)$	$(1,-1,0)$
167.	$(1,-1,-1)$	$(1,-1,1)$
168.	$(1,-1,-1)$	$(1,-1,-1)$
169.	$(1,-1,-1)$	$(-1,0,0)$
170.	$(1,-1,-1)$	$(-1,0,1)$
171.	$(1,-1,-1)$	$(-1,0,-1)$
172.	$(1,-1,-1)$	$(-1,1,0)$
173.	$(1,-1,-1)$	$(-1,1,1)$
174.	$(1,-1,-1)$	$(-1,1,-1)$
175.	$(1,-1,-1)$	$(-1,-1,0)$
176.	$(1,-1,-1)$	$(-1,-1,1)$
177.	$(1,-1,-1)$	$(-1,-1,-1)$
178.	$(-1,0,0)$	$(1,1,1)$
179.	$(-1,0,0)$	$(1,1,-1)$
180.	$(-1,0,0)$	$(1,-1,1)$
181.	$(-1,0,0)$	$(1,-1,-1)$
182.	$(-1,0,0)$	$(-1,1,1)$
183.	$(-1,0,0)$	$(-1,1,-1)$
184.	$(-1,0,0)$	$(-1,-1,1)$
185.	$(-1,0,0)$	$(-1,-1,-1)$
186.	$(-1,0,1)$	$(1,1,-1)$
187.	$(-1,0,1)$	$(1,-1,1)$
188.	$(-1,0,1)$	$(-1,1,-1)$
189.	$(-1,0,1)$	$(-1,-1,1)$
190.	$(-1,0,-1)$	$(1,1,-1)$
191.	$(-1,0,-1)$	$(1,-1,1)$
192.	$(-1,0,-1)$	$(-1,1,-1)$
193.	$(-1,0,-1)$	$(-1,-1,1)$
194.	$(-1,1,0)$	$(1,1,1)$
195.	$(-1,1,0)$	$(1,1,-1)$
196.	$(-1,1,0)$	$(1,-1,1)$
197.	$(-1,1,0)$	$(1,-1,-1)$
198.	$(-1,1,0)$	$(-1,1,1)$
199.	$(-1,1,0)$	$(-1,1,-1)$
200.	$(-1,1,0)$	$(-1,-1,1)$
201.	$(-1,1,0)$	$(-1,-1,-1)$
202.	$(-1,1,1)$	$(0,0,0)$
203.	$(-1,1,1)$	$(0,0,1)$

Table C.13 Hybrid texture (contd).

Sl no.	ϕ'	ϕ''
204.	$(-1,1,1)$	$(0,0,-1)$
205.	$(-1,1,1)$	$(0,1,0)$
206.	$(-1,1,1)$	$(0,1,1)$
207.	$(-1,1,1)$	$(0,1,-1)$
208.	$(-1,1,1)$	$(0,-1,0)$
209.	$(-1,1,1)$	$(0,-1,1)$
210.	$(-1,1,1)$	$(0,-1,-1)$
211.	$(-1,1,1)$	$(1,0,0)$
212.	$(-1,1,1)$	$(1,0,1)$
213.	$(-1,1,1)$	$(1,0,-1)$
214.	$(-1,1,1)$	$(1,1,0)$
215.	$(-1,1,1)$	$(1,1,1)$
216.	$(-1,1,1)$	$(1,1,-1)$
217.	$(-1,1,1)$	$(1,-1,0)$
218.	$(-1,1,1)$	$(1,-1,1)$
219.	$(-1,1,1)$	$(1,-1,-1)$
220.	$(-1,1,1)$	$(-1,0,0)$
221.	$(-1,1,1)$	$(-1,0,1)$
222.	$(-1,1,1)$	$(-1,0,-1)$
223.	$(-1,1,1)$	$(-1,1,0)$
224.	$(-1,1,1)$	$(-1,1,1)$
225.	$(-1,1,1)$	$(-1,1,-1)$
226.	$(-1,1,1)$	$(-1,-1,0)$
227.	$(-1,1,1)$	$(-1,-1,1)$
228.	$(-1,1,1)$	$(-1,-1,-1)$
229.	$(-1,1,-1)$	$(0,0,1)$
230.	$(-1,1,-1)$	$(0,0,-1)$
231.	$(-1,1,-1)$	$(0,1,0)$
232.	$(-1,1,-1)$	$(0,-1,0)$
233.	$(-1,1,-1)$	$(1,0,1)$
234.	$(-1,1,-1)$	$(1,0,-1)$
235.	$(-1,1,-1)$	$(1,1,0)$
236.	$(-1,1,-1)$	$(1,1,-1)$
237.	$(-1,1,-1)$	$(1,-1,0)$
238.	$(-1,1,-1)$	$(1,-1,1)$
239.	$(-1,1,-1)$	$(-1,0,1)$
240.	$(-1,1,-1)$	$(-1,0,-1)$
241.	$(-1,1,-1)$	$(-1,1,0)$
242.	$(-1,1,-1)$	$(-1,1,-1)$
243.	$(-1,1,-1)$	$(-1,-1,0)$

Table C.14 Hybrid texture (contd)

Sl no.	$\phi^{'}$	$\phi^{''}$
244.	$(-1,1,-1)$	$(-1,-1,1)$
245.	$(-1,-1,0)$	$(1,1,1)$
246.	$(-1,-1,0)$	$(1,1,-1)$
247.	$(-1,-1,0)$	$(1,-1,1)$
248.	$(-1,-1,0)$	$(1,-1,-1)$
249.	$(-1,-1,0)$	$(-1,1,1)$
250.	$(-1,-1,0)$	$(-1,1,-1)$
251.	$(-1,-1,0)$	$(-1,-1,1)$
252.	$(-1,-1,0)$	$(-1,-1,-1)$
253.	$(-1,-1,1)$	$(0,0,0)$
254.	$(-1,-1,1)$	$(0,0,1)$
255.	$(-1,-1,1)$	$(0,0,-1)$
256.	$(-1,-1,1)$	$(0,1,0)$
257.	$(-1,-1,1)$	$(0,1,1)$
258.	$(-1,-1,1)$	$(0,1,-1)$
259.	$(-1,-1,1)$	$(0,-1,0)$
260.	$(-1,-1,1)$	$(0,-1,1)$
261.	$(-1,-1,1)$	$(0,-1,-1)$
262.	$(-1,-1,1)$	$(1,0,0)$
263.	$(-1,-1,1)$	$(1,0,1)$
264.	$(-1,-1,1)$	$(1,0,-1)$
265.	$(-1,-1,1)$	$(1,1,0)$
266.	$(-1,-1,1)$	$(1,1,1)$
267.	$(-1,-1,1)$	$(1,1,-1)$
268.	$(-1,-1,1)$	$(1,-1,0)$
269.	$(-1,-1,1)$	$(1,-1,1)$
270.	$(-1,-1,1)$	$(1,-1,-1)$
271.	$(-1,-1,1)$	$(-1,0,0)$
272.	$(-1,-1,1)$	$(-1,0,1)$
273.	$(-1,-1,1)$	$(-1,0,-1)$
274.	$(-1,-1,1)$	$(-1,1,0)$
275.	$(-1,-1,1)$	$(-1,1,1)$
276.	$(-1,-1,1)$	$(-1,1,-1)$
277.	$(-1,-1,1)$	$(-1,-1,0)$
278.	$(-1,-1,1)$	$(-1,-1,1)$
279.	$(-1,-1,1)$	$(-1,-1,-1)$
280.	$(-1,-1,-1)$	$(0,0,1)$
281.	$(-1,-1,-1)$	$(0,0,-1)$
282.	$(-1,-1,-1)$	$(0,1,0)$
283.	$(-1,-1,-1)$	$(0,-1,0)$
284.	$(-1,-1,-1)$	$(1,0,1)$

Table C.15 Hybrid texture (contd).

Sl no.	$\phi^{'}$	$\phi^{''}$
285.	$(-1,-1,-1)$	$(1,0,-1)$
286.	$(-1,-1,-1)$	$(1,1,0)$
287.	$(-1,-1,-1)$	$(1,1,-1)$
288.	$(-1,-1,-1)$	$(1,-1,0)$
289.	$(-1,-1,-1)$	$(1,-1,1)$
290.	$(-1,-1,-1)$	$(-1,0,1)$
291.	$(-1,-1,-1)$	$(-1,0,-1)$
292.	$(-1,-1,-1)$	$(-1,1,0)$
293.	$(-1,-1,-1)$	$(-1,1,-1)$
294.	$(-1,-1,-1)$	$(-1,-1,0)$
295.	$(-1,-1,-1)$	$(-1,-1,1)$
296.	$(1,-1,1)$	$(1,0,1)$

Table C.16 Hybrid texture (contd)

D

Vacuum alignment of ϕ', ϕ'' of disallowed cases

Sl no.	$\phi^{'}$	$\phi^{''}$
1.	$(0,0,0)$	$(0,0,0)$
2.	$(0,0,0)$	$(1,0,0)$
3.	$(0,0,0)$	$(-1,0,0)$
4.	$(0,1,0)$	$(0,0,0)$
5.	$(0,1,0)$	$(1,0,0)$
6.	$(0,1,0)$	$(-1,0,0)$
7.	$(0,-1,0)$	$(0,0,0)$
8.	$(0,-1,0)$	$(1,0,0)$
9.	$(0,-1,0)$	$(-1,0,0)$

Table D.1 Texture zero in the entire 2nd and 3rd row and column of 4×4 matrix.

Sl no.	$\phi^{'}$	$\phi^{''}$
1.	$(0,1,-1)$	$(1,-1,0)$
2.	$(0,1,-1)$	$(-1,1,0)$
3.	$(0,-1,1)$	$(1,-1,0)$
4.	$(0,-1,1)$	$(-1,1,0)$
5.	$(0,0,0)$	$(0,1,0)$
6.	$(0,0,0)$	$(0,-1,0)$
7.	$(0,0,0)$	$(1,-1,0)$
8.	$(0,0,0)$	$(-1,1,0)$
9.	$(0,0,0)$	$(-1,-1,0)$
10.	$(0,0,1)$	$(0,0,0)$

Table D.2 Texture zero in the entire 2nd row and column of 4×4 matrix.

Sl no.	$\phi^{'}$	$\phi^{''}$
11.	$(0,0,1)$	$(0,1,0)$
12.	$(0,0,1)$	$(0,-1,0)$
13.	$(0,0,1)$	$(1,0,0)$
14.	$(0,0,1)$	$(1,1,0)$
15.	$(0,0,1)$	$(1,-1,0)$
16.	$(0,0,1)$	$(-1,0,0)$
17.	$(0,0,1)$	$(-1,1,0)$
18.	$(0,0,1)$	$(-1,-1,0)$
19.	$(0,0,-1)$	$(0,0,0)$
20.	$(0,0,-1)$	$(0,1,0)$
21.	$(0,0,-1)$	$(1,0,0)$
22.	$(0,0,-1)$	$(1,1,0)$
23.	$(0,0,-1)$	$(1,-1,0)$
24.	$(0,0,-1)$	$(-1,0,0)$
25.	$(0,0,-1)$	$(-1,1,0)$
26.	$(0,0,-1)$	$(-1,-1,0)$
27.	$(0,1,0)$	$(0,1,0)$
28.	$(0,1,0)$	$(0,-1,0)$
29.	$(0,1,0)$	$(1,1,0)$
30.	$(0,1,0)$	$(1,-1,0)$
31.	$(0,1,0)$	$(-1,1,0)$
32.	$(0,1,0)$	$(-1,-1,0)$
33.	$(0,1,1)$	$(0,0,0)$
34.	$(0,1,1)$	$(0,1,0)$
35.	$(0,1,1)$	$(0,-1,0)$
36.	$(0,1,1)$	$(1,0,0)$

Table D.3 Texture zero in the entire 2nd row and column of 4×4 matrix.

Sl no.	$\phi^{'}$	$\phi^{''}$
37.	$(0,1,1)$	$(1,1,0)$
38.	$(0,1,1)$	$(1,-1,0)$
39.	$(0,1,1)$	$(-1,0,0)$
40.	$(0,1,1)$	$(-1,1,0)$
41.	$(0,1,1)$	$(-1,-1,0)$
42.	$(0,1,-1)$	$(0,0,0)$
43.	$(0,1,-1)$	$(0,1,0)$
44.	$(0,1,-1)$	$(0,-1,0)$
45.	$(0,1,-1)$	$(1,0,0)$
46.	$(0,1,-1)$	$(1,1,0)$
47.	$(0,1,-1)$	$(-1,0,0)$
48.	$(0,1,-1)$	$(-1,-1,0)$
49.	$(0,-1,0)$	$(0,1,0)$
50.	$(0,-1,0)$	$(0,-1,0)$
51.	$(0,-1,0)$	$(1,1,0)$
52.	$(0,-1,0)$	$(1,-1,0)$
53.	$(0,-1,0)$	$(-1,1,0)$
54.	$(0,-1,0)$	$(-1,-1,0)$
55.	$(0,-1,1)$	$(0,0,0)$
56.	$(0,-1,1)$	$(0,1,0)$
57.	$(0,-1,1)$	$(0,-1,0)$
58.	$(0,-1,1)$	$(1,0,0)$
59.	$(0,-1,1)$	$(1,1,0)$
60.	$(0,-1,1)$	$(-1,0,0)$
61.	$(0,-1,1)$	$(-1,-1,0)$
62.	$(0,-1,-1)$	$(0,0,0)$
63.	$(0,-1,-1)$	$(0,1,0)$
64.	$(0,-1,-1)$	$(0,-1,0)$
65.	$(0,-1,-1)$	$(1,0,0)$
66.	$(0,-1,-1)$	$(1,1,0)$
67.	$(0,-1,-1)$	$(1,-1,0)$
68.	$(0,-1,-1)$	$(-1,0,0)$
69.	$(0,-1,-1)$	$(-1,1,0)$
70.	$(0,-1,-1)$	$(-1,-1,0)$
71.	$(0,0,-1)$	$(0,-1,0)$

Table D.4 Texture zero in the entire 2nd row and column of 4×4 matrix .

Sl no.	ϕ'	ϕ''
1.	$(1,-1,0)$	$(1,0,-1)$
2.	$(1,-1,0)$	$(-1,0,1)$
3.	$(-1,1,0)$	$(1,0,-1)$
4.	$(-1,1,0)$	$(-1,0,1)$
5.	$(0,0,0)$	$(0,0,1)$
6.	$(0,0,0)$	$(0,0,-1)$
7.	$(0,0,0)$	$(1,0,1)$
8.	$(0,0,0)$	$(1,0,-1)$
9.	$(0,0,0)$	$(1,1,0)$
10.	$(0,0,0)$	$(-1,0,1)$
11.	$(0,0,0)$	$(-1,0,-1)$
12.	$(0,1,0)$	$(0,0,1)$
13.	$(0,1,0)$	$(0,0,-1)$
14.	$(0,1,0)$	$(1,0,1)$
15.	$(0,1,0)$	$(1,0,-1)$
16.	$(0,1,0)$	$(-1,0,1)$
17.	$(0,1,0)$	$(-1,0,-1)$
18.	$(0,-1,0)$	$(0,0,1)$
19.	$(0,-1,0)$	$(0,0,-1)$
20.	$(0,-1,0)$	$(1,0,1)$
21.	$(0,-1,0)$	$(1,0,-1)$
22.	$(0,-1,0)$	$(-1,0,1)$
23.	$(0,-1,0)$	$(-1,0,-1)$
24.	$(1,0,0)$	$(0,0,0)$
25.	$(1,0,0)$	$(0,0,1)$
26.	$(1,0,0)$	$(0,0,-1)$
27.	$(1,0,0)$	$(1,0,0)$
28.	$(1,0,0)$	$(1,0,1)$
29.	$(1,0,0)$	$(1,0,-1)$
30.	$(1,0,0)$	$(-1,0,0)$
31.	$(1,0,0)$	$(-1,0,1)$
32.	$(1,0,0)$	$(-1,0,-1)$
33.	$(1,1,0)$	$(0,0,0)$
34.	$(1,1,0)$	$(0,0,1)$
35.	$(1,1,0)$	$(0,0,-1)$
36.	$(1,1,0)$	$(1,0,0)$
37.	$(1,1,0)$	$(1,0,1)$

Table D.5 Texture zero in the entire 3rd row and column of 4×4 matrix.

Sl no.	ϕ'	ϕ''
38.	$(1,1,0)$	$(1,0,-1)$
39.	$(1,1,0)$	$(-1,0,0)$
40.	$(1,1,0)$	$(-1,0,1)$
41.	$(1,1,0)$	$(-1,0,-1)$
42.	$(1,-1,0)$	$(0,0,0)$
43.	$(1,-1,0)$	$(0,0,1)$
44.	$(1,-1,0)$	$(0,0,-1)$
45.	$(1,-1,0)$	$(1,0,0)$
46.	$(1,-1,0)$	$(1,0,1)$
47.	$(1,-1,0)$	$(-1,0,0)$
48.	$(1,-1,0)$	$(-1,0,-1)$
49.	$(-1,0,0)$	$(0,0,0)$
50.	$(-1,0,0)$	$(0,0,1)$
51.	$(-1,0,0)$	$(0,0,-1)$
52.	$(-1,0,0)$	$(1,0,0)$
53.	$(-1,0,0)$	$(1,0,1)$
54.	$(-1,0,0)$	$(1,0,-1)$
55.	$(-1,0,0)$	$(-1,0,0)$
56.	$(-1,0,0)$	$(-1,0,1)$
57.	$(-1,0,0)$	$(-1,0,-1)$
58.	$(-1,1,0)$	$(0,0,0)$
59.	$(-1,1,0)$	$(0,0,1)$
60.	$(-1,1,0)$	$(0,0,-1)$
61.	$(-1,1,0)$	$(1,0,0)$
62.	$(-1,1,0)$	$(1,0,1)$
63.	$(-1,1,0)$	$(-1,0,0)$
64.	$(-1,1,0)$	$(-1,0,-1)$
65.	$(-1,-1,0)$	$(0,0,0)$
66.	$(-1,-1,0)$	$(0,0,1)$
67.	$(-1,-1,0)$	$(0,0,-1)$
68.	$(-1,-1,0)$	$(1,0,0)$
69.	$(-1,-1,0)$	$(1,0,1)$
70.	$(-1,-1,0)$	$(1,0,-1)$
71.	$(-1,-1,0)$	$(-1,0,0)$
72.	$(-1,-1,0)$	$(-1,0,1)$
73.	$(-1,-1,0)$	$(-1,0,-1)$

Table D.6 Texture zero in the entire 3rd row and column of 4×4 matrix.

Sl no.	$\phi^{'}$	$\phi^{''}$
1.	$(0,0,0)$	$(0,1,1)$
2.	$(0,0,0)$	$(0,-1,-1)$
3.	$(0,0,0)$	$(1,-1,-1)$
4.	$(0,0,0)$	$(-1,1,1)$
5.	$(0,0,0)$	$(-1,-1,-1)$
6.	$(0,1,0)$	$(0,1,1)$
7.	$(0,1,0)$	$(1,1,1)$
8.	$(0,1,0)$	$(-1,-1,-1)$
9.	$(0,-1,0)$	$(0,1,1)$
10.	$(0,-1,0)$	$(0,-1,-1)$
11.	$(0,-1,0)$	$(1,1,1)$
12.	$(0,1,0)$	$(1,-1,-1)$
13.	$(0,1,0)$	$(-1,1,1)$
14.	$(0,-1,0)$	$(1,-1,-1)$
15.	$(0,-1,0)$	$(-1,1,1)$
16.	$(0,-1,0)$	$(-1,-1,-1)$
17.	$(1,0,1)$	$(0,0,0)$
18.	$(1,0,1)$	$(1,1,1)$
19.	$(1,0,1)$	$(1,-1,-1)$
20.	$(1,0,1)$	$(-1,0,0)$
21.	$(1,0,1)$	$(-1,1,1)$
22.	$(1,0,1)$	$(-1,-1,-1)$
23.	$(1,1,1)$	$(0,0,0)$
24.	$(1,1,1)$	$(0,1,1)$
25.	$(1,1,1)$	$(0,-1,-1)$
26.	$(1,1,1)$	$(1,0,0)$
27.	$(1,1,1)$	$(1,1,1)$
28.	$(1,1,1)$	$(1,-1,-1)$
29.	$(1,1,1)$	$(-1,0,0)$
30.	$(1,1,1)$	$(-1,1,1)$

Table D.7 $(\mu-\tau)$ symmetry in the entire 4×4 matrix.

Sl no.	$\phi^{'}$	$\phi^{''}$
31.	$(1,1,1)$	$(-1,-1,-1)$
32.	$(1,-1,1)$	$(0,0,0)$
33.	$(1,-1,1)$	$(0,1,1)$
34.	$(1,-1,1)$	$(0,-1,-1)$
35.	$(1,-1,1)$	$(1,0,0)$
36.	$(1,-1,1)$	$(1,1,1)$
37.	$(1,-1,1)$	$(1,-1,-1)$
38.	$(1,-1,1)$	$(-1,0,0)$
39.	$(1,-1,1)$	$(-1,1,1)$
40.	$(1,-1,1)$	$(-1,-1,-1)$
41.	$(-1,0,-1)$	$(0,1,1)$
42.	$(-1,0,-1)$	$(1,1,1)$
43.	$(-1,0,-1)$	$(1,-1,-1)$
44.	$(-1,0,-1)$	$(-1,1,1)$
45.	$(-1,0,-1)$	$(-1,-1,-1)$
46.	$(-1,1,-1)$	$(0,0,0)$
47.	$(-1,1,-1)$	$(0,1,1)$
48.	$(-1,1,-1)$	$(0,-1,-1)$
49.	$(-1,1,-1)$	$(1,0,0)$
50.	$(-1,1,-1)$	$(1,1,1)$
51.	$(-1,1,-1)$	$(1,-1,-1)$
52.	$(-1,1,-1)$	$(-1,0,0)$
53.	$(-1,1,-1)$	$(-1,1,1)$
54.	$(-1,1,-1)$	$(-1,-1,-1)$
55.	$(-1,-1,-1)$	$(0,0,0)$
56.	$(-1,-1,-1)$	$(0,1,1)$
57.	$(-1,-1,-1)$	$(0,-1,-1)$
58.	$(-1,-1,-1)$	$(1,0,0)$
59.	$(-1,-1,-1)$	$(1,1,1)$
60.	$(-1,-1,-1)$	$(1,-1,-1)$
61.	$(-1,-1,-1)$	$(-1,0,0)$
62.	$(-1,-1,-1)$	$(-1,1,1)$
63.	$(-1,-1,-1)$	$(-1,-1,-1)$
64.	$(0,1,0)$	$(0,-1,-1)$
65.	$(1,0,1)$	$(0,1,1)$
66.	$(1,0,1)$	$(0,-1,-1)$
67.	$(1,0,1)$	$(1,0,0)$
68.	$(-1,0,-1)$	$(0,0,0)$
69.	$(-1,0,-1)$	$(0,-1,-1)$
70.	$(-1,0,-1)$	$(1,0,0)$
71.	$(-1,0,-1)$	$(-1,0,0)$
72.	$(0,0,0)$	$(1,1,1)$

Table D.8 $(\mu-\tau)$ symmetry in the entire 4×4 matrix.

E

Vacuum alignment for allowed cases

Sl no.	VEV list	Comment
1.	$\phi' = (0,0,1)$, $\phi'' = (0,0,1)$ $\phi' = (0,0,1)$, $\phi'' = (0,0,-1)$ $\phi' = (0,0,-1)$, $\phi'' = (0,0,1)$ $\phi' = (0,0,-1)$, $\phi'' = (0,0,-1)$ $\phi' = (1,0,0)$, $\phi'' = (0,1,0)$ $\phi' = (1,0,0)$, $\phi'' = (0,-1,0)$ $\phi' = (-1,0,0)$, $\phi'' = (0,1,0)$ $\phi' = (-1,0,0)$, $\phi'' = (0,-1,0)$	8 of such matrices

Table E.1 VEV alignment of triplet flavon fields ϕ', ϕ'' for texture 3 zero symmetric case, that give rise to same complex constraints.

Sl no.	VEV list	Comment
1.	$\phi' = (1,0,1)$, $\phi'' = (0,1,-1)$ $\phi' = (1,0,1)$,$\phi'' = (0,-1,1)$ $\phi' = (1,0,-1)$,$\phi'' = (0,1,1)$ $\phi' = (1,0,-1)$,$\phi'' = (0,-1,-1)$ $\phi' = (-1,0,1)$,$\phi'' = (0,1,1)$ $\phi' = (-1,0,1)$,$\phi'' = (0,-1,-1)$ $\phi' = (-1,0,-1)$,$\phi'' = (0,1,-1)$ $\phi' = (-1,0,-1)$,$\phi'' = (0,-1,1)$	8 of such matrices
2.	$\phi' = (1,0,-1)$, $\phi'' = (1,1,1)$ $\phi' = (1,0,-1)$, $\phi'' = (-1,-1,-1)$ $\phi' = (1,1,1)$, $\phi'' = (0,1,-1)$ $\phi' = (1,1,1)$, $\phi'' = (0,-1,1)$ $\phi' = (-1,0,1)$, $\phi'' = (1,1,1)$ $\phi' = (-1,0,1)$, $\phi'' = (-1,-1,-1)$ $\phi' = (-1,-1,-1)$, $\phi'' = (0,1,-1)$ $\phi' = (-1,-1,-1)$, $\phi'' = (0,-1,1)$	8 of such matrices
3.	$\phi' = (1,0,-1)$, $\phi'' = (1,-1,-1)$ $\phi' = (1,0,-1)$, $\phi'' = (-1,1,1)$ $\phi' = (1,-1,1)$, $\phi'' = (0,1,-1)$ $\phi' = (1,-1,1)$, $\phi'' = (0,-1,1)$ $\phi' = (-1,0,1)$, $\phi'' = (1,-1,-1)$ $\phi' = (-1,0,1)$, $\phi'' = (-1,1,1)$ $\phi' = (-1,1,-1)$, $\phi'' = (0,1,-1)$ $\phi' = (-1,1,-1)$, $\phi'' = (0,-1,1)$	8 of such matrices

Table E.2 VEV alignment of triplet flavon fields ϕ', ϕ'' for $(\mu - \tau)$ symmetric case, that give rise to same complex constraints.

Sl no.	VEV list	Comment
1.	$\phi' = (1,-1,0)$, $\phi'' = (1,-1,0)$ $\phi' = (-1,1,0)$, $\phi'' = (-1,1,0)$ $\phi' = (0,1,-1)$, $\phi'' = (1,0,-1)$ $\phi' = (0,1,-1)$, $\phi'' = (-1,0,1)$ $\phi' = (0,-1,1,)$, $\phi'' = (1,0,-1)$ $\phi' = (0,-1,1)$, $\phi'' = (-1,0,1)$ $\phi' = (1,-1,0)$, $\phi'' = (-1,1,0)$ $\phi' = (-1,1,0)$, $\phi'' = (1,-1,0)$	8 of such matrices
2.	$\phi' = (0,1,1)$, $\phi'' = (1,0,1)$ $\phi' = (0,1,1)$, $\phi'' = (-1,0,-1)$ $\phi' = (0,-1,-1)$, $\phi'' = (1,0,1)$ $\phi' = (0,-1,-1)$, $\phi'' = (-1,0,-1)$ $\phi' = (1,1,0)$, $\phi'' = (1,1,0)$ $\phi' = (1,1,0)$, $\phi'' = (-1,-1,0)$ $\phi' = (-1,-1,0)$, $\phi'' = (-1,-1,0)$ $\phi' = (-1,-1,0)$, $\phi'' = (1,1,0)$	8 of such matrices

Table E.3 VEV alignment of triplet flavon fields ϕ', ϕ'' for texture 1 zero symmetric case, that give rise to same complex constraints.

Sl no.	VEV list	Comment
1.	$\phi' = (0,0,1)$,$\phi'' = (0,1,1)$ $\phi' = (0,0,1)$,$\phi'' = (0,-1,-1)$ $\phi' = (0,0,-1)$,$\phi'' = (0,1,1)$ $\phi' = (0,0,-1)$,$\phi'' = (0,-1,-1)$ $\phi' = (1,0,1)$,$\phi'' = (0,-1,0)$ $\phi' = (1,0,1)$,$\phi'' = (0,1,0)$ $\phi' = (-1,0,-1)$,$\phi'' = (0,1,0)$ $\phi' = (-1,0,-1)$,$\phi'' = (0,-1,0)$	8 of such matrices
2.	$\phi' = (0,0,1)$,$\phi'' = (0,1,-1)$ $\phi' = (0,0,1)$,$\phi'' = (0,-1,1)$ $\phi' = (0,0,-1)$,$\phi'' = (0,1,-1)$ $\phi' = (0,0,-1)$,$\phi'' = (0,-1,1)$ $\phi' = (1,0,-1)$,$\phi'' = (0,1,0)$ $\phi' = (1,0,-1)$,$\phi'' = (0,-1,0)$ $\phi' = (-1,0,1)$,$\phi'' = (0,1,0)$ $\phi' = (-1,0,1)$,$\phi'' = (0,-1,0)$	8 of such matrices

Table E.4 VEV alignment of triplet flavon fields ϕ', ϕ'' for texture 2 zero symmetric case, that give rise to same complex constraints.

F

Light neutrino mass matrix elements

$$
\begin{aligned}
M_{ee} &= c_{12}^2 c_{13}^2 c_{14}^2 m_1 + e^{-i\alpha} c_{13}^2 c_{14}^2 m_2 s_{12}^2 + e^{-i\beta} c_{14}^2 m_3 s_{13}^2 + e^{-i\gamma} m_4 s_{14}^2 \\
M_{e\mu} &= -e^{-i\delta_{24}} c_{14} \left(e^{i\delta_{24}} c_{12} c_{13} c_{23} c_{24} \left(m_1 - e^{-i\alpha} m_2 \right) s_{12} - e^{i\left(\delta_{13}+\delta_{24}\right)} c_{13} c_{24} \left(e^{-i\beta} m_3 \right. \right. \\
&\quad \left. - e^{-i\alpha} m_2 s_{12}^2 \right) s_{13} s_{23} + e^{i\left(2\alpha+\delta_{14}\right)} M c_{13}^2 m_2 s_{12}^2 s_{14} s_{24} - e^{i\delta_{14}} \left(e^{-i\gamma} m_4 - e^{-i\beta} m_3 s_{13}^2 \right) \\
&\quad \left. s_{14} s_{24} + c_{12}^2 c_{13} m_1 \left(e^{i\left(\delta_{13}+\delta_{24}\right)} c_{24} s_{13} s_{23} + e^{i\delta_{14}} c_{13} s_{14} s_{24} \right) \right) \\
M_{e\tau} &= c_{14} \left(- e^{i\left(-\alpha+\delta_{14}\right)} c_{13}^2 c_{24} m_2 s_{12}^2 s_{14} s_{34} + e^{i\delta_{14}} c_{24} \left(e^{-i\gamma} m_4 - e^{-i\beta} m_3 s_{13}^2 \right) s_{14} s_{34} \right. \\
&\quad + c_{12} c_{13} \left(m_1 - e^{-i\alpha} m_2 \right) s_{12} \left(c_{34} s_{23} + e^{i\delta_{24}} c_{23} s_{24} s_{34} \right) + e^{i\delta_{13}} c_{13} \left(e^{-i\beta} m_3 - e^{-i\alpha} \right. \\
&\quad \left. m_2 s_{12}^2 \right) s_{13} \left(c_{23} c_{34} - e^{i\delta_{24}} s_{23} s_{24} s_{34} \right) - c_{12}^2 c_{13} m_1 \left(e^{i\delta_{13}} c_{23} c_{34} s_{13} \right. \\
&\quad \left. \left. + \left(e^{i\delta_{14}} c_{13} c_{24} s_{14} - e^{i\left(\delta_{13}+\delta_{24}\right)} s_{13} s_{23} s_{24} \right) s_{34} \right) \right) \\
M_{\mu\mu} &= e^{i\left(-\gamma+2\delta_{14}-2\delta_{24}\right)} c_{14}^2 m_4 s_{24}^2 + e^{-i\beta} m_3 \left(e^{i\delta_{13}} c_{13} c_{24} s_{23} - e^{i\left(\delta_{14}-\delta_{24}\right)} s_{13} s_{14} s_{24} \right)^2 \\
&\quad + e^{-i\alpha} m_2 \left(c_{12} c_{23} c_{24} + s_{12} \left(- e^{i\delta_{13}} c_{24} s_{13} s_{23} - e^{i\left(\delta_{14}-\delta_{24}\right)} c_{13} s_{14} s_{24} \right) \right)^2 + m_1 \\
&\quad \left(c_{23} c_{24} s_{12} + c_{12} \left(e^{i\delta_{13}} c_{24} s_{13} s_{23} + e^{i\left(\delta_{14}-\delta_{24}\right)} c_{13} s_{14} s_{24} \right) \right)^2
\end{aligned}
$$

$$
\begin{aligned}
M_{\mu\tau} &= e^{i\left(-\gamma+2\delta_{14}-\delta_{24}\right)}c_{14}^2c_{24}m_4s_{24}s_{34}+e^{i\left(2\beta+\delta_{13}\right)}m_3\big(e^{i\delta_{13}}c_{13}c_{24}s_{23}-e^{i\left(\delta_{14}-\delta_{24}\right)}\\
&\quad s_{13}s_{14}s_{24}\big)\big(-e^{-i\left(\delta_{13}-\delta_{14}\right)}c_{24}s_{13}s_{14}s_{34}+c_{13}\big(c_{23}c_{34}-e^{i\delta_{24}}s_{23}s_{24}s_{34}\big)\big)\\
&\quad +m_1\big(-c_{23}c_{24}s_{12}+c_{12}\\
&\quad \big(-e^{i\delta_{13}}c_{24}s_{13}s_{23}-e^{i\left(\delta_{14}-\delta_{24}\right)}c_{13}s_{14}s_{24}\big)\big)\big(s_{12}\big(c_{34}s_{23}+\\
&\quad e^{i\delta_{24}}c_{23}s_{24}s_{34}\big)+c_{12}\big(-e^{i\delta_{14}}c_{13}c_{24}s_{14}s_{34}-e^{i\delta_{13}}s_{13}\big(c_{23}c_{34}\\
&\quad -e^{i\delta_{24}}s_{23}s_{24}s_{34}\big)\big)\big)+e^{-i\alpha}m_2\big(c_{12}c_{23}c_{24}+s_{12}\big(-e^{i\delta_{13}}c_{24}s_{13}\\
&\quad s_{23}-e^{i\left(\delta_{14}-\delta_{24}\right)}c_{13}s_{14}s_{24}\big)\big)\big(-c_{12}\big(c_{34}s_{23}+e^{i\delta_{24}}c_{23}s_{24}s_{34}\big)\\
&\quad +s_{12}\big(-e^{i\delta_{14}}c_{13}c_{24}s_{14}s_{34}-e^{i\delta_{13}}s_{13}\big(c_{23}c_{34}-e^{i\delta_{24}}s_{23}s_{24}s_{34}\big)\big)\big)
\end{aligned}
$$

$$
\begin{aligned}
M_{\tau\tau} &= e^{i\left(-\gamma+2\delta_{14}\right)}c_{14}^2c_{24}^2m_4s_{34}^2+e^{i\left(-\beta+2\delta_{13}\right)}m_3\big(e^{-i\left(\delta_{13}-\delta_{14}\right)}c_{24}s_{13}\\
&\quad s_{14}s_{34}+c_{13}\big(-c_{23}c_{34}+e^{i\delta_{24}}s_{23}s_{24}s_{34}\big)\big)^2+m_1\big(s_{12}\big(c_{34}s_{23}\\
&\quad +e^{i\delta_{24}}c_{23}s_{24}s_{34}\big)+c_{12}\big(-e^{i\delta_{14}}c_{13}c_{24}s_{14}s_{34}-e^{i\delta_{13}}s_{13}\big(c_{23}c_{34}\\
&\quad -e^{i\delta_{24}}s_{23}s_{24}s_{34}\big)\big)\big)^2+e^{-i\alpha}m_2\big(c_{12}\big(c_{34}s_{23}+e^{i\delta_{24}}c_{23}s_{24}s_{34}\big)\\
&\quad -s_{12}\big(-e^{i\delta_{14}}c_{13}c_{24}s_{14}s_{34}-e^{i\delta_{13}}s_{13}\big(c_{23}c_{34}-e^{i\delta_{24}}s_{23}s_{24}s_{34}\big)\big)\big)^2
\end{aligned}
$$

$$
\begin{aligned}
M_{es} &= c_{14}\big(e^{i\delta_{14}}c_{24}c_{34}\big(e^{-i\gamma}m_4-e^{-i\alpha}c_{13}^2m_2s_{12}^2-e^{-i\beta}m_3s_{13}^2\big)s_{14}-\\
&\quad e^{i\delta_{13}}c_{13}\big(e^{-i\beta}m_3-e^{-i\alpha}m_2s_{12}^2\big)s_{13}\big(e^{i\delta_{24}}c_{34}s_{23}s_{24}+c_{23}s_{34}\big)+\\
&\quad c_{12}c_{13}\big(m_1-e^{-i\alpha}m_2\big)s_{12}\big(e^{i\delta_{24}}c_{23}c_{34}s_{24}-s_{23}s_{34}\big)-c_{12}^2c_{13}m_1\\
&\quad \big(e^{i\delta_{14}}c_{13}c_{24}c_{34}s_{14}-e^{i\delta_{13}}s_{13}\big(e^{i\delta_{24}}c_{34}s_{23}s_{24}+c_{23}s_{34}\big)\big)\big)
\end{aligned}
$$

$$
\begin{aligned}
M_{\mu s} &= e^{i\left(2\gamma+2\delta_{14}-\delta_{24}\right)}c_{14}^2c_{24}c_{34}m_4s_{24}+e^{i\left(2\beta+\delta_{13}\right)}m_3\big(e^{i\delta_{13}}c_{13}c_{24}s_{23}\\
&\quad -e^{i\left(\delta_{14}-\delta_{24}\right)}s_{13}s_{14}s_{24}\big)\big(-e^{-i\left(\delta_{13}-\delta_{14}\right)}c_{24}c_{34}s_{13}s_{14}-c_{13}\big(e^{i\delta_{24}}\\
&\quad c_{34}s_{23}s_{24}+c_{23}s_{34}\big)\big)+m_1\big(-c_{23}c_{24}s_{12}+c_{12}\big(-e^{i\delta_{13}}c_{24}s_{13}s_{23}\\
&\quad -e^{i\left(\delta_{14}-\delta_{24}\right)}c_{13}s_{14}s_{24}\big)\big)\big(s_{12}\big(e^{i\delta_{24}}c_{23}c_{34}s_{24}-s_{23}s_{34}\big)+c_{12}\\
&\quad \big(-e^{i\delta_{14}}c_{13}c_{24}c_{34}s_{14}+e^{i\delta_{13}}s_{13}\big(e^{i\delta_{24}}c_{34}s_{23}s_{24}+c_{23}s_{34}\big)\big)\big)\\
&\quad +e^{-i\alpha}m_2\big(c_{12}c_{23}c_{24}+s_{12}\big(-e^{i\delta_{13}}c_{24}s_{13}s_{23}-e^{i\left(\delta_{14}-\delta_{24}\right)}c_{13}\\
&\quad s_{14}s_{24}\big)\big)\big(c_{12}\big(-e^{i\delta_{24}}c_{23}c_{34}s_{24}+s_{23}s_{34}\big)+s_{12}\big(-e^{i\delta_{14}}c_{13}c_{24}\\
&\quad c_{34}s_{14}+e^{i\delta_{13}}s_{13}\big(e^{i\delta_{24}}c_{34}s_{23}s_{24}+c_{23}s_{34}\big)\big)\big)
\end{aligned}
$$

$$
\begin{aligned}
M_{\tau s} &= e^{i\left(-\gamma+2\delta_{14}\right)} c_{14}^2 c_{24}^2 c_{34} m_4 s_{34} + e^{i\left(-\beta+2\delta_{13}\right)} m_3 \big(- e^{-i\left(\delta_{13}-\delta_{14}\right)} c_{24} \\
&\quad c_{34} s_{13} s_{14} - c_{13}\left(e^{i\delta_{24}} c_{34} s_{23} s_{24} + c_{23} s_{34}\right)\big)\big(- e^{-i\left(\delta_{13}-\delta_{14}\right)} c_{24} \\
&\quad s_{13} s_{14} s_{34} + c_{13}\left(c_{23} c_{34} - e^{i\delta_{24}} s_{23} s_{24} s_{34}\right)\big) + m_1\big(s_{12}\left(e^{i\delta_{24}} c_{23} c_{34}\right. \\
&\quad \left. s_{24} - s_{23} s_{34}\right) + c_{12}\big(- e^{i\delta_{14}} c_{13} c_{24} c_{34} s_{14} + e^{i\delta_{13}} s_{13}\left(e^{i\delta_{24}} c_{34} s_{23}\right. \\
&\quad \left. s_{24} + c_{23} s_{34}\right)\big)\big)\big(s_{12}\left(c_{34} s_{23} + e^{i\delta_{24}} c_{23} s_{24} s_{34}\right) + c_{12}\big(- e^{i\delta_{14}} c_{13} c_{24} \\
&\quad s_{14} s_{34} - e^{i\delta_{13}} s_{13}\left(c_{23} c_{34} - e^{i\delta_{24}} s_{23} s_{24} s_{34}\right)\big)\big) + e^{-i\alpha} m_2\big(c_{12}\big(- e^{i\delta_{24}} \\
&\quad c_{23} c_{34} s_{24} + s_{23} s_{34}\big) + s_{12}\big(- e^{i\delta_{14}} c_{13} c_{24} c_{34} s_{14} + e^{i\delta_{13}} s_{13}\left(e^{i\delta_{24}}\right. \\
&\quad \left. c_{34} s_{23} s_{24} + c_{23} s_{34}\right)\big)\big)\big(- c_{12}\left(c_{34} s_{23} + e^{i\delta_{24}} c_{23} s_{24} s_{34}\right) \\
&\quad + s_{12}\big(- e^{i\delta_{14}} c_{13} c_{24} s_{14} s_{34} - e^{i\delta_{13}} s_{13}\left(c_{23} c_{34} - e^{i\delta_{24}} s_{23} s_{24} s_{34}\right)\big)\big)
\end{aligned}
$$

$$
\begin{aligned}
M_{ss} &= e^{-i\left(\gamma+\delta_{14}\right)} c_{14}^2 c_{24}^2 c_{34}^2 m_4 + e^{i\left(-\beta+2\delta_{13}\right)} m_3 \left(e^{-i\left(\delta_{13}-\delta_{14}\right)} c_{24} c_{34} s_{13}\right. \\
&\quad \left. s_{14} + c_{13}\left(e^{i\delta_{24}} c_{34} s_{23} s_{24} + c_{23} s_{34}\right)\right)^2 + m_1\left(s_{12}\left(e^{i\delta_{24}} c_{23} c_{34} s_{24} - \right.\right. \\
&\quad \left.\left. s_{23} s_{34}\right) + c_{12}\big(- e^{i\delta_{14}} c_{13} c_{24} c_{34} s_{14} + e^{i\delta_{13}} s_{13}\left(e^{i\delta_{24}} c_{34} s_{23} s_{24} + \right.\right. \\
&\quad \left.\left. c_{23} s_{34}\right)\big)\right)^2 + e^{-i\alpha} m_2\big(c_{12}\big(- e^{i\delta_{24}} c_{23} c_{34} s_{24} + s_{23} s_{34}\big) \\
&\quad + s_{12}\big(- e^{i\delta_{14}} c_{13} c_{24} c_{34} s_{14} + e^{i\delta_{13}} s_{13}\left(e^{i\delta_{24}} c_{34} s_{23} s_{24} + c_{23} s_{34}\right)\big)\big)^2
\end{aligned}
$$

G

List of Publications

Papers published

1. Neelakshi Sarma, Kalpana Bora, Debasish Borah, Eur.Phys.J. C **79** (2019) no.2, 129 (2019-02-11), DOI: 10.1140/epjc/s10052-019-6584-z. Impact Factor - **5.172**.

2. Kalpana Bora, Neelakshi Sarma, Jaydip Singh, Pramana **89** (2017) no.4, 60 (2017-10-05), DOI: 10.1007/s12043-017-1454-4.

3. Kalpana Bora, Neelakshi Sarma, Springer Conference Proceedings, vol **174** (2015) 345-351, arXiv: 1511.02676.

Papers under preparation/ to be communicated

1. *"Neutrino-carbon interaction at low three-momentum transfer"*

Paper presented, Conferences/Seminars attended

Papers presented:

1. Paper presented (oral) at XXIII DAE-BRNS High Energy Physics Symposium held during December 10-14, 2018 at Indian Institute of Technology, Madras.

2. Paper presented (oral) at UGC-SAP (DRS-III) Sponsored National Seminar on Progresses in Nuclear and High Energy Physics held in the Department of Physics, Gauhati University from 30th to 31st March 2018.

3. Paper presented (poster) at Nu HoRIzons VII held during 21-23 February, 2018 at Harish Chandra Research Institute, Allahabad.

4. Paper presented (oral) at National Conference on Advances in Mathematical Sciences (NCAMS-2016), 22-23 December, 2016, Gauhati University, Guwahati.

5. Paper presented (oral) at Current Issues on Cosmology, Astrophysics, and High Energy Physics, November 2-5,2015, Dibrugarh University, Assam.

6. Paper presented (oral) at XXI DAE-BRNS High Energy Physics Symposium 08-12 December 2014, IIT Guwahati, Assam.

Conferences/Seminars attended:

1. International conference titled '*NuHoRIzons - VI*', HRI Allahabad, March 18-20, 2016.
2. Instructional Workshop in Particle Physics titled '*Sangam @ HRI 2016*' HRI Allahabad, February 15-19, 2016.